MECHANICAL VENTILATION: EFFECTS ON HUMAN DIAPHRAGM GENE EXPRESSION FOLLOWING CARDIOTHORACIC SURGERY AND BREATHING VARIABILITY IN PROLONGED MECHANICAL VENTILATION PATIENTS DURING SPONTANEOUS BREATHING TRIALS

By

TSENG-TIEN HUANG

A DISSERTATION PRESENTED TO THE GRADUATE SCHOOL
OF THE UNIVERSITY OF FLORIDA IN PARTIAL FULFILLMENT
OF THE REQUIREMENTS FOR THE DEGREE OF
DOCTOR OF PHILOSOPHY

UNIVERSITY OF FLORIDA

2009

To my parents, family members, and my dear, Qiong for their love and support

ACKNOWLEDGMENTS

This project would not have been completed without the support and assistance of many people. First, I thank my mentor, Dr. A.D. Martin, for his guidance and continuous support during my graduate education. He is a great model to the researcher I aspire to be. Also, I praise my supervisory committee members: Dr. P.W. Davenport, Dr. J.C. Rosenbek and Dr. David Fuller, for their direction and support throughout my graduate studies. I also thank all laboratory members, who have played a role in my achievements. Finally and most importantly, I am thankful for the experiences shared with my parents and family members throughout my life and career.

TABLE OF CONTENTS

page

LIST OF TABLES

LIST OF FIGURES

Abstract of Dissertation Presented to the Graduate School
of the University of Florida in Partial Fulfillment of the
Requirements for the Degree of Doctor of Philosophy

MECHANICAL VENTILATION: EFFECTS ON HUMAN DIAPHRAGM GENE EXPRESSION FOLLOWING CARDIOTHORACIC SURGERY AND BREATHING VARIABILITY IN PROLONGED MECHANICAL VENTILATION PATIENTS DURING SPONTANEOUS BREATHING TRIALS

By

Tseng-Tien Huang

May 2009

Chair: A.D. Martin
Major: Rehabilitation Sciences

Failure to wean from mechanical ventilation (MV) is a serious problem in acute medical care today. Approximately 5% of patients receiving MV experience difficult weaning, but these patients account for approximately 40-50% of all MV days. Numerous animal studies have documented that MV use leads to diaphragm atrophy, oxidative stress, reduced muscle strength and altered gene expression in as little as 6-24 hours, and this phenomenon has been termed ventilator induced diaphragm dysfunction (VIDD). Additionally, recent human work has documented severe VIDD (diaphragm muscle fibers atrophying ~55%) following approximately 39 hours of MV, and clinical human studies have shown that patients experiencing difficulty weaning have impaired respiratory muscle performance, consistent with changes seen in VIDD models. However, it is unknown how soon the diaphragm begins to start the process of atrophy following the start of mechanical ventilation. We hypothesized that the genes responsible for maintaining diaphragmatic contractile function, stress response, energy transduction would be altered over the course of a 5 hour cardiothoracic surgery.

Two diaphragm biopsies were obtained from 5 male patients (67 +/- 11years) undergoing cardiothoracic surgery. The first biopsy was obtained as soon as the diaphragm was exposed; the

second biopsy was obtained as late in the surgery as possible (4.9 +/- 1.8 hours). We profiled mRNA from the 5 pairs of muscle biopsies with a microarray (Affymetrix Hu U133 plus 2.0). Microarray analysis identified 763 differentially expressed (early vs. late samples) unique gene products ($p< 0.005$) after cardiothoracic surgical procedures. Post-operatively, the genes related to the generalized stress response and redox regulation were upregulated. We also found significantly upregulated expression of cathepsin C (2.7-fold), cathepsin L1 (2.0-fold), and various ubiquitin-conjugating enzymes (E2) (~1.5-fold). Myocyte enhancer factor 2C (MEF2C), a key transcriptional factor for skeletal muscle development and regeneration, was significantly down-regulated (3.5-fold). We conclude that cardiothoracic surgery results in rapid changes in diaphragm gene expression, including genes related to generalized stress response, redox regulation, and proteolysis. This work provides the first data examining the changes of diaphragm gene expression following surgical procedures. These data will lead to future research examining intraoperative pharmacological interventions aimed at preventing VIDD in humans.

Meanwhile, most PMV patients require participating in unsupported, progressively lengthening, spontaneous breathing trials (SBT). Thirty-eight PMV (46+/-23 days) patients (male/female ratio: 16/22, Age 64+/-12yrs) were studied. Breathing pattern (BP) variables including exhaled minute ventilation (V_E), breathing frequency (f), inspired tidal volume (V_T), peak inspiratory flow (PIF), inspiration time (T_I), expiration time (T_E), and duty cycle were measured during the first 30 min of successful and failed SBT and the mean values and coefficients of variation (CV) of these BP variables were calulated. SBT failure was defined with standard criteria. Compared to successful SBT, the failed SBT displayed significantly high PIF and f (31.3+/-9.2 vs. 28.8+/-5.9 L/min and 29+/-11 vs. 26+/-7 breath/min, respectively). The CV of V_E, f and PIF were higher during successful trials. We conclude that selected BP variables are

different within subjects during the first 30 minute interval of failed and successful SBT in PMV patients, reflecting a higher drive to breathe in failed trials. BP CVs variables revealed more significant differences than the mean values.

CHAPTER 1
INTRODUCTION

With the advance in anesthesia and surgical techniques over the past decade, most patients undergoing cardiac surgery are easily weaned from mechanical ventilation within a few hours after surgery (1). However, approximately 5% of cardiac surgical patients require postoperative prolonged mechanical ventilation (PMV), for 7 or more days (2). Additionally, serious complications from PMV use are commonly seen. While receiving MV, the cumulative risk of pneumonia is about 1% per day (3). Other complications of MV include cardiac arrhythmias, deep vein thrombosis, pneumothorax, ascites, aspiration pneumonia, sepsis, gastrointestinal hemorrhage, acute renal failure, and infections (4). These PMV patients repeatedly fail to wean and face a substantial risk of long-term complications and even death (5). Thus, weaning these PMV patients from MV support is one of great challenges in intensive care.

Emerging evidence demonstrates that weaning difficulty is linked to inspiratory muscle dysfunction which results in the inability of the respiratory muscles to maintain adequate ventilation. Specifically, animal studies have shown that respiratory muscle weakness produced by prolonged MV is due to diaphragmatic atrophy and contractile dysfunction (6-11). This decrease in diaphragmatic contractility is time-dependent (8) and may occur with as little as 6-18 hours of MV use (12). Moreover, recent work published in the NEJM has shown that clinically significant diaphragm atrophy occurs in humans following as little as 18-69 hours of MV (13). At the cellular levels, evidence supporting this dysfunction is associated with atrophy (10, 14), oxidative stress (10, 12), myofibrillar disruption (9, 15), and various remodeling responses (6, 11, 14, 16) in the diaphragm. DeRuisseau (17) in 2005 examined gene expression after 6-18 hour of CMV in 5 mice and concluded, ‘Mechanical ventilation resulted in rapid changes in diaphragmatic gene expression and genes in the cell growth/cell maintenance, stress response,

and nucleic acid metabolism categories showed predominant upregulation, whereas genes in the structural protein and energy metabolism categories were predominantly downregulated.' These data imply that gene expression changes start very early following the initiation of MV use. However, no comparable data is available on the acute effects of MV use on the human diaphragm. It is unknown how the mRNA gene expression in the human diaphragm is altered by surgical procedures (including the use of MV) and, more importantly, whether patients undergoing short-term procedures (eg. surgical anesthesia accompanied with MV use) are at risk for developing VIDD.

Specific Aim

To examine the effects of prolonged surgical procedures, which include the use of MV, in mRNA gene expression in human diaphragms.

Hypothesis

The genes responsible for maintaining diaphragmatic contractile function, stress response, energy transduction are influenced over the course of cardiothoracic surgery in humans.

Significance of the Study

This research will expand our knowledge of how the gene expression is influenced by cardiothoracic surgery. The changes of gene expression following surgical procedures may be particularly relevant to understanding the pathophysiological significance of VIDD in patients at risks of post-surgical weaning difficulties. The knowledge of underlying molecular mechanisms of diaphragm dysfunction will help direct efforts to develop rehabilitation and pharmacologic interventions in the pre-, intra- and post-operative periods.

CHAPTER 2
LITERATURE REVIEW

Animal studies in rats have shown that as little as 6 to 18 hours of controlled mechanical ventilation (CMV) results in changes in diaphragmatic gene expression and atrophy (10, 17). Moreover, recent work by Levine et al. in humans has shown that CMV for ~36 hours led to 55% atrophy of diaphragm muscle fibers, increased markers of oxidative stress and upregulation of genes controlling pathways leading to muscle atrophy (13). Clearly, the emerging evidence indicates that short periods of CMV may lead to ventilator-induced diaphragm dysfunction. Thus, the effect of MV-induced diaphragm atrophy and weakening in the ICU patients cannot be ignored.

The objective of this review is twofold 1) outline our current understanding of MV-induced diaphragm dysfunction, and 2) provide a brief overview of signal transduction of muscle unloading.

Mechanical Ventilation-Induced Diaphragmatic Dysfunction

Experimental evidence suggests that controlled mechanical ventilation (CMV), associated with muscle unloading and inactivity, can induce dysfunction of the diaphragm, resulting in an early-onset and progressive decrease in diaphragmatic force generating capacity, called VIDD. The mechanisms of VIDD are not fully elucidated, but include muscle atrophy, oxidative stress, myofibril injury, and various remodeling responses.

Diaphragm Muscle Atrophy

Disuse atrophy following the use of MV develops very rapidly as early as 18 hours and to a significantly greater extent in the diaphragm during CMV than in peripheral skeletal muscles (10). For example, using the rat as an experimental model, Shanely et al.(10) in 2002 reported that the onset of disuse muscle atrophy occurred approximately eight times faster in the

diaphragm compared with locomotor skeletal muscle. Interestingly, they also found that type II fibers exhibited a greater degree of atrophy than type I fibers in the diaphragm during MV. Because the force produced by type I fibers is less than that generated by type II fibers, greater type II fiber atrophy could potentially contribute to the decline of maximal force production by the diaphragm after short-term CMV(18). Moreover, animal MV models demonstrate that diaphragm atrophy results from both decreased rates of protein synthesis,(14) and enhanced rates of proteolysis,(10) which functionally impairs maximal force generation.

Oxidative Stress

It has been shown that diaphragmatic unloading is associated with a rapid onset of oxidative stress following 6 hours of MV (12). Importantly, oxidative stress can contribute to both muscle atrophy and contractile dysfunction (12). Data shows that oxidative stress can modify several proteins associated with excitation-contraction coupling, contributing to a decrease in muscle force production (19). Moreover, MV-induced oxidative stress evokes myofibrillar protein oxidation in the diaphragm (12) and oxidized myofibrillar proteins are sensitive to proteolytic attack by proteases (20). Hence, oxidative stress plays an important role in MV-induced diaphragm contractile dysfunction and atrophy.

Myofibril Injury

Diaphragm muscle inactivity is associated with diaphragm muscle injury (9, 15). After 2-3 days of CMV in rabbits, significant myofibril damage was present in the diaphragm, but not in the soleus (9). It has been shown that myofibril injury contributed to the reduced diaphragm force-generating capacity (-49% in the 3 days of CMV) (9). Structural abnormalities of different subcellular components of diaphragm also could be observed after 2-3 days of CMV in rabbits. These changes consist of disrupted myofibrils, increased numbers of lipid vacuoles in the sarcoplasm, and abnormally small mitochondria containing focal membrane disruptions (15).The

precise mechanisms of injury have not been clearly identified, but mechanical ventilator-induced myofibril injury may involve activation of calpains, which have the ability to degrade several sacromeric proteins and direct cell injury due to augmented oxidative stress (21, 22).

MV-Induced Diaphragm Dysfunction on mRNA Levels

Despite studies in animals which have documented the effects of MV on diaphragm muscle structure and function, the underlying mechanisms regulating rapid diaphragm dysfunction are not fully understood. There are a number of genes encoding for proteins functioning in the initiation of the muscle atrophy process. In mammals, protein degradation involves an ATP-dependent ubiquitin-proteasome pathway (23) (UPP) and is regulated by the muscle-specific ubiquitin ligases (24) (such as E3 ligase), muscle atrophy factor box (25) (MAF-box), and muscle specific RING finger-1(23) (MuRF-1). *In vitro* studies have identified a number of specific mRNAs in the diaphragm that change in response to the use of MV. The mRNA expression of MAF-box (26, 27), MuRF-1,(28) and an E3 ligase (28) in the ubiquitin-proteasome pathway (UPP) are thought to play a role in MV-induced diaphragmatic atrophy and weakness. Zhu et al.(27) demonstrated that MV animals (after 1 day of CMV) increased diaphragmatic mRNA levels of MAF-box and an E3 ligase in the UPP. Moreover, the upregulation of MAF-box mRNA levels occurred before the presence of structural myofibril disarray (injury). Consistent with the above findings, DeRuisseau (28) reported 12 hour of CMV produced an increase in MuRF-1 mRNA levels (19 fold), MAF-box (8.3 fold) in rat diaphragm muscle as compared with the controls. Collectively, CMV increases diaphragmatic levels of key components with the ubiquitin-proteasome pathway contributing to MV-induced proteolysis/atrophy in the diaphragm and the upregulation of atrophic factors in mRNA levels occurs prior to the presence of structural myofibril injury.

Further evidence showing the alterations of mRNA levels after short periods of CMV (6-18 hours) was provided by a gene expression microarray study,(17) demonstrating 354 unique genes with statistically altered expression of at least 1.5 fold in mechanically ventilated rat diaphragms compared with the controls. For the detailed analysis, genes with altered expression were functionally grouped into 4 categories: stress response, protein metabolism, calcium regulation, and energy metabolism. The authors concluded,(17) 'Mechanical ventilation resulted in rapid changes in diaphragmatic gene expression and genes in the cell growth/cell maintenance, stress response, and nucleic acid metabolism categories showed predominant upregulation, whereas genes in the structural protein and energy metabolism categories were predominantly downregulated.' Specifically, stress response genes, including superoxide dismutase-3, slelnoprotein P, peroxiredoxin-3, thioredoxin reductase-1, carbonic anhydrase III, heme oxygenase-1, and metalothionein, demonstrated the largest changes indicating that MV-induced dysfunction involved in oxidative type of stress and some protective adaptations in response to increased oxidative production were also occurred at the earliest time points after the use of MV. Secondly, many protein metabolism genes were altered following 6 and 18 hours of MV. Several members of the cathepsin family of proteases, matrix metalloproteinase-14, tissue inhibitor of metalloproteinase-1 (TIMP-1) were upregulated while calpain-3 (muscle-specific calpain) was downregulated. The upregulation of the cathepsin family in response to MV contributes to overall proteolysis and decreased calpain-3 mRNA level may impact diaphragm muscle apoptosis. Increased TIMP-1 and matrix metalloproteinase-14 may indicate an extracellular matrix remodeling in response to MV. Collectively, changed expression of these protein metabolism genes in response to MV were consistent with previous observations that MV resulted in enhanced protein proteolysis. Third, changes in the expression of genes related to

calcium regulation included calmodulin 1 and 2, calsequsetrin 2, and two calcium ion channel subunits, indicating that dysregulation of intracellular calcium might play a role in the progression of MV-induced diaphragmatic atrophy leading to further diaphragm contractile dysfunction. Finally, altered expression was noted for a large number of genes involved in energy metabolism, indicating that MV alter m-RNA expression patterns of many genes, involved in fat, carbohydrate, and mitochondrial metabolism.

Evidence of VIDD in Humans

Despite the growing evidence from animal models that demonstrates that MV leads to diaphragm dysfunction, very little data are available on the effects of mechanical ventilation on the human diaphragm. There are only two studies that have directly studied the impact of MV on human diaphragm function. Knisely et al. 1998 used a case control design and qualitatively showed massive diaphragm muscle fiber atrophy in a young child ventilated for 47 days compared to a child for 3 days (29). Levine et al. examined biopsy samples obtained from 14 brain-dead organ donors, and showed that 18 to 69 hours of controlled mechanical ventilation was associated with atrophy of both slow-twitch and fast-twitch fibers in the diaphragm (13). Consistent with the animal studies, Levine also showed that diaphragmatic dysfunction accounted for increased cellular stress (+100% caspase-3 mRNA expression) and muscle proteins proteolysis (+200% MAF-box mRNA vs. MBD4 (housekeeping gene); +590% MuRF-1 m-RNA vs. MBD4).

Signaling Mechanisms During Skeletal Muscle Atrophy

The loss of skeletal muscle mass secondary to inactivity or disuse is a common phenomenon known as muscle atrophy or wasting. A variety of conditions lead to muscle atrophy including muscle disuse, multiple disease states, fasting and age-associated atrophy. Regardless of the inciting event, skeletal muscle atrophy is characterized by decreased muscle

fiber cross-section area and protein content, increased insulin resistance, morphological changes (atrophy) of muscle fiber type, and reduced muscle tension. It is well-established that the decrease in protein synthesis and the increase in protein degradation rates account for muscle protein loss due to disuse. However, we are just beginning to understand the molecular signaling mechanisms that lead to protein loss. There is an accumulating literature that is beginning to elucidate upstream molecules and/or signaling mechanisms during skeletal muscle atrophy and several potential signaling molecules/mechanisms have been identified.

TNF-α and Other Cytokines

In general, muscle atrophy due to disuse is initiated by a reduction in muscle contractile activity and muscle tension while muscle atrophy due to disease is initiated by TNF-α or other cytokines. Although both factors contribute to cause to the protein loss, it is unlikely that TNF-α or other cytokines are involved in disuse atrophy. Previous data found no difference in TNF-α protein levels in unloaded muscle (30). Thus, disuse atrophy does not appear to involve the production of TNF-α and is not associated with inflammatory process.

Nuclear Factor Kappa B (NF-kB) Signal

NF-kB is a ubiquitous transcription factor that mediates a variety of processes depending on the cell type and upstream triggers. Incorrect regulation of NF-kB may cause inflammatory and autoimmune diseases, viral infection, and cancer. In mammals, five NF-kB family members have been identified: [p65(Rel A), Rel B, c-Rel, p52, and p50]. All family members are expressed in skeletal muscle, existing in unstimulated cells as heterodimers bound to inhibitory protein Ikappa B (IkB). Activation of NF-kB is achieved by nuclear transport of heterodimers of NF-kB family members and often occurs by the ubiquitination and degradation of the IkB. Also, p50 and p52 can form homodimers and undergo nuclear translocation. Accumulating evidence indicates that a specific NF-kB pathway is required for disuse muscle atrophy (reviewed in Refs.

(31-33)). With unloading, the nuclear levels of p50 and Bcl-3 (a nuclear IkB family member) were markedly increased (30). Meanwhile, mice with a knockout of the p50 gene showed to be resistant to the soleus muscle atrophy that results from 10 days of hindlimb unloading (34). The same result was found when Bcl-3 knockout mice were used(34). These data indicate that NF-kB pathway may be operative during disuse atrophy.

However, the target genes of NF-kB in disuse are currently under investigation. Recent work using transgenic mice revealed some candidate NF-kB targets during muscle atrophy (35). Mice with muscle-specific expression of an activated IkB kinase beta (MIKK) show a distinct skeletal muscle wasting. Specifically, muscle mass in MIKK mice was significantly reduced compared with its wild-type controls, demonstrating that the NF-kB activation by IKKbeta is sufficient to induce muscle atrophy. Cai et al. showed that activation of NF-kB in MIKK mice resulted in increased expression of the E3 ubiquitin ligase MuRF-1, whereas other target genes of NF-kB were not activated in muscle of MIKK mice (35). Previous data has shown that MAF-box and MuRF-1 were upregulated by muscle unloading (36). Thus, it is possible that MuRF-1 transcription is driven by the activation of NF-kB and MuRF-1 may be the target of NF-kB signaling. When MIKK mice were crossed with MuRF-1 -/- mice to create MIKK x MuRF-1 -/- mice, mice with this genotype had a significant reduction in muscle mass, though less than that seen when MIKK mice were crossed with muscle specific expression of IkBα super repressor (MISR) mice. This incomplete inhibition of muscle loss implies that MuRF-1 is not the only crucial mediator of muscle atrophy to be activated by NF-kB pathway.

Another target genes of NF-kB in muscle cell were the proteasome subunits. In the MIKK mice, several proteolytic genes such as C2 and C9 were upregulated and these mRNAs were also upregulated in unloaded and cachectic muscle (36, 37). In addition, microarray data found that

Nedd4 and Mdm2 were upregulated during unloading (36) and these genes could be the targets of NF-kB signaling.

Overall, it is conceivable that NF-kB is a key signaling pathway activated by muscle unloading and may be involved in the activation of proteolytic process. However, the downstream target genes have not been elucidated and this will be an important area for further study.

IGF-1/PI3K/Akt Pathway

The IGF-1/PI3K/Akt pathway is an important signaling pathway for muscle hypertrophy (38). Activation of phosphatidylinositol 3 kinase (PI3K) by upstream ligands such as insulin-like growth factor (IGF-1) leads to activation of the serine/threonine kinase (Akt), which in turn phosphorylates and activates the mammalian target of rapamysin (mTOR) kinase. Activated mTOR can result in increased protein synthesis by phosphorylation and activation of p70S6 kinase, and phosphorylation of eukaryotic translation initiation factor 4E binding protein 1 (4E-BP-1), key regulatory proteins involved in translation and protein synthesis (39). Importantly, this pathway is also thought to be a potent suppressor of proteolysis and the expression of atrophy related ubiquitin ligases. In addition to stimulate muscle protein synthesis through activation of PI3K and Akt, IGF-1 and insulin also reduced the expression of MAF-box (40). Moreover, during the disuse-induced muscle atrophy, Akt protein and phosphorylation levels markedly decreased, as did the activation state of P70S6 kinase (36, 41). In addition, the amount of 4E-BP-1 bound to eukaryotic translation initiation factor 4E(eIF-4E) was increased at 14 days of unloading in rat gastrocnemius muscle, suggesting a role in decrease protein synthesis (36). Furthermore, mice with a knockout of Akt1 gene display severe skeletal muscle atrophy, bone developmental impairment, and severe growth deficiency when compared to wild-type mice (42, 43). Collectively, these results show that IGF-1/PI3K/Akt pathway not only increase overall

protein synthesis, but also suppresses proteolysis and the expression of atrophy-related ubiquitin ligases.

PI3K/Akt/FOXO in Muscle Atrophy

Activation of the PI3K/Akt pathway results in the phosphorylation of the FOXO proteins, which is a subgroup of the forkhead family of transcription factors. In mammals, three members of this family, FOXO1, FOXO3, and FOXO4 have been identified. These have been implicated in regulation of target genes in metabolism, apoptosis, and cell cycle progression (44). When Akt is activated, FOXO is phosphorylated and bound by 14-3-3 protein that mediates its movement from nucleus to cytoplasm. Once phosphorylated FOXO proteins are translocated from the nucleus to cytoplasm, their transcriptional functions will be inhibited (45). Dephosphorylation of FOXO factors leads to FOXO protein to nucleus entry, resulting in suppression of the muscle growth and induction of apoptosis (46).

Evidence showing that IGF-1/PI3K/Akt pathway critically mediated FOXO transcription comes from experiments by Stitt et al.(47). First, they used a pharmacological inhibitor of PI3K and allowed FOXO1 protein to translocate the nucleus. Second, they used a mutant form of FOXO1, which can not be regulated by Akt and remains active in the nucleus, and demonstrated that in the presence of this active, nuclear-localized mutant form of FOXO1, IGF-1 can not inhibit muscle atrophy mediators, the MAF-box or the MuRF1. This finding demonstrates that IGF-1/PI3K/Akt anti-atrophy activity required the blockade of FOXO. The study of transgenic mice specifically over expressing FOXO1 supports this idea since these transgenic mice exhibited less skeletal muscle mass than the non-transgenic controls (48). Enhanced gene expression of Atrogin-1, MuRF-1, and cathepsin L suggested the increase protein degradation contributed to the loss of muscle mass in FOXO1 mice.

FOXO3 was also reported to upregulate the gene expression of Atrogin-1, and IGF-1 was found to reverse the FOXO3 mediated activation of the Atrogin-1 promoter (49). In addition, over-expression of an active form of FOXO3 decreased the skeletal muscle fiber size (49). When FOXO3 activation was blocked by RNAi in muscles, Atrogin-1 induction during muscle atrophy were blunted (49). Collectively, FOXO transcription factors may play a role in muscle atrophy and IGF-1/PI3K/Akt pathway might control these proteins.

Caspase-3 in Muscle Atrophy

Caspase is a specific endoprotease and, in some case, it plays a role in apoptosis (programmed cell death) (50). To date, over twelve proteins belonging to this group have been identified in mammals. In the cells, caspases are expressed as inactive precursors (ie. Procaspases), and activation of caspases can result in events contributing to protein breakdown and apoptosis (50).

Capase-3 activation during muscle atrophy is thought to be involved in the initial steps of myofibrillar degradation. Although the ubiquitin proteasome system, which is thought to be the main proteolytic system during muscle atrophy, can degrade monomeric actin or myosin, it does not break down actomyosin complexes or myofibrils (51). This idea is supported by the evidence that capase-3 activation promotes degradation of actomyosin complexes, and inhibition of caspase-3 activity suppresses the overall rate of proteolysis in diabetic muscle undergoing atrophy (52). In addition, the data shows that caspase-3 inhibition results in the attenuation of myofiber atrophy during diaphragm muscle unloading suggesting that caspase-3 plays a role in muscle protein degradation during muscle disuse (53).

Control of caspase-3 activity is complicated and may involve several interconnected signaling pathways. Powers at al. (2007) proposed that caspase-3 could be activated by oxidative stress, increased cellular calcium, and increased calpain activity (54). Also, multiple lines of

cross talk between pathways were proposed (54). Increased calpain activity can lead to the activation of caspase-3 (55). Thus, cross-talk between the calpain and caspase-3 proteolytic systems may involve in the muscle atrophy during period of disuse; but, the mechanisms under this process are largely unknown.

It is also worth noting that caspase-independent mechanisms, such as the release of apoptosis-inducing factor (AIF) and endonuclease G (EndoG), are involved in myofiber apoptosis in skeletal muscle undergoing atrophy. EndoG is a mitochondrial apoptotic protein and is capable of inducing DNA fragmentation when translocated from mitochondria to nuclei through a caspase-independent pathway (56). Dupont-Versteegden et al. found that the amount of EndoG in nuclei was consistent with myofiber nuclear loss in muscles atrophied in response to hindlimb suspension (57). Moreover, EndoG translocation was very specific for myofiber nuclear apoptosis while very weak activated caspase-3 was seen in myofibers (57). Another protein released from mitochondria upon pro-apoptotic stimulation and capable of inducing apoptosis independent of caspase is apoptosis inducing factor (AIF). Ferreira et al. showed that AIF release was elevated in soleus skeletal muscle during 48 hours of unloading (58). Collectively, these data suggest that mitochondria-associated apoptosis may contribute to the loss of muscle mass in the early phase of muscle atrophy.

Proteolytic Pathways in Skeletal Muscle

Numerous proteolytic systems contribute to the degradation of muscle proteins. The principal proteases in skeletal muscle can be classified into three categories: 1) lysosomal protease; 2) Ca^{2+}-activated proteases (i.e., calpain); and 3) the ubiquitin-proteasome dependent.

Role of lysosomal proteolysis in disuse atrophy

It is believed that lysosomal pathway (i.e. cathepsins) did not play a major role in muscle atrophy. These proteinases (except cathepsin L) were not systematically activated in various

instances of muscle atrophy (59). With the agents that directly inhibit cathespins, myofilbrillar protein degradation rates are not significantly affected in disuse atrophy (31). Cathespins are unlikely to degrade myofibrils, but rather they seem to play a role to degrade membrane proteins, including receptors, ligands, channels, and transporters (60). Moreover, literature shows that proteolysis during muscle atrophy is the interaction of lysosomal and ubiquitin-proteasomal mechanisms. A number of mammalian receptors and ion channels are ubiquitinated and then are degraded by either lysosomal or proteasomal systems. The signal that determines which of these pathways is used is the type of ubiquitin modification that occurs. Intracellular proteins with polyubiquitin chains are easily recognized and degraded by proteasomal systems while the protein substrate with mono- (or di-) ubiquitin modification, then it is degraded by internalization and transport to the lysosome; it is not recognized by the proteasomal systems because of the lack of the polyubiquitin chain (61, 62). Future research on how mono-ubiquitin affects the structure, location, and activity of modified membrane-associated protein will help us understanding the role of the lysosomal systems during muscle atrophy.

Role of calpains in disuse atrophy

Calpains (calpains I and II) are Ca^{2+}-activated proteases that are activated in skeletal muscle during periods of inactivity (63). Although calpains do not directly degrade the contractile proteins actin and myosin, proteins that are involved in the assembly and scaffolding of myofibrils such as titin, vinculin and, nebulin are known calpain substrates (reviewed in Ref. (64)). Moreover, calpain is known to degrade several kinases and phosphatases, including calcium/calmodulin-dependent kinase (CaM kinase II), protein kinase C (PKC-α, PKC-βI, PKC-βII, and PKC-γ), and calcineurin (54). In addition, calpain activity may indirectly influence the rate of protein degradation. Data shows that accumulation of myofibrillar protein fragments

generates a positive feedback resulting in an increase in proteasome activity by the stabilizing association of E3-ubiquitin ligases with their substrates (65). Nonetheless, much work is still needed to unravel the exact roles of calpains during muscle disuse.

Proteasome-mediated proteolysis

Compelling evidence demonstrates that activation of the ubiquitin-proteasome system plays a key role in muscle atrophy. The ubiquitin-proteasome system involves two successive steps. The target protein is first polyubiquitinated and then recognized by the 26S proteasome, which degrades the substrate into peptides(59). Polyubiquitination involves the sequence action of the ubiquitin-activating enzyme (E1), specific ubiquitin-conjugating enzymes (E2), and in many cases specific ubiquitin protein ligase enzyme (E3). Numerous studies demonstrate that there are significant increases in the expression of various components of the ubiquitin-porteasome pathway (UPP) during muscle atrophy (36, 66-68). In addition, inhibition of the components of UPP with agents has also shown significant interference of muscle proteolysis in disuse muscle atrophy (review in Ref(24)).

The E1 enzyme has low expression in skeletal muscle and its mRNA level is not regulated during muscle wasting (59). In mammals, as many as 40 known E2s have been identified but only a small number of E2s (such as $E2_{14K}$, $E2_{20K}$, and UBC4/UBC5 isoforms) are over-expressed during muscle wasting (59).

In mammals, as many as 1000 E3s are recognized but only a very limited number of E3s that upregulated in muscle wasting have been identified (59). Importantly, significant attention has been paid to the increased expression of two muscle-specific E3 enzymes (MAF-box and MuRF-1) in disuse because one signature study demonstrates that mice knocked out for either enzyme were partially resistant to muscle atrophy (69). With the various models of disuse, MAF-

box mRNA levels were increased rapidly before muscle weight loss was detectable, and maintained high expression during the period when overall proteolysis was accelerated (33). This observation suggests that MAF-box may play a role in the initiation and maintenance of accelerated proteolysis. MuRF-1 was also upregulated in several models of disuse atrophy and its mRNA upregulation occurred as early as 12 hours after muscle denervation suggesting that MuRF-1 may involve in the initiation of atrophy process (33). Collectively, both MuRF-1 and MAF-box could be used as early markers of disuse muscle atrophy.

Oxidative Stress

Another area that has received significant attention is the generation of reactive oxygen species (ROS) in muscle unloading. Abundant evidence implicates oxidative stress as a potential regulator of proteolytic pathways leading to muscle atrophy during periods of muscle disuse (review in Ref (54, 70)). The first evidence showing oxidative stress played a key signaling role in the regulation of disuse muscle atrophy was provided by Kondo et al. (71). Their work revealed that immobilization of skeletal muscles was associated with increased free radical production, resulting in oxidative injury in inactive muscle fibers. Importantly, this work also showed that disuse muscle atrophy could be delayed by exogenous antioxidants. These early observations have subsequently been confirmed by others (72, 73).

In order to respond to oxidative stress, cells display adaptive mechanisms involved in increasing their antioxidant defenses. Elevated levels of ROS appear to be detected by redox sensitive regulatory molecules in the cell that can trigger various signal transduction cascades(74). It is believed that oxidative stress contributes to disuse muscle atrophy by influencing the following cell signaling pathways: 1) the activation of NF-kB, and 2) control of the mitogen-activated protein kinases (MAPKs) singaling (54).

Oxidative stress activates NF-kB signal

Accumulating evidence indicates that a specific NF-kB pathway is required for disuse muscle atrophy (as previously discussed). Either exogenous ROS or H_2O_2 triggered ROS could activate NF-kB pathways directly in muscle cells (75). This observation is consistent with the concept that ROS can promote NF-kB activation, which perhaps leads to increased proteolysis through the ubiquitin-proteasome pathway. In contrast, the DNA binding activity of oxidized NF-kB is diminished, suggesting that ROS may also inhibit NF-kB transcriptional activity (54). Nonetheless, it appears that NF-kB activation is under redox control, but how ROS regulates NF-kB transcriptional activity remains largely unknown. Clearly, future research is needed to unravel the uncertainties about the redox regulation of NF-kB in skeletal muscle during periods of inactivity.

Oxidative stress activates MAPK signaling

Another potential link between oxidative stress and muscle disuse atrophy involves the redox regulation of the MAPK activation. It is well established that MAPK can regulate the function of cytoplasmic components and the expression of a variety of genes involved either in survival and proliferation or in the induction of cell death (76). The MAPKs include four subfamilies in skeletal muscle: *1*) extracellular signal-regulated kinases (ERK) 1 and 2 (ERK1/2); *2*) p38 MAPK; *3*) c-Jun NH_2-terminal kinases (JNK); and *4*) ERK5 or big MAPK. These protein kinases contribute to the regulation of life and death decisions in response to various stress signals (i.e. cytokines, growth factors, and cellular stress) (77).

Importantly, MAPKs have been shown to be activated by oxidative stress. Kefalolyianni and associates, for example, found that ERK1/2, JNK, and p38 were activated in skeletal myotubes exposed to H_2O_2 (78). Moreover, the increase of atrogin1/MAF-box was not altered significantly by the ERK inhibitor or the JNK inhibitor, but was blunted by the p38 inhibitor

(33). These data suggest that atrogin1/MAF-box gene is a down-stream target of p38 MAPK signaling. In addition, immobilization of skeletal muscles also resulted in elevated p38 activity during periods of muscle disuse (79). Collectively, these data suggest a potential role for oxidative stress-induced activation of p38 in disuse muscle atrophy.

JNK can be activated in response to many of the same stimuli that activate p38 such as oxidative stress. There is growing evidence that JNK plays an important role in oxidative stress-mediated apoptosis. Because ROS themselves are unable to activate apoptotic cascade, it is hypothesized that a death-signal pathway such as JNK is a mediator between ROS and apoptosis. Similar to p38, JNK activity was significantly elevated in atrophic muscles following a period of immobilization (33). Suppression of JNK by either genetic or pharmacological approaches demonstrates some resistance to ROS-induced apoptosis (80). These findings support a link between ROS, JNK, and apoptosis. However, it is still unknown if JNK activation is response for the myonuclear apoptosis that occurs during disuse muscle atrophy.

Other Candidates Involved in Muscle Atrophy

There are also additional molecular triggers or signaling pathways yet to be elucidated. Additional pathways that contain differentially expressed gene with unloading include those involved with myogenic signaling (MyoD, Mrg1), Notch signaling (transducin-like enhancer of split 4) (Tle4), JAK/STAT signaling, amino acid metabolism, and serine proteases, as well as genes involved in synaptic vesicle remodeling, cell proliferation, and cytoskeletal function (see Ref. (36)for discussion of the full data set). In addition, another microarray study demonstrated that many genes required for ATP production and late steps in glycolysis were down-regulated in multiple types of skeletal muscle atrophy (37). Although there is no obvious relationship between reduced ATP utilization and muscle atrophy, these changes in gene expression would be expected to suppress muscle's capacity to utilize glucose and reduced muscle energy turnover.

Nevertheless, microarray data on global mRNA expression are providing multiple avenues for further study of the regulation of disuse atrophy.

Complexity of Signaling Mechanisms During Skeletal Muscle Atrophy

The more we learn about the disuse atrophy, the more we become aware of its complexity and highly regulated nature. Signals involved in disuse muscle atrophy are summarized in Table 1. Many signaling pathways involved in muscle disuse atrophy are interacted or interdependent with each other. Activation or inhibition of a single pathway may have cascade effects on muscle protein balance, but there is no evidence to prove that the pathway is the sole regulator of the process (33). For example, in muscle cells, ROS may induce activation of both the MAPK and the NF-kB signaling pathway, and the latter promotes increased proteolysis through the ubiquitin-proteasome pathway. Thus, discussing the communications between two or more signaling pathways help us to get a comprehensive understanding of the complexity of muscle atrophy.

Summary and Future Directions

Prolonged periods of skeletal muscle inactivity due to immobilization, hindlimb unloading, or the MV use can result in significant muscle atrophy. The muscle atrophy is characterized as decreased muscle fiber cross-section area and protein content, increased insulin resistance, morphological changes of muscle fiber type, and reduced muscle tension. The decrease in protein synthesis and the increase in protein degradation rates account for the majority of the rapid loss of protein content due to disuse. However, we are just beginning to understand the upstream molecules and signaling mechanisms that lead to protein loss. Literature suggests that NF-kB pathway, IGF-1/PIK3/Akt pathway, and caspase-3 pathway as well as Ubiquitin-proteasome pathway seem to play major roles of protein loss. Factors such as ROS, p38, and JNK are also demonstrative to linking to disuse muscle atrophy, but our current understanding of

how these factors influence the process of muscle atrophy is limited. Furthermore, because of the interplay between signaling pathways, a change in one signal may have multiple effects. Future microarray studies are needed to identify the possible pathways by which proteolysis is modulated and to visualize all the signaling pathways simultaneously, coordinately acting to produce the physiology underlying muscle atrophy. As more research reveals the details of these signaling pathways that are required for atrophy, a much better understanding will be gained of how to treat the atrophic conditions clinically.

Table 2-1. Signals involved in disuse-induced muscle atrophy

Signals	Expression	Function	References
P50, Bcl-3	↑	Promotes protein degradation	(30, 34)
PI3K, Akt	↓	Promotes protein degradation Inhibits protein synthesis	(49)
Nedd4, Mdm2	↑	Promotes protein degradation	(36)
Caspase-3	↑	Promotes protein degradation	(52)
EndoG, AIF	↑	Promotes protein degradation	(57, 58)
Calpains	↑	Promotes protein degradation	(64)
MAF-box, MuRF-1	↑	Promotes protein degradation	(69)
ROS	↑	Promotes protein degradation	(71)
P38	↑	Promotes protein degradation	(79)
JNK	↑	Promotes protein degradation?	(54)
FOXO1, FOXO3	↑	Promotes protein degradation	(48, 49)

CHAPTER 3
METHODS AND MEASUREMENTS

Research Design

A prospective, observational, repeated-measures design was conducted in this project.

Subjects

Seven male patients between 50 to 80 years of age undergoing scheduled cardiothoracic surgical operations at Shands Hospital at the University of Florida were recruited to enroll in this prospective study. The investigative protocol was approved by the Institutional Review Broad at University of Florida. In addition, patients signed a separate clinical consent form for their cardiothoracic surgical procedures. Exclusion criteria included NYHA Class III or IV Cardiac Disease, history of stroke, cerebrovascular disease, spinal cord injury or progressive neuromuscular disease, cardiothoracic surgery within the previous 12 weeks, any prior history of pneumonectomy or lung surgery, a skeletal pathology such as scoliosis, FEV1 <60% of age-predicted value, and malignancy.

Anesthetic Management

A preoperative dose of intravenous vancomycin (1-4 mg) was given. A standard anesthesia regimen was used in all patients. Subjects were administered general anesthesia and endotracheally intubated by the anesthesiologist. Controlled mechanical ventilation was maintained at 5 cycles per minute with a tidal volume of 5-7 mL/kg. Anesthetic induction consisted of fentanyl, propofol, versed, vancomycin, and vecuronium. Intraoperative paralysis maintenance was with vecuronium (0.6-0.8 mg/kg) /or pancuronium (0.1-0.12 mg/kg). Analgesia was maintained during cardiopulomnary bypass (CPB) with fentanyl and versed infusion, which changed to propofol infusion after CPB. Intraoperatively, hypertension was treated with

labetolol, nipride, and hydralazine. Hypotensive episodes were treated with intravenous mannitol. No patient received corticosteroids before, during, or after the operation.

Surgical Management

All patients underwent a median sternotomy and CPB. Standard aortic, valve replacement surgery was performed by the same surgeon, Dr. Thomas M. Beaver. Hypothermic CPB (temperatures of 18-24°C) with a retro-grade blood cardioplegia was used in all patients. Hypothermic circulatory arrest was performed. Mean arterial pressure of 50-80 mmHg and blood flows of 2.4-2.8 $\cdot$ $min^{-1} \cdot m^{-2}$ were maintained during CPB. The hematocrit was maintained at >20% during CPB. The use of vasoactive drugs was at the discretion of the anesthesiologist managing the case. Patients were actively rewarmed to 36.5°C before removal of the aortic crossclamp and weaning from CPB. After surgery, all patients were transferred to the cardiothoracic intensive care unit for the recovery.

Diaphragm Biopsies

Two full-thickness biopsy specimens (approximately 6 mm diameter) were taken from the antero-lateral aspect of the right or left diaphragm near the costal margin during surgery. The first biopsy was obtained immediately after exposing the diaphragm during cardiothoracic surgery; the second biopsy was obtained as late in surgery as possible. Each specimen was stabilized by using RNAlater® solution (Ambion Inc. Austin, TX, USA) and then transferred to liquid nitrogen and stored at -80°C for microarray analysis. The RNAlater® solution stabilized and protected RNA in fresh specimens and then the specimen could be indefinitely stored at -20°C or below until further analysis.

The safety and ethics of obtaining diaphragm samples from humans must be addressed. Numerous studies have been published in which non-therapeutic, experimental human diaphragm tissue samples during cardiac surgeries (81-88) and no complication was reported.

Isolation of Total RNA

Total RNA was isolated with a RneasyTM Mini Kit (Qiagen Inc) and processed according to the manufacturer's instructions. Briefly, a portion of the costal diaphragm (~20mg) was homogenized with Polytron homogenizer and centrifuged at full speed for 3 min (4°C) to remove insoluble material if necessary. The sample was added two volumes of 100% ethanol and centrifuged at 10,000g for 1 min until the lysate/ethanol was mixed. Then the sample was added one volume of Lysis solution. Following transfer of the aqueous phase to a new tube, RNA was precipitated and washed twice with 500µL-700 µL Wash solution (e.g. 75% ethanol). The concentration and purity of the extracted RNA was processed according to the standard protocol. In addition, the high quality of total RNA was determined by capillary electrophoresis using an Agilent bioanlysis system (Bioanalyzer 2001; Agilent, Palo Alto, CA).

Microarray Processing

Complementary Ribonucleic Acid (cRNA) Synthesis and Microarray Hybridization

The microarray processing and the following analysis were performed in Dr. Henry Baker's laboratory at University of Florida. In brief, cRNA was synthesized based on the two-step amplification protocol outlined by the manufacturer (Affymetrix, High Wycombe, UK), using 0.4 µg of total RNA as starting material. Secondly, cRNA was transcribed *in vitro* with the incorporation of biotinylated nucleotides using an ENZO Bio Array High Yield RNA Transcript Labeling kit (T7; Enzo Life science, Farmingdale, NY), and the Biotin-labeled product was hybridized onto an Affymetrix Hu U133 plus 2.0 GeneChip, in which contains 54,675 probe sets representing over 38,500 well-substantiated human genes. Staining and washing followed the protocol (EukGEWSv4; Affymetrix) using a fluidics station (Affymetrix).

Data Acquisition (Scanning)

The arrays were scanned with a scanner (Affymetrix) and the fluorescence intensity calculated using Affymetrix Gene Chip Operating Software (GCOS). Chip to chip normalization was accomplished using dChip (Wong laboratory, Department of Biostatistics, Harvard School of Public Health, Cambridge, MA) normalization protocols. An expression matrix was modeled using the perfect match-only model algorithms of dChip. The detail of this model is described elsewhere (89). Briefly, each probe set of Affymetrix GeneChip was represented by ~16-20 perfectly matched oligonucletides. Comparison of the hybridization pattern of the perfect match-only pairs allowed for estimating the signal intensity of the true target transcript as well as eliminating non-specific hybridization signals.

Microarray Data Analysis and Biostatistics

Affymetrix Microarray Suite, version 5.0 (MAS 5.0, Stanford, CA) was used to identify probe sets whose hybridization signal intensity was at or below background levels. These probe sets were referred to as “absent”. Probe sets whose signal intensity were absent on all arrays under study were excluded in the following high-level statistical analysis. A transcript was required to be present on all the chips in the early- and late-surgical conditions in reporting differentially expressed genes.

High-level Statistical Analysis

High level statistical analysis was performed using algorithms within the software package dChip and BRB Array Tools (for details, see http//linus.nci.nih.gov/BRB-ArrayTools.html). In Dr. Baker’s laboratory, a 3-step general approach to the high-level statistical analysis of microarray datasets was developed and it consists of: 1) Unsupervised Analysis of Gene Expression Patterns, 2) Supervised Analysis of Gene Expression patterns, and 3) path analysis.

Unsupervised analysis of gene expression patterns

Initially, an unsupervised analysis was applied to assess the similarity and differences in apparent gene expression profiles among the samples. For this purpose, the dataset was passed through a variation filter to remove probe sets whose hybridization signal intensities did not vary much across the data set. By ranking on coefficient of variation, the top half of the dataset was identified and subjected to the next step. Secondly, principal component analysis (PCA), a form of multidimensional scaling, was used to identify similarities between specimens and to identify outliers (90). In PCA, the dimensionality of the dataset was reduced to the principal components. The first principal component accounts for most of the variance in the dataset, followed by the second principal component and so on. In addition, the principal components could be used to identify similarities in expression patterns among arrays without imposing structure. We performed PCA on the datasets in conjunction with cluster analysis. The results were visualized as a dendrogram on top of the cluster image.

Supervised analysis of gene expression patterns

The aim of supervised analysis was identify a list of genes that were differentially expressed between early-surgery and late-surgery samples (paired by patients). Probe sets whose hybridization signal intensities differed between early-surgery and late-surgery samples at the $p<0.005$ level of significance (using a modified Student's t test) were identified.

The reason for choosing $p<0.005$ level of significance is justified below. The key statistical issue in the supervised analysis involves controlling for the multiple comparisons. To appreciate this, consider an example in which there are 1,000 genes and 10 subjects in two groups. Using a two-sample t test with a significance level of 0.05, we would expect 50 of the gene expressions to be significant by chance alone. Several methods to alleviate this problem are possible 1) to adjust for multiple comparisons using a Bonferroni adjustment. Using a Bonferroni adjustment

would result in a per comparison significance level of 0.05/1000=0.00005, which might be too conservative because of the difficulty in achieving statistical significance, and 2) to control the False Discovery Rate (FDR), which is widely considered to be a more appropriate criterion in this context. A landmark paper by Storey and Tibshirani (91) in 2003 described the basics of FDR. In this method, let F be the number of false positives and T be the number of true positives. The FDR for an experiment is the expected proportion of F/(F+T), or the ratio of the false positives divided by all positives. There are a number of methods available for controlling FDR, including a selection of conservative p value. Typically, a p-value of 0.005 to identify significant probes sets at this level of significance one would expect one false positive by chance alone out of 500 probe sets analyzed. Therefore, in this study, a p-value of <0.005 was used to identify significance probe sets between early-surgery and late-surgery samples.

Path analysis

Once probe sets were identified that were differentially expressed between early-surgery and late-surgery samples, NetAffx query (http://www.affymetrix.com/analysis/index.affx) was undertaken for retrieving Gene Ontology (GO) annotations of the significant probe sets. This web available software was used for functional annotation clustering. By using this GO-enriched gene list, the Pathway-Express, one of a package of microarray tools, (http://vortex.cs.wayne.edu/projects.htm) was used to provide searchable pathways that related to the significant gene products in our study. The aim of this path analysis was to produce biological meaningful knowledge from the huge amount of data resulting from the microarray experiments. When a user submit a list of genes, which show significant differentially different in a given condition, the Pathway-Express searches the Onto-Tools database and builds a list of all associated pathways. The Onto-Tools database currently containes signaling pathways from Kyoto Encyclopedia of Genes and Genomes (KEGG) (http://www.genome.jp/kegg/). The

Pathway-Express performs a classical enrichment analysis based on a hypergeometric distribution in order to identify those pathways that contain a proportion of differentially expressed genes that is significant from what is expressed just by chance (92). This analysis produces a set of p-values that characterize the significance of the pathway from this statistical perspective (a lower p-value corresponds to a higher significance). Lastly, a freeware program of Advanced Pathway Painter v 2.08 (http://www.gsa-online.de/eng/app.html) was used to visualize the functional relationship among the significant gene products in these biological pathways.

CHAPTER 4
RESULTS AND DISCUSSION

Patient Collective and Clinical Data

Seven male patients fulfilled the entry criteria and were enrolled in the study. However, two subjects' data were excluded due to a diaphragm scarring in one case and the other case whose biopsy samples were possibly mislabeled (early-surgical and late-surgical conditions). Therefore, only five patients' data were reported and analyzed. Clinical baseline characteristics, such as age, height, weight, name of surgery, and type of anesthesia were given in Table 4-1.

The patients underwent to cardiothoracic surgical procedures with a mean (+/-SD) duration of 4.9+/-1.8 hours. The patients' age ranged from 54 to 78 years with a mean (+/-SD) of 67+/-11 years. Cardio-pulmonary bypass (CPB) time ranged from 159 to 266 minutes with a mean (+/-SD) of 218+/-51 minutes. One of the five subjects did not complete the planned hypothermic circulatory arrest because an isoelectric EEG was noted upon reaching the selective low temperature. Total cross clamp time ranged from 42 to 204 minutes with a mean (+/-SD) of 142+/-66 minutes. All subjects tolerated surgery without event and no study-related post-operative complications were noted.

Microarray Data Analysis and Biostatistics

Unsupervised Analysis of Gene Expression Patterns

Ten diaphragm muscle biopsy samples were obtained: five early-surgery and five late-surgery samples (paired by patients). Of these 10 arrays investigated, the expression of 2558 probe sets was not above background on any array and these probe sets were classified "absent" and excluded from further analysis. Of the remaining 52117 probe sets detected above background on at least one array, only 3318 probe sets were identified by the variation filter as having a CV of greater than 0.5 and were subjected to hierarchical cluster analysis. Figure 4-1

showed the hierarchical cluster analysis of the 10 arrays based on the expression level of the 3318 probe sets whose expression level varied the most.

Supervised Analysis of Gene Expression Patterns

Supervised microarray analysis identified 1081 probe sets differentially expressed (early vs. late) samples at $p < 0.005$ confidence level. Among these 1081 probe sets, 763 unique known genes were identified. The majority of transcripts (601/763) were upregulated.

To obtain initial information regarding the functionality of those genes that differentially expressed between early-surgical and late surgical conditions, the NetAffx query was undertaken for retrieving Gene Ontology (GO) annotations of those genes. The list of annotated genes was grouped into18 functional categories (Figure 4-2). Because of the number of differentially expressed genes, we elected to narrow our discussion to selected categories including generalized stress response and redox regulation (Table 4-2), protein membolism (Table 4-3), energy metabolism (Table 4-4), and muscle specific regulatory genes (Table 4-5). Remaining functional categories not presented in the discussion together within the list of expressed sequence tags were summarized in the tables of Appendix (A1-A11).

Path Analysis

Out of the 763 unique products, the Pathway-Express analysis considered 212 focus genes in its database. Scrutinizing the functional and biological linkage between these genes, the Janus kinase/signal transducers and activators of transcription (JAK/STAT) pathway (n=16, p value<0.0001) (Figure 4-3), the p53 signaling pathway (n=10, p value<0.0001) (Figure 4-4), the ErbB signaling pathway (n=7, p value=0.03), and the MAPK signaling pathway (n=15 p value=0.04) were identified (Table 4-6).

Discussion

Genome-wide gene expression profiling has created unique opportunities to investigate complex biological processes regulated at the transcriptional level. A previous study used the microarray technique to describe the molecular response associated with ventilator-induced muscle atrophy (VIDD) in an animal model (17). To our knowledge, this is the first repeated measures genome-wide profiling study examining molecular responses associated with diaphragm inactivity/MV in humans. Using gene expression profiling, we identified 763 unique transcripts that were differentially expressed ($p<0.005$) between early-surgical and late-surgical conditions. The majority of transcripts (601/763) were up-regulated. The list of differentially expressed genes was grouped into 18 functional groups. The objective of this study was to assess some of the transcriptional factors that are responsible for maintaining contractile function, stress response, protein metabolism, and energy metabolism, and how they were affected in the course of cardiothoracic surgery.

Generalized Stress Responsive and Redox Regulation Genes

Interleukin 6

During cardiothoracic surgical procedure, we observed increased expression in a number of genes linked to inflammatory and/or immune response. For example, interleukin 6 (IL6), a known proinflammatory cytokine, was significantly upregulated (15.6-fold). It is noted that, with cachexia, IL6 are the key triggers of muscle wasting, but IL6-induced muscle atrophy also occurs in the healthy animals (93). Meanwhile, IL6 may interact with a JAK/STAT signaling pathway, leading to changes in the expression of the suppressors of cytokine signaling (SOCS) family, and that this process may play a role in muscle atrophy with disuse (36). The JAK-STAT signaling takes part in the regulation of cellular responses to cytokines and growth factors. The deletion of SOCS genes in mice leads to significant overgrowth (94). In the present investigation, we

observed an increase of several SOCS mRNAs in the diaphragm including suppressor of cytokine signaling 1 (SOCS1) (4.7-fold), suppressor of cytokine signaling 2 (SOCS2) (3.1-fold), and suppressor of cytokine signaling 3 (SOCS3) (9.4-fold) as well as signal transducer and activator of transcription 3 (STAT3) (1.6-fold). The Path analysis identified that during the surgical procedure, increased expression of IL6 was associated with the increased expression of those genes (Figure 4-2). More interesting, a previous study found that there was a significant negative correlation between SOCS3 mRNA and myofibrillar protein content in the IL6-induced atrophied muscle (93). Collectively, this suggests that IL6 triggers an intracellular cascade including a JAK/STAT pathway during the cardiothoracic surgical procedure and this process possibly regulates the cellular response in the context of diaphragm unloading.

Despite previous studies in the animals suggested that cytokines e.g. IL6 are unlikely to involve in disuse muscle atrophy, we detected a significant increase in the mRNA for cytokines, namely IL6 (15.6-fold) and IL8 (9.2-fold). This is most likely due to the fact that our model is not a pure MV inactivity paradigm with the addition of surgery. Our surgery/MV model, however, is the **actual** clinical situation that often leads to VIDD and difficult weaning in humans, and thus, our results indicate that cytokines may affect diaphragm muscle and are relevant to the clinical management of these patients.

Oxidative stress

Oxidative stress has been implicated as a contributing factor to disuse muscle atrophy and a rapid onset of oxidative stress can occur following as early as 3-6 hours of MV (12). Consistent with a previous study (28), we found several genes upregulated in the diaphragm responsible for oxidative stress, including peroxiredoxin 6 (PRDX6) (2-fold), superoxide dismutase 2, mitochondrial (SOD2) (2.9-fold) and thioredoxin (TXN) (1.9-fold).

PRDX6 is an antioxidant enzyme that can reduce H_2O_2 and alkyl hydroperoxide to water and alcohol, respectively (95). PRDX6 is widely expressed in all the vital organs including the skeletal muscle (96). Additionally, Wang et al.(97) have shown that PRDX6 is a unique non-redundant antioxidant that functions independently of other antioxidant proteins such as catalase (CAT), glutathione (GPX), and superoxide dismutase (SOD). In the present investigation, we observed an increase in PRDX6 mRNA in the diaphragm during the surgical procedure, suggesting that the PRDX6 antioxidant properties might play a role in the human diaphragm muscle unloading.

It is well established that in quiescent cells, much of reactive oxygen species (ROS) are produced as byproduct of mitochondrial respiration when electrons leak from the electron transfer chain (ETC). The mitochondrial production of ROS results in the oxidation of mitochondrial lipids, protein, and DNA (98). SOD2, one of the enzymes of superoxide dismutase, converts superoxide to oxygen plus hydrogen peroxide and serves as the primary defense against mitochondrial superoxide. Therefore, it is not surprising that we detected an increase of SOD2 mRNA in our study. In mammals, three isoforms of superoxides are present. SOD1 is located in cytoplasm, SOD2 in the mitochondria, and SOD3 in the extracellular region. In the present investigation, we observed an increase of mRNA expression level in SOD2, but not in SOD1 and SOD3 in the diaphragm. This finding was consistent with previous observation that the diaphragm of 12 hour MV animals exhibited increased mRNA expression for SOD2 and no change in the mRNA expression of SOD1 was detected(99). Additionally, Chen et al.(100) found that the antioxidant systems eg. glutathione (GSH) and thioredoxin (TXN) were functionally distinct in cells and they showed that mitochondrial TXN-2 was more sensitive to oxidation than cytoplasmic TXN-1 by exogenously added peroxides. Hence, oxidative stress in

mitochondria may present an early signal of diaphragm unloading and play an important role in our surgery/MV model. This intriguing possibility awaits further confirmation.

TXN is a small (12 kD) globular, ubiquitous enzyme whose function is involved in antioxidant defense mechanisms such as the elimination of peroxide and the reduction of oxidized proteins. In the present investigation, we observed an increase in TXN mRNA in the diaphragm during the surgical procedure. This finding is consistent with the animal study reporting (101) that the expression of TXN is significantly increased by 2- and 4-day hindlimb unloading, which precedes the muscle weight loss. More interesting, TXN involves in various cellular process via redox signaling pathway, some of which are thought to be closely associated with muscle atrophy (101). Specifically, TXN can exert suppressive effects on the process of muscle atrophy as follows: (1) TXN suppresses the activation of NF-kB via the inhibition of I-kB breakdown, which then inhibits the NF-kB-induced activation of ubiquitin pathways (102) and (2) TXN works with PRDX to eliminate ROS production, which in turn suppresses the ROS-mediated activation of NF-kB, FOXO, and the ubiquitin-proteasome system.

Collectively, our data suggests that increased expression of a series of antioxidant genes, including PRDX6, SOD2 and TXN, participate in establishing an antioxidant firewall and their antioxidant properties are important in response to oxidative insult in the human diaphragm muscle unloading.

Protein Metabolism

Disuse atrophy can be detected following as little as 18 hours of MV use (10). In muscle atrophy, the balance between protein synthesis and degradation is shifted. The majority of muscle protein loss results from the acceleration of muscle protein degradation (103). At least three proteolytic systems are known to be involved in muscle protein degradation. These include lysosomal proteolysis, calcium-activated proteasomes, and ubiqutin-proeasome dependent

pathway. Several studies have shown members of each of these pathways are upregulated during disuse (17, 36, 37, 104, 105). Consistent with previous studies, our data indicates that cardiothoracic surgical procedures with MV support increase the proteolytic processes, which may cause significant atrophy of the human diaphragm. The parallel regulation of these proteolytic pathways under the surgical procedure was discussed as follows:

Proteasome-mediated proteolysis

Proteasome-mediated proteolysis is thought to be responsible for the majority of protein breakdown that occurs during disuse atrophy (24). This proteolytic process is characterized by the concerted action of ubiqutin-conjugating enzymes that link chains of polyubiqutin onto target proteins for degradation by either the 26S proteasome or the 20S protease core (106). In the present investigation, we found that mRNAs for polyubiqutination were upregulated in the diaphragm including several ubiqutin-conjugating enzymes (UBE2) and ubiquitin specific peptidases (USP). Although the USP itself does not involve in proteasome binding, the upregulation of the USP enzymes may assist to recycle free ubiquitin efficiently when the ubiquitin-proteasome systems is activated (59).

More importantly, we found a 2.6-fold upregulation of the ubiquitin protein ligase enzyme (E3) in the diaphragm. Tripartite motif-containing 63 (TRIM63) (otherwise known as MuRF-1) is a muscle-specific E3 identified being important to the regulation of protein loss during atrophy. Thus, the modest upregulation of TRIM63 in the diaphragm indicates that patients undergoing a short-term surgical procedure (4.9+/-1.8 hours), including the use of MV, are at risk for developing VIDD. Interestingly, our data demonstrated *downregulation* in another muscle-specific E3 gene, namely F-box protein 32 (FBXO32) (otherwise known as MAF-box). FBXO32 is a component of an SCF-type (Skp1/Cdc53/F-box complex) E3 ubiquitin ligase that determines substrate specificity for proteasome degradation. This protein is specifically

expression in cardiac and skeletal muscle and has previously been identified as a marker of muscle atrophy (25). In this study, we found a 3.5-fold *downregulation* of FBXO32 in the muscle samples. Previous animal work showed that 12 hours of MV resulted in significant elevations in mRNA levels in both FBXO32 (MAFbx) (3.8-fold) and MuRF-1 (19-fold)(28). However, in contrast to the animal studies, a consistent elevation of MAFbx and MuRF-1 mRNA has not been observed in published human muscle disuse studies (review in Ref.(107)). For example, de Boer et al.(108) showed 10 days of limb immobilization to result in elevated mRNA levels of MuRF-1, but not FBXO32, in the vastus lateralis of healthy human volunteers. These observations question the role of MuRF-1 and FBXO32 consistently in human muscle disuse atrophy. Further work is required to explain these important observations.

Lysosomal proteolysis

As mentioned earlier, cellular proteins can be targeted by lysosomal enzymes, known as cathepsins. In the present investigation, we observed an increase in cathepsin C (CTSC) (2.7-fold) and cathepsin L1 (CTSL1) (2.0-fold) mRNA in the diaphragm during the surgical procedure. Although cathepsin are unlikely to degrade the bulk of myobrillar proteins, some reports have suggested that cathepsin may play a special role in turnover of membrane proteins, including receptors, ligands, channels, and transporters (60). Meanwhile, literature suggests that proteolysis during muscle atrophy represents an interaction of lysosomal and ubiquitin-proteasomal mechanisms (31). In support of this, we found that upregulation of cathepsins were coordinated with an increase of protein ubiquitination in the diaphragm, suggesting that lysosomal proteolysis may play a role in human diaphragm muscle disuse during the cardiothoracic surgical procedure.

Calcium-activated proteasomes

Calpains (such as calpains I and II) are Ca^{2+} -activated proteases that are activated in skeletal muscle during periods of inactivity (63). Calpain substrates include proteins that are involved in the assembly and scaffolding of myofibrils. For example, nebulin and titin, two proteins that connect myofilament to the Z-disc, are known calpain substrates (64). However, calpains cleave their protein substrate, rather than completely degrading them, thereby generating fragments (63). It has been hypothesized that these fragments resulting from calpain cleavage become substrates for the ubiqutin-proeasome dependent pathway (UPP). In support of this hypothesis, Menconi et al. (109) demonstrate that calpain activation in myotubes results in a dose- and time-dependent increase in proteasome activity.

Additionally, Smith et al. (110) demonstrated that the calpain proteases act upstream of the UPP and calpain activation are sufficient to activate the UPP. However, in the present investigation, no change in mRNA levels for calpains was found, concomitantly with the UPP. We admit that, because of our study design, we may have missed early or transient increases in the expression of calpains. In fact, the mRNA level of calpain does not necessarily reflect its *in vivo* activity because 1) calpain's activity varies with cytosolic calcium concentration and 2) its activity is further regulated by its inhibitor, calpastatin, and membrane phospholipids (111).

Protein synthesis

Consistent with the idea that decreased protein synthesis is involved in the loss of protein during muscle disuse, two nuclear genes coding for mitochondrial ribosomal proteins were modestly downregulated, including mitochondrial ribosomal protein S25 (MRPS25) (1.4-fold decrease) and mitochondrial ribosomal protein L47 (MRPL47) (1.8-fold decrease). Several mRNAs encoding eukaryotic translation initial factors (EIFs), the elongation factor 2 (ELL2), and the termination factor 1 (ETF1) were upregulated in the diaphragm in response to the

cardiothoracic surgical procedure. In addition, the surgical procedure was associated with increased ribosomal protein S24 (PRS24) (2.4-fold) and S6 (RPS6) (2.4-fold) mRNA, a 40S ribosome subunit. Overall, this suggests that the diaphragm may upregulate the protein translation capacity after the cardiothoracic surgery; however, the rate of mitochondrial protein synthesis is decreased.

Energy Metabolism

During cardiothoracic surgical procedures, use of controlled MV exposes the diaphragm to a unique mode of disuse. The diaphragm is simultaneously unloaded, electrically quiescent and phasically shortened by cyclical lung inflation. In addition, neuromuscular junctions are blocked by neuromuscular blocking agents. Under such conditions, the energy metabolic requirements of the diaphragm are decreased, which likely impacts the rate of cellular energy turnover. Previous muscle disuse studies have demonstrated that many genes required for ATP production and the key regulatory steps of the glycolysis/gluconeogenesis were down-regulated (17, 37). Consistent with this, we observed a decreased expression of malate dehydrogenase 1 (MDH1) (2.2-fold decrease). MDH1 is important in transporting NADH equivalents across the mitochondrial membrane, controlling tricarboxylic acid (TCA) cycle pool size and providing contractile function (112). It plays a crucial role both in the malate-aspartate shuttle and the TCA cycle in all aerobic tissues of mammals, including the skeletal muscles (113). A decreased expression of MDH1 suggests that during the surgical procedure the diaphragm tends to decreased reliance on carbohydrate oxidation because less metabolic requirements are needed.

In addition, an increase in pyruvate dehydrogenase kinase, isoform 4 mRNA level (PDK4) (4.0-fold), a mitochondrial enzyme responsible for regulation of pyruvate dehydrogenase complex (PDC), was observed. PDC is able to catalyze the oxidation of pyruvate to acetyl-CoA in the mitochondria. Induction of PDK4 will inhibit the PDC activity and decrease carbohydrate

oxidation; thereby conserve glucose and the substrate for gluconeogenesis (114). More importantly, activation of PDK4 may enhance the oxidation of fatty acids by inactivation of PDC (115). Therefore, an increased expression of PDK4 suggests that the diaphragm during the surgical procedure tends to utilize fatty acid, rather than carbohydrate, as a fuel source. These observations seemingly conflict with previous studies showing that unloading muscle is associated with a fiber type switch (from slow to fast myosin fiber types) as well as metabolic changes including increased substrate-level activation of glycolysis and inhibition of fatty acid oxidation. For example, Wittwer et al. reported a downregulation of the capacity to oxidize fatty acids and an increase in glycolytic capacity in prolonged unloading of rat soleus muscle (116). The cause of this discrepancy is unknown; however one explanation may be that an early adaptation to unloading-induced metabolic deregulation occurs via increasing lipid utilization, while in the later phase of unloading metabolic flexibility is lost, resulting in enhanced reliance on glucose utilization concomitant with lipid accumulation in tissue. In support of this hypothesis, Mazatti et al. found that 24 hours of muscle unloading rather than 12 days of muscle unloading resulted in significantly the upregulation of peroxisome proliferators-activated receptor δ (Ppar δ), indicating an adaptive response to lipid utilization following muscle unloading (117). Further studies are needed to test this hypothesis.

A downregulation of phosphoenolpyruvate carboxykinase 1 (PCK1) (2.3-fold decrease) which plays a role in the regulation of gluconeogenesis was observed. This finding was not anticipated since the diaphragm is not considered to be a major site of glucose synthesis. Collectively, the surgical procedure alters mRNA expression patterns of the genes encoding key energy metabolism enzymes and results in an impairment of muscle carbohydrate metabolism as indicated by the upregulation of PDK4 mRNA.

Muscle-specific Regulatory Genes

Several muscle-specific regulatory genes were affected during the cardiothoracic surgery, including myogenic differentiation 1 (MYOD1) (2-fold increase), myogenic factor 5 (MYF5) (1.6-fold decrease), supervillin (SVIL) (2-fold increase), and myocyte enhancer factor 2C (MEF2C) (3.5-fold decrease) as well as mesenchyme homeobox 2 (MEOX2) (3.5-fold decrease). MYOD is one member of myogenic transcription factors, which can stimulate and modulate the transcription of muscle-specific genes and thus are able to contribute to muscle plasticity (118). While its role in adult muscle is not fully understood, it implicated in fiber phenotype adaptation in limb muscles. Although it is still controversial, several studies have shown that an adaptation from slow to fast phenotype was associated with elevated MYOD1 mRNA expression. Consistent with previous finding (36), upregulation of MYOD1 was seen during the initial stage of atrophy. However, upregulation of MYOD1 also has been seen with increased muscle loading (119). Additionally, in MYOD1 knockout mice, MYOD1 deletion resulted in a decrease in diaphragm maximal titanic tension, along with decrements in peak power output (120). These conflicting findings raise a question as to whether MYOD1 gene expression is dependent on interaction of the co-activators or inhibitors present in different activity paradigms. In support of this hypothesis, Stevenson et al. demonstrated that in a microarray study the expression pattern of MYOD1 and Mrg1, a transcriptional co-activator, were tightly co-regulated ($r^2 = 0.96$) during muscle disuse atrophy (36). Further studies are needed in progress to test this hypothesis.

MYF5, another member of myogenic transcription factors, was downregulated (1.6-fold). MYF5 plays an integral role in the initiation and control of skeletal muscle development (121). In adult muscle, MYF5 is expressed in satellite cells (122) and upregulation of MYF5 also has been reported after a single bout of exercise, indicating that upregulation of MYF5 is associated with load-mediated satellite activation (123). Additionally, MYF5 is also present in muscle

spindles in adult muscle (122), and therefore MYF5 expression could be also reflected to muscle spindle activity in the diaphragm.

We observed an upregulation of SVIL mRNA (2-fold increase). SVIL is an actin-binding protein and it expresses in muscle-enriched tissue, especially skeletal muscle (124). The role of SVIL in muscle is still under investigation. It forms a high-affinity link between the actin cytoskeleton and the plasma membrane (sarcolemma) of striated muscle cells. Although dystrophin is required for sarcolemmal integrity (125), SVIL may provide an additional anchor maintaining the integrity and organization of the sarcolemma of striated muscle cells during the mechanical stresses associated with load-induced stretching and muscle contraction (126). Additionally, SVIL may mediate the interaction between actin filaments and myosin II, functioning as membrane-associated scaffold (127). The upregulation of SVIL in our study suggests that this protein might be involved in the atrophy process following the surgical procedure. However, the role of SVIL in muscle disuse remains elusive.

MEF2C, a transcriptional factor for skeletal muscle development and regeneration, was downregulated (3.5-fold decrease) in the study. MEF2 proteins, MEF2A, -B, -C, and –D, usually cooperate with myogenic transcriptional factor family to drive skeletal muscle development during embryogenesis, but little is known about the role of MEF2C in the adult muscle. Potthoff et al. recently shows that MEF2C is an essential regulator of the M-line-specific protein, myomesin, and M protein and that loss of MEF2C in skeletal muscle resulted in improper sacromere organization (128). Additionally, a 14-days spaceflight suppressed MEF2C protein production, and with 9 days recovery in a 1 G environment MEF2C protein content returnd to the normal level, suggesting that MEF2C could be a key transcriptional factor for skeletal muscle atrophy and reloading (129). Collectively, MEF2C is sensitive to muscle loading/unloading

conditions and the downregulated MEF2C might impair contractile function because MEF2C is essential for sarcomere assembly.

Path Analysis

Path analysis via PathwayExpress identified that during the cardiothoracic surgical procedure affected the JAK-STAT, p53, ErbB, and MAPK signaling pathways (Table 4-2). Among these pathways, the JAK-STAT pathway appears to be key because it not only modulates the cell cycle, the apoptosis process and the MAPK signaling, but also is the signaling pathway that is most significantly modulated as indicated by the p-value <0.0001. The JAK/STAT pathway is a intracellular signal-transducing pathway that is activated by oxygen radicals, various cytokines, and growth factors in various disease states and is also recognized as an important membrane-to-nucleus signaling pathway for a variety of stress responses and oxidative stress [see review ref (130)]. A critical outcome of JAK/STAT activity is the translocation of STAT to the nucleus, leading to alterations in the transcription and expression of a number of specific target genes (131). In the context of the surgery/MV, we observed the upregulation of specific target genes involved in PIM1 (pim-1) (3.5-fold increase), MYC (c-Myc) (8.0-fold increase), and CISH (CIS) (6.8-fold increase) thereby possibly modulating cell proliferation, development, immunity, and cell cycle (Figure 4-2).

Another key pathway identified in this study is the p53 signaling pathway (p<0.0001). P53 is a sequence-specific transcriptional factor and it can activate its downstream target in a manner to induce cell growth arrest (132). In this study, many downstream targets of p53 revealed altered mRNA levels (Figure 4-3).GADD45A, B, and G are genes that promote cell growth arrest are upregulated during the surgical procedure (3.0-fold increase, 10.2-fold increase, and 4.3-fold increase, respectively). A cyclin-dependent kinase inhibitor 1 (p21) (otherwise known as CDKN1A) (4.9-fold increase) is also upregualted. P21 plays a cooperative role with GADD45

proteins in inducing cell growth arrest (133). Also, it is well-known that p53 can mediate apoptotic cell death by elevating the transcriptional expression of several proapoptotic genes (e.g., Bax, PUMA, Noxa, and DR4/5) (134, 135). However, whether p53-induced apoptosis plays a role in skeletal muscle remains unknown. Siu and his college (136) found that p53 and its target genes were related to the unloading-induced apoptosis in the animal models. Consistent with this finding, two p53-induced proapoptotic genes were upregulated in this study, including Noxa (otherwise known as PMAIP1) (2.8-fold increase) and DR5 (otherwise known as TNFRSF10B) (2.5-fold increase). These data indicate that Noxa and DR5 may involve in the apoptotic responses during the unloading-induced muscle atrophy. However, it is noted that p53 induces either cell cycle arrest or apoptosis depending on specific cellular contexts. For example, previous data demonstrates that the activation of apoptotic targets (eg. noxa or/and DR5) alone is not sufficient to induce apoptosis in some cells and the induction of GADD45 mediated by p21 may inhibit cell apoptosis (135). Nevertheless, our data suggests that the p53 signal pathway controlling in apoptosis/cell cycle arrest through it targets may play an additional role in muscle atrophy process during the surgical procedure.

Summary and Conclusion

In summary, we found that cardiothoracic surgery results in rapid changes in diaphragm gene expression. We identified 763 transcripts that were differentially expressed ($p<0.005$) between early-surgical and late-surgical samples. Genes could be categorized into 18 functional groups, of which we chose to focus on four categories for discussion. The major findings includes: 1) surgical stress-related genes demonstrated the largest changes, which likely trigger an intracellular cascade including a JAK/STAT pathway during the cardiothoracic surgical procedure and this process possibly regulates the cellular response in the context of diaphragm unloading; 2) an increased expression of antioxidant genes occurred, which may be related to

protective adaptations in response to stress, including increased oxidant production in mitochondria; 3) several proteolytic related genes, including ubiqutin-conjugating enzymes (E2) and MuRF-1 (E3), were upregulated, indicating that the cardiothoracic surgical procedure increased the proteolytic processes, which may lead to significant atrophy of the human diaphragm; 4) the diaphragm during the surgical procedure tends to decrease activity of the glycolytic enzymes, concomitant with an decrease in gluconeogenic capacity in the muscle; 5) several muscle-specific regulatory genes were affected by the cardiothoracic surgical procedure; however, their physiological role in muscle disuse remains elusive; and 6) the p53 signal pathway involved in negative growth control through it targets, may play an additional role in the muscle atrophy process during the surgical procedure. Our microarray data illuminate how the mRNA expression in the human diaphragm is affected by a surgical procedure (including the use of CMV). The changes in gene expression following surgical procedures may be particularly relevant to understanding the pathogenesis of VIDD in patients at risk of post-surgical weaning difficulties. The knowledge of underlying molecular mechanisms of diaphragm dysfunction may help direct efforts to develop rehabilitation and pharmacologic interventions in the preoperative and postoperative periods. Further studies are anticipated to confirm and to clarify the biological relevance of our study.

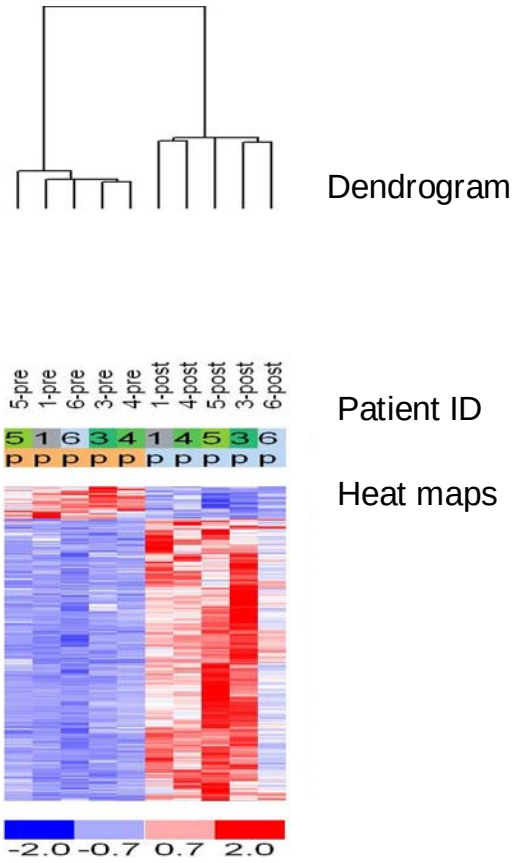

Figure 4-1. Unsupervised cluster analysis. This figure shows the hierarchal cluster pattern of the hybridization signal intensities of 3318 probe sets that display a CV>0.5. In the heat map, the intensity of the color indicates relative expression for each individual gene. The intensity of the color red indicates relative greater than the mean for that individual gene, blue indicates expression less than the mean, and the white indicates mean expression. The dendrogram of the clustering is displayed above and is used to identify similarities in expression patterns among the arrays.

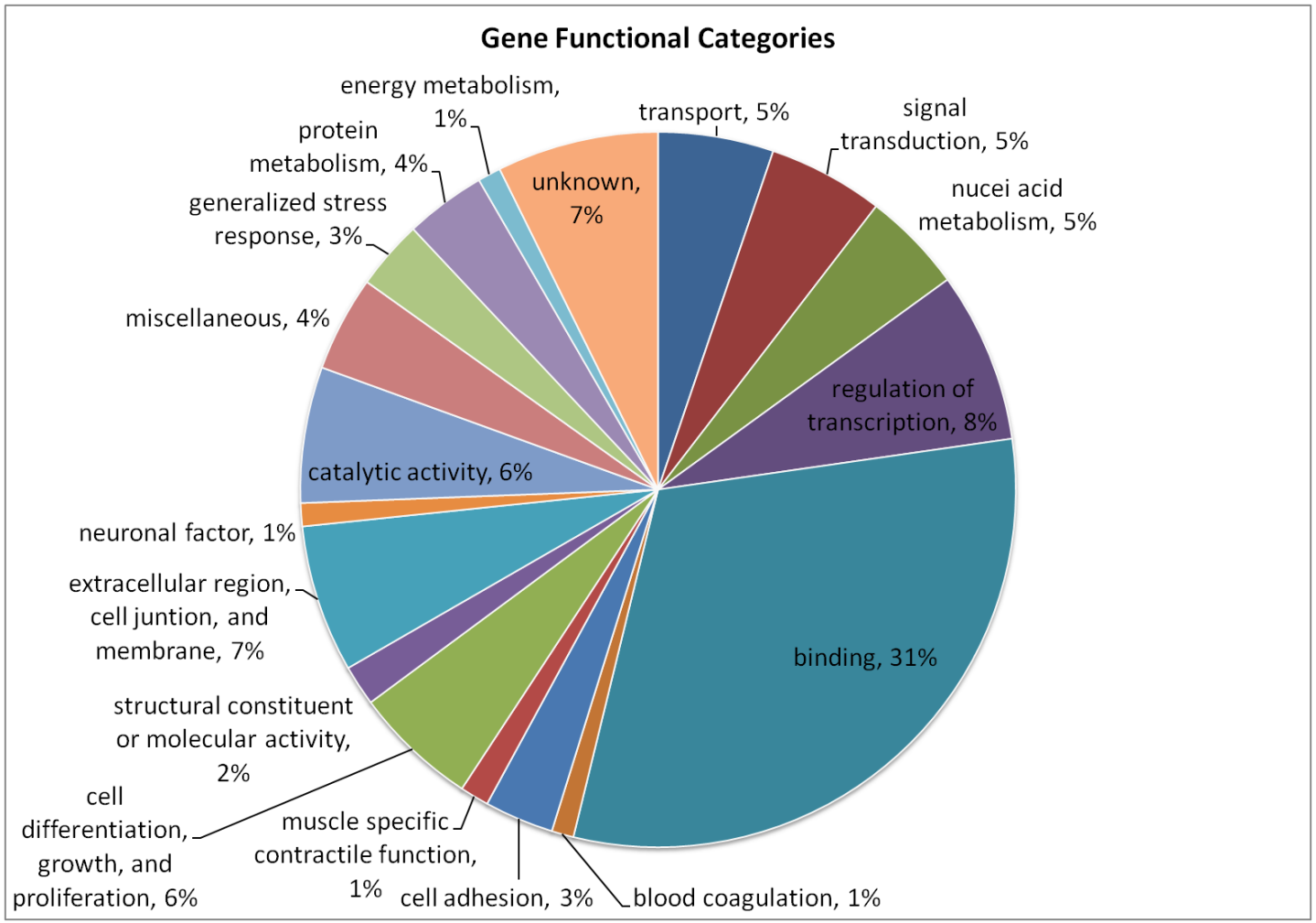

Figure 4-2. Functional classification of 763 genes differentially expressed in early- vs. late- surgical conditions.

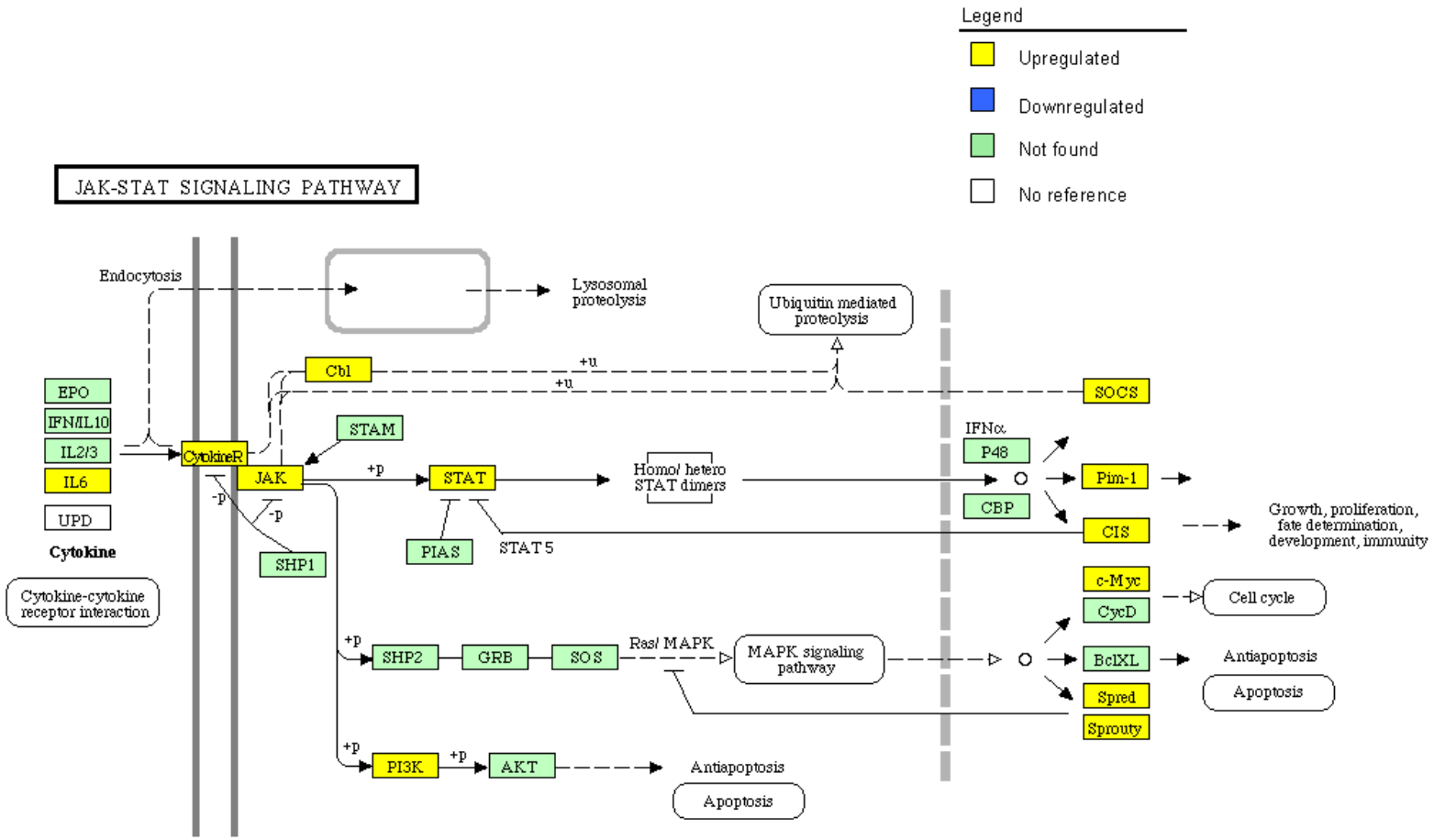

Figure 4-3. JAK-STAT signaling pathway. Yellow and blue indicate overexpressed and underexpressed genes in the chips, respectively. Light green indicates that the gene was not present in the chips or its expression did not change significantly after surgery. White indicates that the gene has no reference in the KEGG database and the function of this gene is unknown. p, phosphorylation; u, ubiquitination.A large oval represents a link to another pathway map. Solid line indicates a direct effect while dash line indicates an indirect effect.

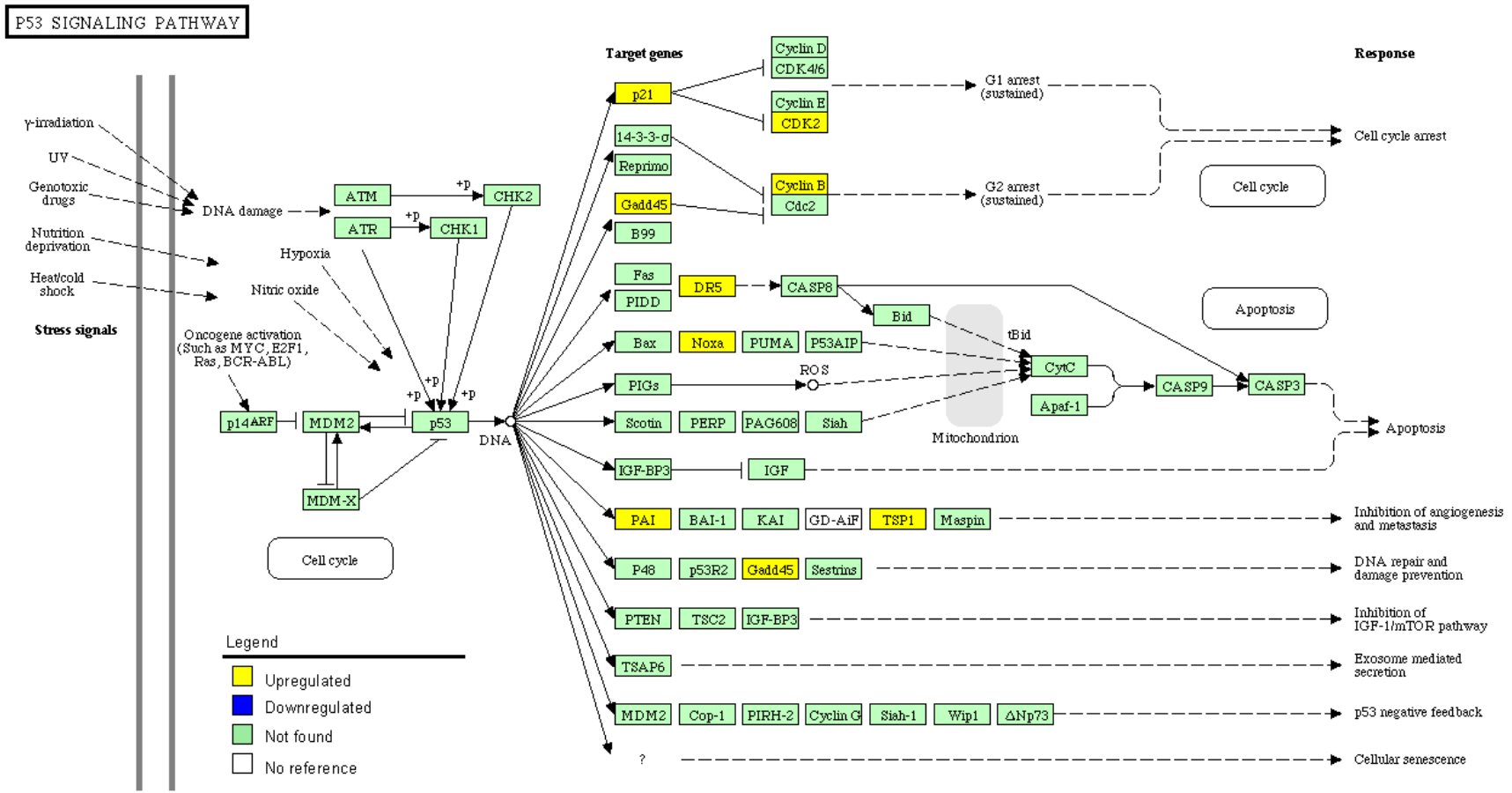

Figure 4-4. p53 signaling pathway. Yellow and blue indicate overexpressed and underexpressed genes in the chips, respectively. Light green indicates that the gene was not present in the chips or its expression did not change significantly after surgery. White indicates that the gene has no reference in the KEGG database and the function of this gene is unknown. p, phosphorylation; u, ubiquitination.A large oval represents a link to another pathway map. Solid line indicates a direct effect while dash line indicates an indirect effect.

Table 4-1. Clinical baseline characteristics of five patients undergoing cardiothoracic surgery

Patient ID	Age	Height (cm)	Weight (Kg)	Type of Surgery	Type of anesthesia	CPB time (mins)	HCA time (mins)	CP time (mins)
1	56	183	155	Aortic, valve replacement (AVR) ascending	general endotracheal	243	15	202
3	76	174	87	Resection and replacement of the ascending aorta and proximal arch; replacement of the aortic valve	general endotracheal	159	10	135
4	71	182	100	Replacement of the ascending and arch aorta	general endotracheal	166	24	42
5	54	183	110	Ascending and aortic arch replacement	general endotracheal	266	5	204
6	78	180	100	Aortic root remodeling w/ preservation of the aortic valve and sinuses	general endotracheal	255	N/A	130

Characteristics of patients undergoing cardiothoracic surgery. CPB time, cardiopulmonary bypass time; HCA time, hypothermic circulatory arrest time; CP time, cross clamp time.

Table 4-2. List of genes related to generalized stress response and redox regulation that are significantly different after surgery

Probe set	Symbol	Fold change	Description	Function
200989_at	HIF1A	2.6	hypoxia-inducible factor 1, alpha subunit (basic helix-loop-helix transcription factor)	response to hypoxia
209189_at	FOS	6.8	v-fos FBJ murine osteosarcoma viral oncogene homolog	inflammatory response
202376_at	SERPINA 3	5.8	serpin peptidase inhibitor, clade A (alpha-1 antiproteinase, antitrypsin), member 3	inflammatory response
213146_at	JMJD3	4.3	jumonji domain containing 3	inflammatory response
206157_at	PTX3	20.5	pentraxin-related gene, rapidly induced by IL-1 beta	inflammatory response
211506_s_at	IL8	9.2	interleukin 8	inflammatory response
204470_at	CXCL1	7.4	chemokine (C-X-C motif) ligand 1 (melanoma growth stimulating activity, alpha)	inflammatory response
207850_at	CXCL3	5.1	chemokine (C-X-C motif) ligand 3	inflammatory response
209774_x_at	CXCL2	8.3	chemokine (C-X-C motif) ligand 2	inflammatory response
205207_at	IL6	15.6	interleukin 6 (interferon, beta 2)	inflammatory response
203372_s_at	SOCS2	3.1	suppressor of cytokine signaling 2	JAK-STAT cascade
210001_s_at	SOCS1	4.7	suppressor of cytokine signaling 1	JAK-STAT cascade
208992_s_at	STAT3	1.6	signal transducer and activator of transcription 3 (acute-phase response factor)	JAK-STAT cascade
227697_at	SOCS3	9.4	suppressor of cytokine signaling 3	JAK-STAT cascade
220088_at	C5AR1	5.1	complement component 5a receptor 1	immune response
205403_at	IL1R2	6.8	interleukin 1 receptor, type II	immune response
206637_at	P2RY14	-2.1	purinergic receptor P2Y, G-protein coupled, 14	immune response
212196_at	IL6ST	2.0	interleukin 6 signal transducer (gp130, oncostatin M receptor)	immune response
206087_x_at	HFE	-1.7	hemochromatosis	immune response
236947_at	SEMA3C	-1.7	sema domain, immunoglobulin domain (Ig), short basic domain, secreted, (semaphorin) 3C	immune response
203574_at	NFIL3	4.2	nuclear factor, interleukin 3 regulated	immune response
242751_at	PRDX6	1.9	peroxiredoxin 6	response to oxidative stress
215223_s_at	SOD2	2.9	superoxide dismutase 2, mitochondrial	response to oxidative stress
208864_s_at	TXN	1.9	thioredoxin	cell redox homeostasis

Table 4-3. Expression of protein metabolism genes that are significantly different in the diaphragm after surgery

Probe set	Symbol	Fold change	Description	Function
201195_s_at	SLC7A5	2.2	solute carrier family 7 (cationic amino acid transporter, y+ system), member 5	amino acid metabolism
225647_s_at	CTSC	2.7	cathepsin C	lysosome
202087_s_at	CTSL1	2.0	cathepsin L1	lysosome
200881_s_at	DNAJA1	1.9	DnaJ (Hsp40) homolog, subfamily A, member 1	protein folding
200664_s_at	DNAJB1	2.8	DnaJ (Hsp40) homolog, subfamily B, member 1	protein folding
208810_at	DNAJB6	1.7	DnaJ (Hsp40) homolog, subfamily B, member 6	protein folding
210187_at	FKBP1A	2.3	FK506 binding protein 1A, 12kDa	protein folding
225827_at	EIF2C2	1.7	eukaryotic translation initiation factor 2C, 2	protein synthesis
208624_s_at	EIF4G1	1.6	eukaryotic translation initiation factor 4 gamma, 1	protein synthesis
1554309_at	EIF4G3	1.9	eukaryotic translation initiation factor 4 gamma, 3	protein synthesis
211787_s_at	EIF4A1	2.6	eukaryotic translation initiation factor 4A, isoform 1	protein synthesis
208707_at	EIF5	1.9	eukaryotic translation initiation factor 5	protein synthesis
201574_at	ETF1	1.8	eukaryotic translation termination factor 1	protein synthesis
223481_s_at	MRPL47	-1.8	mitochondrial ribosomal protein L47	protein synthesis
224873_s_at	MRPS25	-1.4	mitochondrial ribosomal protein S25	protein synthesis
1555878_at	RPS24	2.4	ribosomal protein S24	protein synthesis
238156_at	RPS6	2.4	ribosomal protein S6	protein synthesis
225954_s_at	MIDN	4.3	midnolin	protein modification
236975_at	USP12	1.8	ubiquitin specific peptidase 12	ubiquitin thiolesterase activity
231990_at	USP15	2.2	ubiquitin specific peptidase 15	ubiquitin thiolesterase activity
220370_s_at	USP36	1.9	ubiquitin specific peptidase 36	ubiquitin thiolesterase activity
241762_at	FBXO32	-3.5	F-box protein 32	ubiquitin-protein ligase activity
236972_at	TRIM63	2.6	tripartite motif-containing 63 (MuRF-1)	ubiquitin-protein ligase activity

Table 4-3. Continued.

Probe set	Symbol	Fold change	Description	Function
222435_s_at	UBE2J1	1.7	ubiquitin-conjugating enzyme E2, J1 (UBC6 homolog, yeast)	ubiquitin-protein ligase activity
243046_at	UBE2D3	1.8	ubiquitin-conjugating enzyme E2D 3 (UBC4/5 homolog, yeast)	ubiquitin-protein ligase activity
65521_at	UBE2D4	1.5	ubiquitin-conjugating enzyme E2D 4 (putative)	ubiquitin-protein ligase activity
202779_s_at	UBE2S	1.6	ubiquitin-conjugating enzyme E2S	ubiquitin-protein ligase activity
202779_s_at	UBE2S	1.6	ubiquitin-conjugating enzyme E2S	ubiquitin-protein ligase activity

Table 4-4. List of genes related to energy metabolism that are significantly different in the diaphragm after surgery

Probe set	Symbol	Fold change	Description	Function
240187_at	PPP1R3C	-2.8	protein phosphatase 1, regulatory (inhibitor) subunit 3C	carbohydrate metabolism
204748_at	PTGS2	5.2	prostaglandin-endoperoxide synthase 2 (prostaglandin G/H synthase and cyclooxygenase)	fatty acid metabolism
209184_s_at	IRS2	2.0	insulin receptor substrate 2	glucose metabolism
205960_at	PDK4	4.0	pyruvate dehydrogenase kinase, isozyme 4	glucose metabolism
235374_at	MDH1	-2.2	malate dehydrogenase 1, NAD (soluble)	glycosis
206932_at	CH25H	8.6	cholesterol 25-hydroxylase	lipid metabolism
243296_at	PBEF1	5.1	pre-B-cell colony enhancing factor 1	NAD biosynthesis
208383_s_at	PCK1	-2.3	phosphoenolpyruvate carboxykinase 1 (soluble)	regulation of gluconeogenesis

Table 4-5. List of muscle-specific genes related to contractile functions that are significantly different in the diaphragm after surgery

Probe set	Symbol	Fold change	Description	Function
215795_at	MYH7B	-2.4	myosin, heavy chain 7B, cardiac muscle, beta	actin binding
222976_s_at	TPM3	1.6	tropomyosin 3	actin binding
1567107_s_at	TPM4	2.1	tropomyosin 4	actin binding
1569512_at	SVIL	1.9	supervillin	actin filament binding
236395_at	MEF2C	-3.5	myocyte enhancer factor 2C	muscle development
206201_s_at	MEOX2	-3.5	mesenchyme homeobox 2	muscle development
242795_at	MYOT	-2.8	myotilin	muslce contraction
207424_at	MYF5	-1.6	myogenic factor 5	myogenic differentiation
206657_s_at	MYOD1	2.0	myogenic differentiation 1	myogenic differentiation
211926_s_at	MYH9	1.7	myosin, heavy chain 9, non-muscle	unknown

Table 4-6. Significant signaling pathways that were identified by Path Analysis

Signaling pathway	Up-regulated transcripts	Down-regulated transcripts	P value
JAK-STAT	CBLB, CISH, CSF3, IFNGR1, IL6, IL6ST, JAK1,MYC, PIK3R3, PIM1, SOCS1, SOCS2, SOCS3, SPRED1, SPRY1,STAT3	----	<0.0001
p53	CCNB2, CDK2, CDKN1A, GADD45A, GADD45B, GADD45G, PMAIP1, SERPINE1, THBS1, TNFRSF10B	----	<0.0001
ErbB	ABL2, CBLB, CDKN1A, MYC, PAK6, PIK3R3	CDKN1B	0.03
MAPK	ACVR1B, DUSP1, DUSP4, DUSP5, DUSP6, FOS, GADD45A, GADD45B, GADD45G, IL1R1, IL1R2, MAPKAPK2, MYC, NLK, NRA41	----	0.04

CHAPTER 5
BREATHING VARIABILITY DURING SPONTANEOUS BREATHING TRIALS IN PROLONGED MECHANICAL VENTILATION PATIETNS

Background and Significance

Mechanical ventilation is one of the cornerstone treatments for patients in intensive care units (ICUs). However, prolonged mechanical ventilation (PMV) is associated with increased risk of significant long-term complications including mortality and high health care cost (137, 138). One common method for weaning patients is progressively lengthening spontaneous breathing trials (SBT) without ventilation support, until weaning is accomplished (139). Evaluation of the breathing pattern during SBT may improve clinical assessment of how patients are tolerating SBT and may predict ultimate weaning outcome (140). Therefore, any significant alteration in the breathing pattern of patients during the SBT requires investigation.

Previous studies of breathing pattern during weaning trials have been largely confined to mean values of the breathing parameters (141-145). Little attention has been focused on the variability in breathing pattern during weaning trials. Recently, evidence of the importance of the breathing variability in ICU patients was provided by Wysocki et al. 2006, who showed that reduced breathing variability, quantified by using coefficient of variation (CV), during a 60 min SBT was associated with a high incidence of acute weaning failure in the ICU patients (146). They also suggest that breathing variability indices, e.g. CV, are sufficient to distinguish successful cases from those who fail and may serve as a weaning predictor. Bien et al. reported that breathing pattern variability (measured by CV and the parameters of standard deviations) in patients who failed to weaning trials was significantly lower than those who passed weaning trials (147). In contrast, EI-Khatib el al. and Engoren found that the patients who failed to be separated from the ventilator had a lower breathing variability than the patients who succeeded (148, 149).

Therefore, we designed a prospective study in the ICU patients to investigate the breathing variability during weaning trials. To eliminate any differences arising from different patient samples, each patient served as his or her own control. We hypothesized that compared with successful SBT bouts, the failed SBT bouts would demonstrate a significant lower breathing pattern variability.

Literature Review

Respiratory failure, requiring MV support, is characterized by impairment of respiratory mechanics and gas exchange. The severity of this impairment changes according to the pathophysiologic development of the disease. After resolution of respiratory failure, most patients are easily weaned, but as many as 20% of mechanically ventilated patients experience difficulty weaning (150, 151). According to the European Respiratory Society's classification in 2007, prolonged mechanical ventilatory (PMV) support is defined by a patient who fails at least three weaning attempts or requires > 7 days of weaning after the first weaning attempt (137). These patients repeatedly fail to wean and face a substantial risk of long-term complications and even death (5, 138). It is estimated that ICU mortality of PMV patients is about 25% (150, 152). Thus, weaning these patients from MV support is one of the great challenges in intensive care.

Weaning Trials in Weaning Protocols

Weaning trials are recommended for MV patients who are considered to be ready- to-wean. In general, a weaning trial involves reducing the support provided by the ventilator while monitoring for evidence of respiratory distress or altered gas exchange. There are several different ways to perform a weaning trial. One common method for weaning patients is having the patient perform progressively lengthening spontaneous breathing trials (SBT) without mechanical ventilation support, until weaning is accomplished (139). During a SBT, a patient with a tracheostomy is removed from the ventilator to breathe spontaneously with supplemental

oxygen via a T-piece tube for a predetermined amount of time. During a SBT, the patient is carefully observed, vital signs and the adequacy of ventilation and/or gas exchange are measured. Additionally, evidence suggests that breathing pattern represents the response of the respiratory system to physiologic distress. For instance, during the SBT, patients adopt a breathing pattern that differs substantially from the pattern used when receiving MV support (145). The alteration of breathing patterns reflects global respiratory system performance. Thus, breathing pattern analysis may be a helpful means of monitoring respiratory performance in PMV patients during SBT (140, 145).

Breathing Pattern Analysis

The traditional strategy of breathing pattern analysis is to divide the breathing parameters into two parts: 1) mean value of the parameters (obtained by averaging over many breathing cycles) and 2) variability of the parameters (e.g. measured by the standard deviation and/or coefficients of variation). More often, the mean values have been regarded as the true output of the respiratory control system and the measure of variability considered as an uncorrelated random (white) noise superimposed on the output of the respiratory controller. However, emerging evidence shows that breath-to-breath variability of respiratory parameters is not random (153-155) and may be explained either by a central neural mechanism or by instability of feedback loops (156-159). For example, in healthy humans, stimulation of the central/peripheral chemoreceptors with isocapnic hypoxia increased the gross breathing variability whereas external resistive loadings or elastic loadings decreased the breathing variability (159-161). These findings indicate that changes in the variability of respiratory parameters are specific and unique. Analysis of variability may reflect different physiological influences on the control of breathing.

Reproducibility of Breathing Parameters

A potential argument against studying the use of breathing pattern as weaning measurements could be made by citing the fact that breathing pattern in humans has shown its diversity and individuality: the breath-to-breath and day-to-day variability in breathing pattern. In order to properly use the breathing pattern as an evaluative tool, it is essential to know whether the breathing pattern parameters are reproducible. In 1988, Tobin MJ et al. designed a series of experiments that separately examined the breath-to-breath and day-to-day variability in breathing pattern in healthy volunteers. They reported that breath-to-breath variability in breathing pattern over a 15-min period in 65 healthy subjects revealed large coefficient of variations, suggesting inter-individual breath-to-breath reproducibility of tests of respiratory control was limited (162). However, by examining day-to-day data, the constancy of the average breathing pattern (mean of a 15-min recording) was acceptable when measured repeatedly (162).

The following studies further examined the reproducibility of breathing pattern parameters in critically-ill, intubated patients. Krieger et al. investigated the variability of the breathing pattern before and after extubation in 50 clinically ready-to- wean patients and they found that the CV for frequency and inspired tidal volume measured during a weaning trial over a 15-min recording were nearly identical pre-extubation and post-extubation, highlighting intra-individual breath-to-breath reproducibility was relatively stable (163). Yang KL also found a similar result(164). He examined the reproducibility of breathing pattern parameters obtained on three weaning trials over a period of 15 minutes in 30 ICU patients whose primary diagnoses consisted of pneumonia, ARDS, neuromuscular diseases, chronic heart failure, and COPD. He found that the CV for frequency, inspired tidal volume, and minute ventilation did not show any significant difference over three weanig trials indicating that breathing pattern parameters, measured with the CV, were reliable from one trial to the next with bedside instruments.

From the literature, we have learned that breathing pattern recording over a period of time exhibits inherent dynamics and fluctuations. This variability of breathing pattern is not random and demonstrates its diversity and individuality. This breath-to-breath variability is quite diverse among the healthy humans, but this irregular breathing pattern is reproducible for the same subjects under the same conditions, even in the critically-ill patients.

Physiological Grounds of Breathing Pattern Variability

Research into breathing behavior of mammals demonstrates that the control of breathing is an integrative process that results from the interactions between several central neuronal networks (including the cerebral cortex that allows behavioral and volitional modulation of respiration during wakefulness) and/or feedback modulations by mechanical and chemical afferents (159, 165-167). The confluence of these complex interactions should result in some degrees of variability in breathing pattern. However, this inherently dynamical behavior may become static (having reduced variability over a period of time) under high stress (168) or under some pathological conditions (169, 170). For instance, it has shown that loading respiration, in healthy humans mechanically (elastic and resistive) tends to reduce breathing variability (160, 161). Another striking case is people with compensated chronic heart failure (CHF). These patients usually demonstrate an oscillatory breathing pattern characterized by cyclical respiration (periodic breathing) during the daytime (171). This periodic breathing would enhance peripheral chemosensitivity in CHF, which in turn would result in instability of cardio-respiratory control (170). If peripheral chemoreceptor over-activity couples with impaired baroreflex sensitivity, it would lead to slow the oscillations in blood pressure and respiration, representing a reduced variability in breathing pattern (172, 173).

Additionally, experimental animal studies in acute lung injury demonstrated that application of variations in frequency and tidal volume during mechanical ventilation could

improve lung function and gas exchange, compared with a conventional volume-cycled MV mode (174, 175). This observation suggests that breathing variability added to mechanical ventilation provides an optimal level of physiological improvement. It is speculative that breathing variability in physiological rhythms is invariabile and of the reserves to response challenges (176). A respiratory controller with some degrees of variability may allow flexible responses to environmental/physiological changes by modulating the control parameters (177). As pointed out by Dejours et al. (1961), 'an infinite number of possible combinations of the ventilatory components exists capable of achieving the same minute ventilation. The number of combinations decreases when the demand for ventilation increases and at maximal ventilatory values all individuals tend to exhibit more similar patterns (178).'

Breathing Pattern during Weaning

A number of breathing pattern parameters have been reported to be associated with the success or failure of ventilator discontinuation (139, 179-181). Reported weaning predictors including vital capacity, tidal volume, respiratory rate, minute ventilation, rapid shallow breathing index (RSBI), and maximal inspiratory pressure (PImax) have been developed and applied in clinical settings. Moreover, integrated factors also have been employed (139), for example, CROP index (CROP = dynamic compliance multiplies by maximal inspiratory pressure by PaO_2/P_AO_2 and divides this product by the respiratory rate). However, analysis of receiver operating characteristics curves (ROC) has shown none of these indices are sufficiently sensitive and specific to be useful in predicting the success of ventilation discontinuation, especially in the elderly and/or in the PMV patients (139).

Studies of examining the breathing pattern, maximal inspiratory pressure, and lung mechanics in patients being weaned from MV displayed inconsistent findings (143, 144). Del Rosario et al. reported that patients who failed to wean had a higher respiratory rate and RSBI by

comparing with successfully weaned groups. PImax and dynamic intrinsic positive airway pressure (PEEPi), measured from the oesophageal pressure were similar to both groups (143). On the contrary, Jubran and collegues found that at the early phase of a weaning trial, the failure group developed rapid shallow breathing and a higher value of PEEPi than the successful group. Over the weaning course, the respiratory resistance increased in the failure group whereas it remains unchanged in the success group (144). At the end of weaning trials, they found that 13 of 17 failure-to-wean patients increased in $PaCO_2$ whereas 4 showed a decrease in $PaCO_2$. They concluded that the patients who fail to wean developed rapid shallow breathing at the onset of the weaning trial and progressively increased in respiratory resistance and PEEPi, representing an excessive load to the respiratory muscles. This combination of increased mechanical load with rapid shallow breathing led to inefficient CO_2 clearance, which was the dominant determinant of weaning failure in the overall group. However, that rapid shallow breathing developed at the onset of weaning trials in the failure group is not a universal phenomenon. Capdevia et al. investigated 17 patients receiving PMV (average length of MV support > 20 days) and found that at the onset of weaning trials, high respiratory rate and low tidal volume values were observed in both success and failure groups, without significant inter-group differences (142). But, they agreed that PEEPi increased in response to the increased respiratory rate in the failure group throughout the weaning period (142).

It seems that an excessive inspiratory load imposed on the respiratory muscles is an essential determinant of weaning failure. This excessive load leads to increase in the required breathing energy expenditure with a concomitant of breathing pattern alterations (144). Additionally, it is accepted that a high neural drive persisted over the weaning period in failure-to-wean patients (145). The presence of a high neural drive indicates that the respiratory muscles

continue to generate large inspiratory pressure to cope with this excessive load rather than a decrease in respiratory motor output. If the mechanical loads excessive to the capacity that respiratory muscle can generate, this imbalance will lead to respiratory distress and eventually, the weaning failure will ensue.

The importance of the load-capacity balance on the weaning outcome of PMV patients has been highlighted by a recent study. Purro et al. have shown that in the presence of a high neural drive to breathe, the patients with a high load/capacity index (such as Pdi/Pdimax > 0.4) were unweanable (where Pdi is the pressure required for tidal breathing and Pdimax is maximal pressure that the respiratory muscles can generate) (182). They also found that a positive linear relationship between the load/capacity index and the effective inspiratory impedance (P0.1/tidal volume/inspiratory time and P0.1 is the value of airway pressure 100ms after the beginning of the occluded inspiration) ($r = 0.61$). Thus, they suggested that non-invasive methods such as breathing pattern and P0.1 might help to identify the patients who fail to wean.

However, it was shown that the value of P0.1 would be underestimated in the presence of hypercapnia or in the patients with abnormal lung mechanics (183). Additionally, it is reported that a progressive deterioration in respiratory mechanics during SBT in the patients who fail to wean and Pdimax probably decreased by the end of the weaning trials (184). Moreover, in clinical settings, it is impractical to measure the ratio of Pdi/Pdimax on a breath-by-breath basis during the weaning trials. Thus, an accessible and alternate index to represent the relationship of the load-capacity balance is needed.

Breathing Variability during Weaning

Few investigators have attempted to examine the breathing variability during weaning (146-149). Bien et al. reported that breathing pattern variability (measured by CV and the parameters of standard deviations) in patients who failed weaning trials was significantly lower

than those who passed their weaning trials (147). Accordingly, they also reported that the area under the ROC curves of these breathing variability indices was within the range of 0.73-0.80. Wysocki et al. showed that reduced breathing variability, quantified by using CV, during a 60 min SBT was associated with a high incidence of acute weaning failure in the ICU patients (146). In contrast, El-Khatib et al. and Engoren found that breathing variability measured by entropy indices was more irregular (higher) in patients who failed extubation compared to patients who passed extubation trials (148, 149). It is hard to explain the inconsistency of these findings because of the nature of the corresponding populations and different experimental conditions. Nevertheless, all authors agree that breathing variability may potentially serve as a weaning predictor for the ICU patients.

It is speculative that breathing variability is likely to be a reflection of a load-capacity balance of respiratory system. Previous studies have shown that external resistive loadings or elastic loadings decreased breathing variability during loaded respiration in healthy humans (160, 161). Additionally, it was reported that respiratory variability was reduced in patients with restrictive lung disease, compared with that of healthy subjects (169). Caminal et al. examined breathing variability in the respiratory volume signals based on non-linear prediction methods in a group of 20 patients on weaning trials from MV and each patient placed under two different levels of pressure support ventilation (PSV), classified as low PSV (5+/-2 cm H_2O) and high PSV (12+/-2 cm H_2O). They found an inverse relationship between the levels of PSV and the breathing variability in tidal volume and inspiratory time (185). These results suggest that breathing variability might parallel to the load-capacity balance of the respiratory system and a high breathing variability indicates a large respiratory reserve. However, this supposition needs further studies to approve it.

In summary, patients requiring long-term MV support face a high risk of mortality/mobility during their hospitalization. SBT are recommended for patients who are ready-to-wean. Evaluation of breathing pattern during SBT may be helpful to assess the effectiveness of weaning protocols. Many breathing parameters represented by the mean values have been reported to be associated with the success or failure of SBT. However, none of these predictors are universally accepted and they lose their discriminatory power in the PMV population.

On the other hand, analysis of breathing variability, reflecting different physiological influences on the control of breathing, may provide an alternate method to predict weaning outcome. Recently, Wysocki et al. demonstrated that reduced breathing variability, quantified by using CV, during a 60 min SBT was associated with a high incidence of acute weaning failure in the ICU patients (146). It was suggested that breathing variability indices, e.g. CV, are sufficient to distinguish successful and failed cases and may potentially serve as a weaning predictor. In contrast, El-Khatib el al. and Engoren found that the patients who failed to be separated from the ventilator had a lower breathing variability than the patients who succeeded (148, 149).

Therefore, we designed a prospective study in ICU patients with prolonged MV support to investigate the breathing variability during the weaning trials. To eliminate any differences arising from a different patient population, each patient served as his or her own control. We hypothesized that compared with successful SBT bouts, the failed SBT bouts would show lower breathing pattern variability.

Methods

Subjects

Thirty-eight tracheostomized PMV patients who were clinically stable (no fever, pain, or anxiety, etc.), with normal hemodynamic conditions, without any evident signs of respiratory

distress (total breathing frequency < 35 breaths/min), and whose primary physician considered them ready to undergo a trial of weaning were enrolled in the study. The investigative protocol was approved by the Institutional Review Broad at University of Florida and informed consent was obtained from the subjects or next of kin.

The patients had received an average of 46±23 days of MV support before study entry. The pertinent characteristics of patients in this study are listed in Table 5-1. That the patients were included in this study should have 1): demonstrate an improvement or resolution of the underlying causes of respiratory failure and adequate gas exchange (eg. PaO2 above 60 mmhg while breathing with a FiO2 of 0.5 or less); 2): be medically stable and ready to be weaned from the ventilator as determined by the attending physician; 3): demonstrate an intact phrenic nerve; 4): have a hemoglobin level above 10 g/dl and body temperature of > 36.5 and < 38.5 °C; and 5): be stable cardiovascular system (eg. HR < 140 beats/min; stable blood pressure) and stable metabolic status (eg. Acceptable electrolytes). Patients with spinal cord injury, progressive neuromuscular diseases, primary cardiomyopathy, hepatic failure or requiring continuous analgesic agents that would depress respiratory drive were excluded. In addition to the above listed criteria, to qualify for inclusion, patients' baseline ventilator setting had to meet the following specifications: SIMV≤6 breaths/min, pressure support ≤ 15 cmH_2O, PEEP≤ 8 cm H_2O, and $FiO_2 \leq 0.5$.

All patients participated in progressively lengthening SBT daily. The daily test of SBT was conducted by disconnecting the patients from mechanical ventilation without any form of ventilatory support and each patient spontaneously breathed through a T-tube circuit, with the FiO_2 set at the same level as that used during mechanical ventilation. On the first day of SBT, the subject was asked to breathe off the ventilator as tolerated. The SBT durations were progressed

per protocol. For example, the duration of the SBT was increased daily in the following progression: 1, 2, 3, 4, 6, 9, and 12 hours. On the day of SBT, the patients were maintained a semirecumbent position (head of bed at 30 degrees) and received oxygen supplementation to maintain percutaneous oxygen saturation (SpO2) at > 90%. Between two daily SBTs, the subjects would rest on MV support. In addition, before performing a SBT, the subjects would be suctioned, if necessary, to minimize secretions.

Study Procedure

During the SBT, the subject was allowed to breathe off the ventilator per predetermined duration. A SBT was conducted by disconnecting the patient from the ventilator with any form of ventilatory support and the FiO_2 was provided during MV was maintained with a T-piece adapter. The SBT was started at approximately 09:00 am each morning. Patients were maintained in a semirecumbent position (head of bed at 30°) and they received supplemental oxygen between FiO_2 of 0.3 to 0.5 to keep oxygen saturation (SpO_2) at least 90%. The patients were continuously monitored during SBT by the ICU clinical staff.

A computerized pulmonary monitoring system (CO_2SMO Plus, Novametrix Medical System Inc. Wallingford, Connecticut, USA), incorporating an adult flow sensor placed between the tracheal canula and the T-piece of the breathing circuit, was used to measure the breathing pattern variables. Exhaled minute ventilation (V_E), breathing frequency (f), inspired tidal volume (V_T), peak inspiratory flow (PIF), inspiration time (T_I), expiration time (T_E), and the duty cycle (T_I/Ttot) were recorded electronically with Analysis Plus software (Novametrix Medical System Inc. Wallingford, Connecticut, USA). The criteria for terminating a SBT were hypertension (systolic blood pressure > 180 mm Hg), tachycardia (heart rate > 120 beats/minute or 30 beats/min over pretrial values), SpO_2 < 90% lasting for more than 5 minutes, breathing frequency > 40 breaths/min lasting more than 5 minutes, diaphoresis, paradoxical breathing pattern,

significant accessory muscle use, persistent dysrhythmias, anxiety, or the patient requesting to be returned to MV support. Failure in a SBT (denoted as "failed") was defined as inability to sustain spontaneous breathing efforts for the predetermined duration of SBT followed by reconnection of mechanical ventilation whereas when a subject successfully completes a scheduled SBT, this bout would be denoted as "successful."

Data Analysis and Statistical Analysis

V_E, f, V_T, T_I, T_E, PIF, and T_I/Ttot were acquired on a breath-to-breath basis for a period of the the SBT tolerated duration, and the reported data were their average values over the first 30 minutes of a fail/successful SBT for each subject. Breathing variability was also calculated and expressed as the coefficient of variation (CV).

Results were reported as mean±SD. Paired t tests were used to compare the spontaneous breathing pattern between the failed and successful bouts. Statistical significance was set at $p<0.05$. The analyses were carried out using SPSS 14.0 software (version 14, SPSS Institute Inc).

Results

Table 5-2 showed mean value and CV of seven breathing variables during a failed/successful SBT bout for each subject. Compared to the successful bouts, the failed bouts had higher mean values for PIF and f (31.3+/-9.2 vs. 28.8+/-5.9 L/min and 29+/-11 vs. 26+/-7 breaths/min, respectively) (Table 5-2). The CV for V_E, f, and PIF were significantly lower during the failed SBT bout, whereas the CV for V_T, T_I, T_E, and T_I/Ttot in the failed bout did not reach a significant difference (Table 5-2).

Discussion

The main finding of this study is that the mean values of PIF and f were higher during the first 30 minute interval of failed SBT in PMV patients, reflecting a higher drive to breathe in failed SBT trials. Secondly, among selected breathing variables, breathing variability, quantified

by the CVs, revealed more significant differences than the mean values. This finding suggests that analysis of the CVs provides additional information, which is ignored by the mean data.

Previous studies (142, 145) have demonstrated that changes in breathing pattern, including increased respiratory drive and decreased T_I were associated with weaning failure; however, little is known about the breathing pattern during off the ventilator SBT in patients receiving PMV support. During the first 30 minute interval of failed SBT, we found that the mean value of PIF was higher, compared with the successful bout; whereas the mean value of T_I did not reach significance. This finding agrees with the previous data that there is a higher drive to breathe in failed SBT bout. The presence of a high neural drive indicates that the respiratory muscles continue to generate large inspiratory pressures to cope with this excessive load rather than a decrease in respiratory motor output. However,if an imbalance between the load faced by the respiratory muscles and their neuromuscular competence occurs, which can cause the inability to sustain spontaneous breathing and/or hypercapnia, and thus, this imbalance will lead to respiratory distress and sooner or later the weaning failure will ensue.

We also found that reduced breathing variability, quantified by the CV for V_E, PIF, and f during the first 30 minute interval of failed SBT, compared with the successful SBT bout. These findings are consistent with the literature. Bien et al. reported that CVs of PIF was lower in the post-operative SIRS patients who failed to weaning trials than those who passed their weaning trials(147). Consistently, Wysocki et al. showed that reduced breathing variability, quantified by using CV, during a 60 min SBT was associated with a high incidence of acute weaning failure in the ICU patients (146). Alteration of breathing variability may reflect different physiological influences on the control of breathing (186). In this study, we observed reduced variability of V_E, PIF, and f suggesting that breathing variability may provide additional information to how the

PMV patients adapts to an increased ventilation workload such as an off ventilator SBT and the breathing variability data, measured on CVPIF, is more sensitive to reflect this adaptation during a SBT than the mean value of PIF.

It is speculative that breathing variability is likely to be a reflection of a load-capacity balance of respiratory system. Earlier studies (160, 161) have shown that loading respiration, in healthy humans mechanically (elastic and resistive) tends to reduce breathing variability in CVV_E and CVT_E. Moreover, Caminal et al.(185) examined breathing variability in the respiratory volume signals based on non-linear prediction methods in a group of 20 patients on weaning trials from MV and each patient placed under two different levels of pressure support ventilation (PSV), classified as low PSV (5±2 cm H_2O) and high PSV (12±2 cm H_2O). They found an inverse relationship between the levels of PSV and the breathing variability in tidal volume and inspiratory time. These results suggest that breathing variability might parallel to the load-capacity balance of the respiratory system and a high breathing variability indicates a large respiratory reserve.

In contrast, El-khatib et al. found that breathing patterns during CPAP trials (5-7.5 cm H_2O) were more irregular in patients who failed extubation compared to patients who weaned (148). They reported that the CV of peak flow and tidal volume in passed and failed group were 11.6+/-4.1% vs. 29.9 +/- 12% and 9.1+/-4.1% vs. 26.1+/- 6.9%. These inconsistencies might be due to differences in study designs. First, in El-khatib et al.'s study, 60 min of peak flow and tidal volume was recorded under SIMV conditions, but not on spontaneous respiration through a T-piece circuit. Breathing variability was then measured on spontaneous breaths occurring between SIMV breaths. Of note, under SIMV conditions, no information on spontaneous breathing pattern in time can be obtained due to the presence of mechanical breaths. In addition,

spontaneous breaths with CPAP (5-7.5 cm H_2O) tended to be slower and deeper compared with spontaneous breaths without CPAP and this slower and deeper breathing behavior may increase the gross breathing variability because of greater elimination of carbon dioxide (187, 188). Our patients were disconnected from mechanical ventilators and did not receive any ventilatory support during SBT. Thus, the present work and the study by El-khatib et al. are not fully comparable.

Engoren found that weaning failure patients had a lower breathing variability, measured as Approximate Entropy (AppEn), than the patients who succeeded (149). AppEn is a mathematical approach to quantify the regularity of a system and a high AppEn value often indicates unpredictability and random variation in a system (189). They suggested a more complex tidal volume pattern corresponded to a failed SBT. However, a high entropy value does not always occur in parallel to increased variations if the variability is not random (190). For example, in animal studies, increased inspired CO_2 (from 2.5% to 5% CO_2) resulted in a decreased CV in V_E but increased AppEn (190). In addition, data has shown that an increase in the entropy (such as AppEn) does not always indicate an increase in dynamical complexity. A typical example is that a randomized time series has higher entropy than the original time series although the process of randomization destroys inherent correlation and degrades the information content of the original signal(191).

Summary and Conclusion

We found that among the selected breathing pattern variables includingV_E, f, V_T, T_I, T_E, PIF, and T_I/Ttot, the mean value of PIF and f were significantly different within subjects during the first 30 minutes interval of failed and successful SBT in PMV patients, reflecting a higher drive to breathe in failed trials. Secondly, among selected breathing variables including V_E, f, and PIF, breathing variability, quantified by the CVs, reveal more significant differences than the

mean values. This finding suggests that analysis of the CVs provides additional information, which is ignored by the mean data.

Table 5-1. Demographic characteristic of the prolonged mechanical ventilation patients

Patient No	Age/ Gender	Cause of ICU admission	Days of MV support	NIF* (cm H_2O)	SAPS II
1	39/F	Hepatobiliary surgery for neoplasm	43	45.2	19
2	66/M	ARDS	23	37.0	32
3	47/M	Chronic Heart Failure	35	39.9	24
4	65/M	Myocardiac Infarct with CPR/code event	29	43.1	40
5	59/F	GI surgery, not for neoplasm	38	47.0	27
6	61/M	Hepatobiliary surgery for neoplasm	19	42.0	28
7	75/F	Craniotomy, not for neoplasm	81	31.9	36
8	72/F	ARDS	107	36.5	53
9	62/F	Post-surgical acute respiratory failure	38	24.6	32
10	60/F	COPD exacerbation	29	32.2	21
11	75/M	Sepsis with shock	44	38.7	28
12	55/M	Liver Transplant	15	64.5	37
13	59/F	Sepsis with shock	43	70.9	40
14	68/F	Hypercapnic respiratory failure	32	52.0	37
15	67/F	Esophageal surgery	63	59.3	23
16	57/F	Pneumonia (non-aspiration)	46	79.7	39
17	78/M	other:burn	51	75.5	40
18	67/F	Abdominal aortic aneurysm (AAA) repair	26	45.2	35
19	66/F	Esophageal surgery	27	28.9	43
20	39/M	Portal vein thrombosis	13	50.8	13
21	41/M	Multiple trauma	40	20.4	38
22	77/F	GI surgery, not for neoplasm	89	12.3	22
23	77/M	GI surgery, not for neoplasm	21	52.4	36
24	81/M	Multiple trauma	53	36.4	44
25	64/M	Multiple trauma	48	87.0	34
26	55/F	Post-surgical acute respiratory failure	54	41.4	26
27	55/F	MVR/aortic root replacement/ R pulmonary artery repair	63	42.1	19
28	69/F	New CVA or intracranial hemorrhage (ICH)	44	64.3	32
29	64/M	Dissecting abdominal aortic aneurysm	15	27.5	40
30	61/F	ARDS	43	81.4	32
31	57/F	Liver Transplant	47	42.3	29
32	63/M	Abdominal aortic aneurysm (AAA) repair	57	57.2	35
33	87/F	Cardiac valve replacement	106	40.3	35
34	68/F	New CVA or intracranial hemorrhage (ICH)	60	34.2	36
35	40/F	Multiple trauma	31	91.5	21
36	72/F	GI surgery, not for neoplasm	47	63.7	18
37	69/M	Myocardiac Infarct with CPR/code event	41	45.6	28
38	77/M	Post-surgical acute respiratory failure	67	72.8	40
Mean	64		46	48.9	32
SD	12		23	19	9

*NIF, negative inspiratory force; SAPS II, simplified acute physiology score II.

Table 5-2. Breathing pattern variables in the Successful vs. Failed spontaneous breathing trials

	Mean			CV, %		
	Successful	Failed	P Value	Successful	Failed	P Value
Ve (L/min)	7.87±2.03	8.20±2.94	0.36	18.11±9.4	14.49±7.35	0.03
RR (breath/min)	25.6±7.2	28.98±11.2	0.02	17.4±11.03	13.38±6.04	0.02
Vt (ml)	306.2±68.4	296.9±82.2	0.42	15.98±12.7	14.78±14.52	0.35
PIF (L/min)	28.8±5.88	31.34±9.2	0.04	19.11±9.25	14.88±19.11	0.01
Ti (sec)	0.96±0.21	0.90±0.24	0.07	20.98±18.47	18.15±11.11	0.21
Te (sec)	1.58±0.42	1.54±0.8	0.72	27.71±14.31	24.68±12.9	0.42
Ti/Ttot	0.38±0.06	0.39±0.07	0.75	19.03±10.9	18.59±10.1	0.42

CV, coefficient of variation; Ve minute ventilation; RR, respiratory rate; Vt, inspired tidal volume; PIF, peak inspiratory flow; Ti, inspiration time; Te, expiration time; Ti/Ttot, duty cycle; Data provides as Mean±SD.

CHAPTER 6
CONCLUSIONS AND FUTURE DIRECTION

In our first preliminary microarray study, we conclude that cardiothoracic surgery results in rapid changes in diaphragm gene expression, including genes related to generalized stress response, redox regulation, proteolysis, and energy metabolism. Further studies are needed to confirm and to clarify the biological relevance of our data.

In our second study, we conclude that the mean value of PIF and f were significantly different within subjects during the first 30 minutes interval of failed and successful SBT in PMV patients, reflecting a higher drive to breathe in failed trials. Secondly, among selected breathing variables including V_E, f, and PIF, breathing variability, quantified by the CVs, revealed more significant differences than the mean values. This finding suggests that analysis of the CVs provides additional information, which is ignored by the mean data. This study enhances our understanding of the breathing variability changes that occur in weaning failure patients. Information gained from this study may provide insights for improved weaning strategies. We believe that a better understanding of mechanisms, which contributed to the weaning failure, could help to improve the care of prolonged mechanical ventilation patients. Further work is needed to clarify the mechanisms of reduced breathing pattern variability in the failure of the spontaneous breathing trials.

APPENDIX
GENE FUNCTIONAL CATEGORIES

Gene functional categories and description were obtained from several public databases including gene ontology (Amigo; http://www.godatabase.org/cgi-bin/amigo/go.cgi), PubMed (http://www.ncbi.nlm.nih.gov/entrez/query.fcgi), OMIM (http://www.ncbi.nih.gov/entrez/query.fcgi?db=OMIM), and NetAffx (http://www.affymetix.com/analysis/netaffx/index.affx).

Table A-1. Expression of transport genes that are significantly different in the diaphragm after surgery

Probe set	Symbol	Fold change	Description	Function
200787_s_at	PEA15	1.8	phosphoprotein enriched in astrocytes 15	carbohydrate transport
202497_x_at	SLC2A3	5.0	solute carrier family 2 (facilitated glucose transporter), member 3	carbohydrate transport
209681_at	SLC19A2	3.3	solute carrier family 19 (thiamine transporter), member 2	folic acid transport
221020_s_at	SLC25A32	1.8	solute carrier family 25, member 32	folic acid transport
201088_at	KPNA2	2.1	karyopherin alpha 2 (RAG cohort 1, importin alpha 1)	intracelluar protein transport
1565875_at	NUP153	1.6	nucleoporin 153kDa	intracelluar protein transport
241425_at	NUPL1	1.4	nucleoporin like 1	intracelluar protein transport
200750_s_at	RAN	1.5	RAN, member RAS oncogene family	intracelluar protein transport
207624_s_at	RPGR	1.7	retinitis pigmentosa GTPase regulator	intracelluar protein transport
212902_at	SEC24A	1.8	SEC24 related gene family, member A (S. cerevisiae)	intracelluar protein transport
223225_s_at	SEH1L	2.6	SEH1-like (S. cerevisiae)	intracelluar protein transport
223209_s_at	SELS	1.5	selenoprotein S	intracelluar protein transport
235670_at	STX11	2.5	syntaxin 11	intracelluar protein transport
212112_s_at	STX12	1.7	syntaxin 12	intracelluar protein transport
221662_s_at	SLC22A7	1.7	solute carrier family 22 (organic anion transporter), member 7	ion transport
212110_at	SLC39A14	4.1	solute carrier family 39 (zinc transporter), member 14	ion transport
223044_at	SLC40A1	-1.7	solute carrier family 40 (iron-regulated transporter), member 1	ion transport
219911_s_at	SLCO4A1	3.0	solute carrier organic anion transporter family, member 4A1	ion transport
202068_s_at	LDLR	5.3	low density lipoprotein receptor (familial hypercholesterolemia)	lipid transport
230494_at	SLC20A1	2.6	solute carrier family 20 (phosphate transporter), member 1	phosphate transport
220948_s_at	ATP1A1	2.0	ATPase, Na+/K+ transporting, alpha 1 polypeptide	potassium ion transport
242836_at	ATP1B3	2.6	ATPase, Na+/K+ transporting, beta 3 polypeptide	potassium ion transport
209112_at	CDKN1B	-1.6	cyclin-dependent kinase inhibitor 1B (p27, Kip1)	potassium ion transport
237007_at	KCNB2	1.6	potassium voltage-gated channel, Shab-related subfamily, member 2	potassium ion transport
206765_at	KCNJ2	-2.1	potassium inwardly-rectifying channel, subfamily J, member 2	potassium ion transport
229953_x_at	LCA5	-1.9	Leber congenital amaurosis 5	protein transport

Table A-1. Continued.

Probe set	Symbol	Fold change	Description	Function
227247_at	PLEKHA8	-1.5	pleckstrin homology domain containing, family A (phosphoinositide binding specific) member 8	protein transport
221704_s_at	VPS37B	1.5	vacuolar protein sorting 37 homolog B (S. cerevisiae)	protein transport
224953_at	YIPF5	-1.6	Yip1 domain family, member 5	protein transport
206170_at	ADRB2	1.8	adrenergic, beta-2-, receptor, surface	regulation of sodium ion transport
218708_at	NXT1	2.6	NTF2-like export factor 1	RNA export from nucleus
237648_x_at	NHEDC2	1.6	Na+/H+ exchanger domain containing 2	sodium ion transport
229199_at	SCN9A	-1.8	sodium channel, voltage-gated, type IX, alpha subunit	sodium ion transport
205896_at	SLC22A4	3.6	solute carrier family 22 (organic cation transporter), member 4	sodium ion transport
242836_at	ATP1B3	2.6	ATPase, Na+/K+ transporting, beta 3 polypeptide	sodium:potassium-exchaning ATPase activity
205856_at	SLC14A1	-2.4	solute carrier family 14 (urea transporter), member 1 (Kidd blood group)	water transport
243166_at	SLC30A5	-1.5	solute carrier family 30 (zinc transporter), member 5	zinc ion transport
243524_at	SLC30A7	2.0	solute carrier family 30 (zinc transporter), member 7	zinc ion transport
1561886_a_at	SLC39A14	3.4	solute carrier family 39 (zinc transporter), member 14	zinc ion transport

Table A-2. Expression of signal transduction genes that are significantly different in the diaphragm after surgery

Probe set	Symbol	Fold change	Description	Function
210517_s_at	AKAP12	2.4	A kinase (PRKA) anchor protein (gravin) 12	signal transduction
215483_at	AKAP9	-1.5	A kinase (PRKA) anchor protein (yotiao) 9	signal transduction
210390_s_at	CCL15	1.7	chemokine (C-C motif) ligand 15	signal transduction
209287_s_at	CDC42EP3	1.5	CDC42 effector protein (Rho GTPase binding) 3	signal transduction
218157_x_at	CDC42SE1	2.2	CDC42 small effector 1	signal transduction
1555730_a_at	CFL1	1.6	cofilin 1 (non-muscle)	signal transduction
227481_at	CNKSR3	2.2	CNKSR family member 3	signal transduction
205898_at	CX3CR1	-2.6	chemokine (C-X3-C motif) receptor 1	signal transduction
208335_s_at	DARC	2.7	Duffy blood group, chemokine receptor	signal transduction
205419_at	EBI2	3.7	Epstein-Barr virus induced gene 2 (lymphocyte-specific G protein-coupled receptor)	signal transduction
212951_at	GPR116	1.5	G protein-coupled receptor 116	signal transduction
223620_at	GPR34	-2.3	G protein-coupled receptor 34	signal transduction
233953_at	GUCA1C	2.1	guanylate cyclase activator 1C	signal transduction
211676_s_at	IFNGR1	1.9	interferon gamma receptor 1	signal transduction
216944_s_at	ITPR1	1.6	inositol 1,4,5-triphosphate receptor, type 1	signal transduction
212723_at	JMJD6	2.1	jumonji domain containing 6	signal transduction
212935_at	MCF2L	2.0	MCF.2 cell line derived transforming sequence-like	signal transduction
225478_at	MFHAS1	1.9	malignant fibrous histiocytoma amplified sequence 1	signal transduction
230550_at	MS4A6A	-1.7	membrane-spanning 4-domains, subfamily A, member 6A	signal transduction
217302_at	OR2F2	1.5	olfactory receptor, family 2, subfamily F, member 2	signal transduction
219155_at	PITPNC1	2.2	phosphatidylinositol transfer protein, cytoplasmic 1	signal transduction

Table A-2. Continued.

Probe set	Symbol	Fold change	Description	Function
226122_at	PLEKHG1	2.7	pleckstrin homology domain containing, family G (with RhoGef domain) member 1	signal transduction
215894_at	PTGDR	-1.6	prostaglandin D2 receptor (DP)	signal transduction
209050_s_at	RALGDS	2.0	ral guanine nucleotide dissociation stimulator	signal transduction
208370_s_at	RCAN1	1.7	regulator of calcineurin 1	signal transduction
209324_s_at	RGS16	4.5	regulator of G-protein signaling 16	signal transduction
202388_at	RGS2	5.4	regulator of G-protein signaling 2, 24kDa	signal transduction
224390_s_at	RGS8	1.9	regulator of G-protein signaling 8	signal transduction
209941_at	RIPK1	1.9	receptor (TNFRSF)-interacting serine-threonine kinase 1	signal transduction
236606_at	SAV1	1.5	salvador homolog 1 (Drosophila)	signal transduction
209723_at	SERPINB9	2.0	serpin peptidase inhibitor, clade B (ovalbumin), member 9	signal transduction
226837_at	SPRED1	2.2	sprouty-related, EVH1 domain containing 1	signal transduction
230212_at	SPRY1	1.7	sprouty homolog 1, antagonist of FGF signaling (Drosophila)	signal transduction
202286_s_at	TACSTD2	2.6	tumor-associated calcium signal transducer 2	signal transduction
209295_at	TNFRSF10B	2.5	tumor necrosis factor receptor superfamily, member 10b	signal transduction
227345_at	TNFRSF10D	2.9	tumor necrosis factor receptor superfamily, member 10d, decoy with truncated death domain	signal transduction
203120_at	TP53BP2	1.8	tumor protein p53 binding protein, 2	signal transduction
215411_s_at	TRAF3IP2	1.7	TRAF3 interacting protein 2	signal transduction
230192_at	TRIM13	-1.5	tripartite motif-containing 13	signal transduction
200641_s_at	YWHAZ	1.5	tyrosine 3-monooxygenase/tryptophan 5-monooxygenase activation protein, zeta polypeptide	signal transduction

Table A-3. Expression of nuclei acid metabolism genes that are significantly different in the diaphragm after surgery

Probe set	Symbol	Fold change	Description	Function
204510_at	CDC7	1.9	cell division cycle 7 homolog (S. cerevisiae)	DNA replication
209101_at	CTGF	2.8	connective tissue growth factor	DNA replication
201970_s_at	NASP	1.7	nuclear autoantigenic sperm protein (histone-binding)	DNA replication
241797_at	NFIX	-1.5	nuclear factor I/X (CCAAT-binding transcription factor)	DNA replication
238992_at	POLI	-2.1	polymerase (DNA directed) iota	DNA replication
209868_s_at	RBMS1	1.5	RNA binding motif, single stranded interacting protein 1	DNA replication
226153_s_at	CNOT6L	1.5	CCR4-NOT transcription complex, subunit 6-like	mRNA processing
200033_at	DDX5	1.8	DEAD (Asp-Glu-Ala-Asp) box polypeptide 5	mRNA processing
201386_s_at	DHX15	1.6	DEAH (Asp-Glu-Ala-His) box polypeptide 15	mRNA processing
201303_at	EIF4A3	2.1	eukaryotic translation initiation factor 4A, isoform 3	mRNA processing
229007_at	LOC283788	-1.7	hypothetical protein LOC283788	mRNA processing
236907_at	PABPC1	2.2	poly(A) binding protein, cytoplasmic 1	mRNA processing
212015_x_at	PTBP1	2.0	polypyrimidine tract binding protein 1	mRNA processing
201586_s_at	SFPQ	2.5	splicing factor proline/glutamine-rich (polypyrimidine tract binding protein associated)	mRNA processing
209024_s_at	SYNCRIP	1.8	synaptotagmin binding, cytoplasmic RNA interacting protein	mRNA processing
202750_s_at	TFIP11	2.3	tuftelin interacting protein 11	mRNA processing
222748_s_at	TXNL4B	1.9	thioredoxin-like 4B	mRNA processing
229630_s_at	WTAP	2.5	Wilms tumor 1 associated protein	mRNA processing
204252_at	CDK2	1.6	cyclin-dependent kinase 2	regulation of DNA replication

Table A-3. Continued.

Probe set	Symbol	Fold change	Description	Function
223397_s_at	NIP7	2.7	nuclear import 7 homolog (S. cerevisiae)	ribosome assembly
218156_s_at	TSR1	1.6	TSR1, 20S rRNA accumulation, homolog (S. cerevisiae)	ribosome assembly
234295_at	DBR1	-1.7	debranching enzyme homolog 1 (S. cerevisiae)	RNA splicing
201055_s_at	HNRNPA0	1.7	heterogeneous nuclear ribonucleoprotein A0	RNA splicing
227110_at	HNRNPC	1.5	heterogeneous nuclear ribonucleoprotein C (C1/C2)	RNA splicing
212028_at	RBM25	1.6	RNA binding motif protein 25	RNA splicing
222443_s_at	RBM8A	1.8	RNA binding motif protein 8A	RNA splicing
201070_x_at	SF3B1	1.5	splicing factor 3b, subunit 1, 155kDa	RNA splicing
200892_s_at	SFRS10	1.8	splicing factor, arginine/serine-rich 10 (transformer 2 homolog, Drosophila)	RNA splicing
214882_s_at	SFRS2	1.6	splicing factor, arginine/serine-rich 2	RNA splicing
206108_s_at	SFRS6	1.6	splicing factor, arginine/serine-rich 6	RNA splicing
213649_at	SFRS7	1.6	splicing factor, arginine/serine-rich 7, 35kDa	RNA splicing
213175_s_at	SNRPB	1.6	small nuclear ribonucleoprotein polypeptides B and B1	RNA splicing
201478_s_at	DKC1	1.8	dyskeratosis congenita 1, dyskerin	rRNA processing
211951_at	NOLC1	2.0	nucleolar and coiled-body phosphoprotein 1	rRNA processing
212422_at	PDCD11	1.6	programmed cell death 11	rRNA processing

Table A-4. Expression of regulation of transcription genes that are significantly different in the diaphragm after surgery

Probe set	Symbol	Fold change	Description	Function
1560765_a_at	ARHGAP22	1.9	Rho GTPase activating protein 22	regulation of transcription
213138_at	ARID5A	2.2	AT rich interactive domain 5A (MRF1-like)	regulation of transcription
1558000_at	ARID5B	3.1	AT rich interactive domain 5B (MRF1-like)	regulation of transcription
225557_at	AXUD1	6.4	AXIN1 up-regulated 1	regulation of transcription
204194_at	BACH1	1.9	BTB and CNC homology 1, basic leucine zipper transcription factor 1	regulation of transcription
201101_s_at	BCLAF1	1.5	BCL2-associated transcription factor 1	regulation of transcription
201170_s_at	BHLHB2	2.7	basic helix-loop-helix domain containing, class B, 2	regulation of transcription
200777_s_at	BZW1	1.6	basic leucine zipper and W2 domains 1	regulation of transcription
204093_at	CCNH	1.7	cyclin H	regulation of transcription
1555411_a_at	CCNL1	4.2	cyclin L1	regulation of transcription
212501_at	CEBPB	2.2	CCAAT/enhancer binding protein (C/EBP), beta	regulation of transcription
207630_s_at	CREM	3.3	cAMP responsive element modulator	regulation of transcription
202776_at	DNTTIP2	1.8	deoxynucleotidyltransferase, terminal, interacting protein 2	regulation of transcription
226952_at	EAF1	1.5	ELL associated factor 1	regulation of transcription
212418_at	ELF1	1.8	E74-like factor 1 (ets domain transcription factor)	regulation of transcription
226099_at	ELL2	7.3	elongation factor, RNA polymerase II, 2	regulation of transcription
242868_at	EPAS1	2.2	endothelial PAS domain protein 1	regulation of transcription
1561167_at	ETV6	2.1	ets variant gene 6 (TEL oncogene)	regulation of transcription
202768_at	FOSB	5.2	FBJ murine osteosarcoma viral oncogene homolog B	regulation of transcription
218880_at	FOSL2	3.3	FOS-like antigen 2	regulation of transcription
1569477_at	FOXO3	2.0	forkhead box O3	regulation of transcription
218458_at	GMCL1	-1.6	germ cell-less homolog 1 (Drosophila)	regulation of transcription
222830_at	GRHL1	2.3	grainyhead-like 1 (Drosophila)	regulation of transcription
213844_at	HOXA5	-2.0	homeobox A5	regulation of transcription
205453_at	HOXB2	-1.6	homeobox B2	regulation of transcription
228904_at	HOXB3	-1.7	homeobox B3	regulation of transcription

Table A-4. Continued.

Probe set	Symbol	Fold change	Description	Function
208930_s_at	ILF3	1.4	interleukin enhancer binding factor 3, 90kDa	regulation of transcription
1557174_a_at	IRAK1BP1	-2.0	interleukin-1 receptor-associated kinase 1 binding protein 1	regulation of transcription
202531_at	IRF1	4.5	interferon regulatory factor 1	regulation of transcription
203297_s_at	JARID2	1.6	jumonji, AT rich interactive domain 2	regulation of transcription
201473_at	JUNB	4.1	jun B proto-oncogene	regulation of transcription
200704_at	LITAF	3.2	lipopolysaccharide-induced TNF factor	regulation of transcription
201862_s_at	LRRFIP1	2.1	leucine rich repeat (in FLII) interacting protein 1	regulation of transcription
209348_s_at	MAF	-1.7	v-maf musculoaponeurotic fibrosarcoma oncogene homolog (avian)	regulation of transcription
218559_s_at	MAFB	2.6	v-maf musculoaponeurotic fibrosarcoma oncogene homolog B (avian)	regulation of transcription
36711_at	MAFF	8.7	v-maf musculoaponeurotic fibrosarcoma oncogene homolog F (avian)	regulation of transcription
226206_at	MAFK	1.5	v-maf musculoaponeurotic fibrosarcoma oncogene homolog K (avian)	regulation of transcription
227538_at	MED26	1.6	mediator complex subunit 26	regulation of transcription
1552330_at	MGC16385	-1.6	hypothetical protein MGC16385	regulation of transcription
205932_s_at	MSX1	1.9	msh homeobox 1	regulation of transcription
225344_at	NCOA7	1.9	nuclear receptor coactivator 7	regulation of transcription
210162_s_at	NFATC1	1.5	nuclear factor of activated T-cells, cytoplasmic, calcineurin-dependent 1	regulation of transcription
1567013_at	NFE2L2	1.9	nuclear factor (erythroid-derived 2)-like 2	regulation of transcription
223217_s_at	NFKBIZ	3.9	nuclear factor of kappa light polypeptide gene enhancer in B-cells inhibitor, zeta	regulation of transcription
209706_at	NKX3-1	1.7	NK3 homeobox 1	regulation of transcription

Table A-4. Continued.

Probe set	Symbol	Fold change	Description	Function
202600_s_at	NRIP1	2.1	nuclear receptor interacting protein 1	regulation of transcription
202861_at	PER1	2.5	period homolog 1 (Drosophila)	regulation of transcription
205251_at	PER2	1.9	period homolog 2 (Drosophila)	regulation of transcription
209034_at	PNRC1	1.8	proline-rich nuclear receptor coactivator 1	regulation of transcription
206036_s_at	REL	1.8	v-rel reticuloendotheliosis viral oncogene homolog (avian)	regulation of transcription
222815_at	RNF12	2.1	ring finger protein 12	regulation of transcription
204900_x_at	SAP30	1.6	Sin3A-associated protein, 30kDa	regulation of transcription
219993_at	SOX17	4.1	SRY (sex determining region Y)-box 17	regulation of transcription
213654_at	TAF5L	1.9	TAF5-like RNA polymerase II, p300/CBP-associated factor (PCAF)-associated factor, 65kDa	regulation of transcription
203313_s_at	TGIF1	4.1	TGFB-induced factor homeobox 1	regulation of transcription
229983_at	TIGD2	-1.6	tigger transposable element derived 2	regulation of transcription
215111_s_at	TSC22D1	1.6	TSC22 domain family, member 1	regulation of transcription
204094_s_at	TSC22D2	2.2	TSC22 domain family, member 2	regulation of transcription
235170_at	ZNF92	-1.5	zinc finger protein 92	regulation of transcription

Table A-5. Expression of binding genes that are significantly different in the diaphragm after surgery

Probe set	Symbol	Fold change	Description	Function
205304_s_at	KCNJ8	-1.6	potassium inwardly-rectifying channel, subfamily J, member 8	ATP binding
236114_at	RUNX1	2.7	runt-related transcription factor 1 (acute myeloid leukemia 1; aml1 oncogene)	ATP binding
213918_s_at	NIPBL	1.7	Nipped-B homolog (Drosophila)	binding
227467_at	RDH10	1.8	retinol dehydrogenase 10 (all-trans)	binding
202083_s_at	SEC14L1	2.4	SEC14-like 1 (S. cerevisiae)	binding
225212_at	SLC25A25	3.8	solute carrier family 25 (mitochondrial carrier; phosphate carrier), member 25	binding
32091_at	SLC25A44	1.7	solute carrier family 25, member 44	binding
229169_at	TTC18	-1.5	tetratricopeptide repeat domain 18	binding
1554588_a_at	TTC30B	-2.0	tetratricopeptide repeat domain 30B	binding
212859_x_at	MT1E	3.5	metallothionein 1E	cadmium ion binding
217165_x_at	MT1F	3.5	metallothionein 1F	cadmium ion binding
204745_x_at	MT1G	3.5	metallothionein 1G	cadmium ion binding
206461_x_at	MT1H	3.4	metallothionein 1H	cadmium ion binding
217546_at	MT1M	11.4	metallothionein 1M	cadmium ion binding
208581_x_at	MT1X	3.3	metallothionein 1X	cadmium ion binding
216513_at	DCT	3.0	dopachrome tautomerase (dopachrome delta-isomerase, tyrosine-related protein 2)	copper ion binding
225987_at	STEAP4	1.9	STEAP family member 4	copper ion binding
220936_s_at	H2AFJ	-1.7	H2A histone family, member J	DNA binding
211997_x_at	H3F3B	1.9	H3 histone, family 3B (H3.3B)	DNA binding
214509_at	HIST1H3I	1.6	histone cluster 1, H3i	DNA binding
209317_at	POLR1C	1.9	polymerase (RNA) I polypeptide C, 30kDa	DNA binding
1554770_x_at	ZNF785	-1.8	zinc finger protein 785	DNA binding

Table A-5. Continued.

Probe set	Symbol	Fold change	Description	Function
1552316_a_at	GIMAP1	-1.9	GTPase, IMAP family member 1	GTP binding
226402_at	CYP2U1	-1.6	cytochrome P450, family 2, subfamily U, polypeptide 1	heme binding
235985_at	PITPNB	1.9	phosphatidylinositol transfer protein, beta	lipid binding
213629_x_at	MT1JP	3.6	metallothionein 1J (pseudogene)	metal ion binding
233085_s_at	OBFC2A	2.7	oligonucleotide/oligosaccharide-binding fold containing 2A	nucleic acid binding
212027_at	RBM25	1.5	RNA binding motif protein 25	nucleic acid binding
221213_s_at	SUHW4	-2.1	suppressor of hairy wing homolog 4 (Drosophila)	nucleic acid binding
201873_s_at	ABCE1	1.5	ATP-binding cassette, sub-family E (OABP), member 1	nucleotide binding
213198_at	ACVR1B	1.7	activin A receptor, type IB	nucleotide binding
228201_at	ARL13B	1.7	ADP-ribosylation factor-like 13B	nucleotide binding
203586_s_at	ARL4D	1.6	ADP-ribosylation factor-like 4D	nucleotide binding
242727_at	ARL5B	1.5	ADP-ribosylation factor-like 5B	nucleotide binding
209186_at	ATP2A2	1.9	ATPase, Ca++ transporting, cardiac muscle, slow twitch 2	nucleotide binding
230387_at	ATP2C1	-1.6	ATPase, Ca++ transporting, type 2C, member 1	nucleotide binding
219487_at	BBS10	-1.9	Bardet-Biedl syndrome 10	nucleotide binding
204258_at	CHD1	2.8	chromodomain helicase DNA binding protein 1	nucleotide binding
203104_at	CSF1R	-1.8	colony stimulating factor 1 receptor, formerly McDonough feline sarcoma viral (v-fms) oncogene homolog	nucleotide binding
240221_at	CSNK1A1	1.6	casein kinase 1, alpha 1	nucleotide binding
207945_s_at	CSNK1D	2.4	casein kinase 1, delta	nucleotide binding
203302_at	DCK	-1.7	deoxycytidine kinase	nucleotide binding
232541_at	EGFR	2.3	epidermal growth factor receptor (erythroblastic leukemia viral (v-erb-b) oncogene homolog, avian)	nucleotide binding

Table A-5. Continued.

Probe set	Symbol	Fold change	Description	Function
210287_s_at	FLT1	3.5	fms-related tyrosine kinase 1 (vascular endothelial growth factor/vascular permeability factor receptor)	nucleotide binding
210005_at	GART	1.7	phosphoribosylglycinamide formyltransferase, phosphoribosylglycinamide synthetase, phosphoribosylaminoimidazole synthetase	nucleotide binding
232024_at	GIMAP2	-2.7	GTPase, IMAP family member 2	nucleotide binding
219243_at	GIMAP4	-1.7	GTPase, IMAP family member 4	nucleotide binding
236583_at	GIMAP5	-1.7	GTPase, IMAP family member 5	nucleotide binding
228071_at	GIMAP7	-2.0	GTPase, IMAP family member 7	nucleotide binding
227692_at	GNAI1	-1.7	guanine nucleotide binding protein (G protein), alpha inhibiting activity polypeptide 1	nucleotide binding
240452_at	GSPT1	2.1	G1 to S phase transition 1	nucleotide binding
201277_s_at	HNRPAB	1.9	heterogeneous nuclear ribonucleoprotein A/B	nucleotide binding
213076_at	ITPKC	3.7	inositol 1,4,5-trisphosphate 3-kinase C	nucleotide binding
223380_s_at	LATS2	1.6	LATS, large tumor suppressor, homolog 2 (Drosophila)	nucleotide binding
201461_s_at	MAPKAPK2	1.6	mitogen-activated protein kinase-activated protein kinase 2	nucleotide binding
225613_at	MAST4	1.9	microtubule associated serine/threonine kinase family member 4	nucleotide binding
200768_s_at	MAT2A	2.5	methionine adenosyltransferase II, alpha	nucleotide binding
238624_at	NLK	1.4	nemo-like kinase	nucleotide binding
207075_at	NLRP3	2.4	NLR family, pyrin domain containing 3	nucleotide binding
211949_s_at	NOLC1	1.7	nucleolar and coiled-body phosphoprotein 1	nucleotide binding
1555310_a_at	PAK6	1.7	p21(CDKN1A)-activated kinase 6	nucleotide binding
221918_at	PCTK2	1.9	PCTAIRE protein kinase 2	nucleotide binding
227255_at	PDIK1L	-1.6	PDLIM1 interacting kinase 1 like	nucleotide binding
202464_s_at	PFKFB3	3.8	6-phosphofructo-2-kinase/fructose-2,6-biphosphatase 3	nucleotide binding
209193_at	PIM1	3.5	pim-1 oncogene	nucleotide binding

Table A-5. Continued.

Probe set	Symbol	Fold change	Description	Function
219622_at	RAB20	1.9	RAB20, member RAS oncogene family	nucleotide binding
221014_s_at	RAB33B	-1.6	RAB33B, member RAS oncogene family	nucleotide binding
223467_at	RASD1	5.7	RAS, dexamethasone-induced 1	nucleotide binding
212168_at	RBM12	1.6	RNA binding motif protein 12	nucleotide binding
212099_at	RHOB	3.0	ras homolog gene family, member B	nucleotide binding
223169_s_at	RHOU	2.8	ras homolog gene family, member U	nucleotide binding
209941_at	RIPK1	1.9	receptor (TNFRSF)-interacting serine-threonine kinase 1	nucleotide binding
218088_s_at	RRAGC	1.6	Ras-related GTP binding C	nucleotide binding
200754_x_at	SFRS2	1.6	splicing factor, arginine/serine-rich 2	nucleotide binding
1562948_at	SMC5	1.5	structural maintenance of chromosomes 5	nucleotide binding
202693_s_at	STK17A	2.0	serine/threonine kinase 17a	nucleotide binding
205214_at	STK17B	3.3	serine/threonine kinase 17b	nucleotide binding
202307_s_at	TAP1	2.3	transporter 1, ATP-binding cassette, sub-family B (MDR/TAP)	nucleotide binding
218459_at	TOR3A	2.0	torsin family 3, member A	nucleotide binding
213726_x_at	TUBB2C	1.6	tubulin, beta 2C	nucleotide binding
202932_at	YES1	1.7	v-yes-1 Yamaguchi sarcoma viral oncogene homolog 1	nucleotide binding
1553696_s_at	ZNF569	-1.8	zinc finger protein 569	nucleotide binding
224632_at	GPATCH4	1.6	G patch domain containing 4	nuleic acid binding
220330_s_at	SAMSN1	6.7	SAM domain, SH3 domain and nuclear localization signals 1	phosphotyrosine binding

Table A-5. Continued.

Probe set	Symbol	Fold change	Description	Function
205681_at	BCL2A1	11.3	BCL2-related protein A1	protein binding
208536_s_at	BCL2L11	1.5	BCL2-like 11 (apoptosis facilitator)	protein binding
202710_at	BET1	-1.8	BET1 homolog (S. cerevisiae)	protein binding
218723_s_at	C13orf15	2.6	chromosome 13 open reading frame 15	protein binding
230424_at	C5orf13	-1.7	chromosome 5 open reading frame 13	protein binding
212923_s_at	C6orf145	3.1	chromosome 6 open reading frame 145	protein binding
221003_s_at	CAB39L	2.0	calcium binding protein 39-like	protein binding
205899_at	CCNA1	1.5	cyclin A1	protein binding
232768_at	CCNB2	1.5	cyclin B2	protein binding
229900_at	CD109	2.0	CD109 molecule	protein binding
218351_at	COMMD8	-1.6	COMM domain containing 8	protein binding
202437_s_at	CYP1B1	1.9	cytochrome P450, family 1, subfamily B, polypeptide 1	protein binding
230568_x_at	DLL3	1.6	delta-like 3 (Drosophila)	protein binding
201041_s_at	DUSP1	3.7	dual specificity phosphatase 1	protein binding
225656_at	EFHC1	1.9	EF-hand domain (C-terminal) containing 1	protein binding
212418_at	ELF1	1.8	E74-like factor 1 (ets domain transcription factor)	protein binding
220386_s_at	EML4	1.7	echinoderm microtubule associated protein like 4	protein binding
224657_at	ERRFI1	4.0	ERBB receptor feedback inhibitor 1	protein binding
222853_at	FLRT3	-2.6	fibronectin leucine rich transmembrane protein 3	protein binding
205436_s_at	H2AFX	1.8	H2A histone family, member X	protein binding
201631_s_at	IER3	3.6	immediate early response 3	protein binding
206245_s_at	IVNS1ABP	1.7	influenza virus NS1A binding protein	protein binding
222728_s_at	JOSD3	1.8	Josephin domain containing 3	protein binding

Table A-5. Continued.

Probe set	Symbol	Fold change	Description	Function
226479_at	KBTBD6	-1.8	kelch repeat and BTB (POZ) domain containing 6	protein binding
223412_at	KBTBD7	-2.0	kelch repeat and BTB (POZ) domain containing 7	protein binding
205150_s_at	KIAA0644	-1.7	KIAA0644 gene product	protein binding
243589_at	KIAA1267	-1.6	KIAA1267	protein binding
226370_at	KLHL15	1.7	kelch-like 15 (Drosophila)	protein binding
203068_at	KLHL21	1.6	kelch-like 21 (Drosophila)	protein binding
203835_at	LRRC32	2.0	leucine rich repeat containing 32	protein binding
1559580_at	LRRC39	-3.1	leucine rich repeat containing 39	protein binding
222231_s_at	LRRC59	2.0	leucine rich repeat containing 59	protein binding
233487_s_at	LRRC8A	1.6	leucine rich repeat containing 8 family, member A	protein binding
200797_s_at	MCL1	2.0	myeloid cell leukemia sequence 1 (BCL2-related)	protein binding
202431_s_at	MYC	8.0	v-myc myelocytomatosis viral oncogene homolog (avian)	protein binding
208093_s_at	NDEL1	1.9	nudE nuclear distribution gene E homolog (A. nidulans)-like 1	protein binding
224958_at	NUFIP2	1.7	nuclear fragile X mental retardation protein interacting protein 2	protein binding
225842_at	PHLDA1	3.0	pleckstrin homology-like domain, family A, member 1	protein binding
211580_s_at	PIK3R3	2.8	phosphoinositide-3-kinase, regulatory subunit 3 (p55, gamma)	protein binding
202327_s_at	PKD1	2.0	polycystic kidney disease 1 (autosomal dominant)	protein binding
202446_s_at	PLSCR1	3.3	phospholipid scramblase 1	protein binding
204286_s_at	PMAIP1	2.8	phorbol-12-myristate-13-acetate-induced protein 1	protein binding
37028_at	PPP1R15A	2.2	protein phosphatase 1, regulatory (inhibitor) subunit 15A	protein binding
202886_s_at	PPP2R1B	1.7	protein phosphatase 2 (formerly 2A), regulatory subunit A, beta isoform	protein binding
208965_s_at	PYHIN1	3.0	pyrin and HIN domain family, member 1	protein binding

Table A-5. Continued.

Probe set	Symbol	Fold change	Description	Function
225039_at	RPE	-1.5	ribulose-5-phosphate-3-epimerase	protein binding
201070_x_at	SF3B1	1.5	splicing factor 3b, subunit 1, 155kDa	protein binding
212470_at	SPAG9	1.5	sperm associated antigen 9	protein binding
201060_x_at	STOM	2.3	stomatin	protein binding
218335_x_at	TNIP2	1.6	TNFAIP3 interacting protein 2	protein binding
208900_s_at	TOP1	2.3	topoisomerase (DNA) I	protein binding
233970_s_at	TRMT6	1.6	tRNA methyltransferase 6 homolog (S. cerevisiae)	protein binding
242116_x_at	ANKRD17	1.6	ankyrin repeat domain 17	RNA binding
201376_s_at	HNRPF	1.6	heterogeneous nuclear ribonucleoprotein F	RNA binding
236699_at	MBNL2	1.4	muscleblind-like 2 (Drosophila)	RNA binding
205135_s_at	NUFIP1	1.9	nuclear fragile X mental retardation protein interacting protein 1	RNA binding
224956_at	NUFIP2	1.8	nuclear fragile X mental retardation protein interacting protein 2	RNA binding
203737_s_at	PPRC1	3.3	peroxisome proliferator-activated receptor gamma, coactivator-related 1	RNA binding
238122_at	RBM12B	-1.8	RNA binding motif protein 12B	RNA binding
212028_at	RBM25	1.6	RNA binding motif protein 25	RNA binding
208804_s_at	SFRS6	1.6	splicing factor, arginine/serine-rich 6	RNA binding
213175_s_at	SNRPB	1.6	small nuclear ribonucleoprotein polypeptides B and B1	RNA binding
220104_at	ZC3HAV1	2.1	zinc finger CCCH-type, antiviral 1	RNA binding
201531_at	ZFP36	4.5	zinc finger protein 36, C3H type, homolog (mouse)	RNA binding
211965_at	ZFP36L1	3.0	zinc finger protein 36, C3H type-like 1	RNA binding
201369_s_at	ZFP36L2	2.2	zinc finger protein 36, C3H type-like 2	RNA binding
227188_at	C21orf63	2.5	chromosome 21 open reading frame 63	sugar binding
210732_s_at	LGALS8	1.8	lectin, galactoside-binding, soluble, 8 (galectin 8)	sugar binding

Table A-5. Continued.

Probe set	Symbol	Fold change	Description	Function
222162_s_at	ADAMTS1	4.1	ADAM metallopeptidase with thrombospondin type 1 motif, 1	zinc ion binding
1562275_at	ADAMTS9	8.4	ADAM metallopeptidase with thrombospondin type 1 motif, 9	zinc ion binding
203322_at	ADNP2	1.6	ADNP homeobox 2	zinc ion binding
244519_at	ASXL1	1.7	additional sex combs like 1 (Drosophila)	zinc ion binding
231270_at	CA13	1.7	carbonic anhydrase XIII	zinc ion binding
202284_s_at	CDKN1A	4.9	cyclin-dependent kinase inhibitor 1A (p21, Cip1)	zinc ion binding
239648_at	DCUN1D3	2.4	DCN1, defective in cullin neddylation 1, domain containing 3 (S. cerevisiae)	zinc ion binding
201693_s_at	EGR1	6.7	early growth response 1	zinc ion binding
205249_at	EGR2	6.1	early growth response 2 (Krox-20 homolog, Drosophila)	zinc ion binding
206115_at	EGR3	4.1	early growth response 3	zinc ion binding
208989_s_at	FBXL11	1.5	F-box and leucine-rich repeat protein 11	zinc ion binding
204224_s_at	GCH1	4.6	GTP cyclohydrolase 1 (dopa-responsive dystonia)	zinc ion binding
208066_s_at	GTF2B	1.6	general transcription factor IIB	zinc ion binding
224569_s_at	IRF2BP2	1.5	interferon regulatory factor 2 binding protein 2	zinc ion binding
225142_at	JHDM1D	1.6	jumonji C domain-containing histone demethylase 1 homolog D (S. cerevisiae)	zinc ion binding
224933_s_at	JMJD1C	2.1	jumonji domain containing 1C	zinc ion binding
1556060_a_at	KIAA1702	1.8	KIAA1702 protein	zinc ion binding
202393_s_at	KLF10	2.8	Kruppel-like factor 10	zinc ion binding
221841_s_at	KLF4	3.1	Kruppel-like factor 4 (gut)	zinc ion binding
224606_at	KLF6	2.8	Kruppel-like factor 6	zinc ion binding
203542_s_at	KLF9	2.6	Kruppel-like factor 9	zinc ion binding
215322_at	LONRF1	1.8	LON peptidase N-terminal domain and ring finger 1	zinc ion binding
204575_s_at	MMP19	3.2	matrix metallopeptidase 19	zinc ion binding
212185_x_at	MT2A	2.4	metallothionein 2A	zinc ion binding

Table A-5. Continued.

Probe set	Symbol	Fold change	Description	Function
221715_at	MYST3	1.7	MYST histone acetyltransferase (monocytic leukemia) 3	zinc ion binding
215073_s_at	NR2F2	-1.9	nuclear receptor subfamily 2, group F, member 2	zinc ion binding
202340_x_at	NR4A1	3.7	nuclear receptor subfamily 4, group A, member 1	zinc ion binding
209959_at	NR4A3	4.6	nuclear receptor subfamily 4, group A, member 3	zinc ion binding
210391_at	NR6A1	1.4	nuclear receptor subfamily 6, group A, member 1	zinc ion binding
211564_s_at	PDLIM4	1.8	PDZ and LIM domain 4	zinc ion binding
1557852_at	PHC2	2.2	polyhomeotic homolog 2 (Drosophila)	zinc ion binding
215281_x_at	POGZ	-1.5	pogo transposable element with ZNF domain	zinc ion binding
228964_at	PRDM1	2.7	PR domain containing 1, with ZNF domain	zinc ion binding
203749_s_at	RARA	1.9	retinoic acid receptor, alpha	zinc ion binding
205178_s_at	RBBP6	1.8	retinoblastoma binding protein 6	zinc ion binding
219897_at	RNF122	1.6	ring finger protein 122	zinc ion binding
218738_s_at	RNF138	1.8	ring finger protein 138	zinc ion binding
226104_at	RNF170	-1.7	ring finger protein 170	zinc ion binding
213038_at	RNF19B	1.8	ring finger protein 19B	zinc ion binding
201846_s_at	RYBP	2.4	RING1 and YY1 binding protein	zinc ion binding
243166_at	SLC30A5	-1.5	solute carrier family 30 (zinc transporter), member 5	zinc ion binding
219480_at	SNAI1	1.6	snail homolog 1 (Drosophila)	zinc ion binding
230380_at	THAP2	3.4	THAP domain containing, apoptosis associated protein 2	zinc ion binding
212665_at	TIPARP	6.2	TCDD-inducible poly(ADP-ribose) polymerase	zinc ion binding
202643_s_at	TNFAIP3	3.2	tumor necrosis factor, alpha-induced protein 3	zinc ion binding
202871_at	TRAF4	1.5	TNF receptor-associated factor 4	zinc ion binding
235081_x_at	TRIM65	-1.7	tripartite motif-containing 65	zinc ion binding

Table A-5. Continued.

Probe set	Symbol	Fold change	Description	Function
241755_at	UQCRC2	-1.7	ubiquinol-cytochrome c reductase core protein II	zinc ion binding
1554036_at	ZBTB24	2.3	zinc finger and BTB domain containing 24	zinc ion binding
227162_at	ZBTB26	-1.6	zinc finger and BTB domain containing 26	zinc ion binding
236557_at	ZBTB38	1.6	zinc finger and BTB domain containing 38	zinc ion binding
206098_at	ZBTB6	-1.5	zinc finger and BTB domain containing 6	zinc ion binding
218810_at	ZC3H12A	2.1	zinc finger CCCH-type containing 12A	zinc ion binding
222451_s_at	ZDHHC9	2.2	zinc finger, DHHC-type containing 9	zinc ion binding
208078_s_at	ZEB1	6.0	zinc finger E-box binding homeobox 1	zinc ion binding
217741_s_at	ZFAND5	3.9	zinc finger, AN1-type domain 5	zinc ion binding
207090_x_at	ZFP30	-1.5	zinc finger protein 30 homolog (mouse)	zinc ion binding
201531_at	ZFP36	4.5	zinc finger protein 36, C3H type, homolog (mouse)	zinc ion binding
201369_s_at	ZFP36L2	2.2	zinc finger protein 36, C3H type-like 2	zinc ion binding
216960_s_at	ZNF133	-1.4	zinc finger protein 133	zinc ion binding
219854_at	ZNF14	-1.5	zinc finger protein 14	zinc ion binding
206314_at	ZNF167	-1.9	zinc finger protein 167	zinc ion binding
219495_s_at	ZNF180	-1.6	zinc finger protein 180	zinc ion binding
213218_at	ZNF187	-1.6	zinc finger protein 187	zinc ion binding
200828_s_at	ZNF207	1.5	zinc finger protein 207	zinc ion binding
233461_x_at	ZNF226	-1.6	zinc finger protein 226	zinc ion binding
242919_at	ZNF253	-1.8	zinc finger protein 253	zinc ion binding
1558700_s_at	ZNF260	-1.9	zinc finger protein 260	zinc ion binding

Table A-5. Continued.

Probe set	Symbol	Fold change	Description	Function
1562991_at	ZNF292	1.9	zinc finger protein 292	zinc ion binding
233952_s_at	ZNF295	2.5	zinc finger protein 295	zinc ion binding
227613_at	ZNF331	3.6	zinc finger protein 331	zinc ion binding
228927_at	ZNF397	-1.6	zinc finger protein 397	zinc ion binding
209944_at	ZNF410	1.6	zinc finger protein 410	zinc ion binding
205514_at	ZNF415	-1.6	zinc finger protein 415	zinc ion binding
1554007_at	ZNF483	-2.4	zinc finger protein 483	zinc ion binding
1562211_a_at	ZNF491	1.7	zinc finger protein 491	zinc ion binding
1553957_at	ZNF564	-1.8	zinc finger protein 564	zinc ion binding
1553696_s_at	ZNF569	-1.8	zinc finger protein 569	zinc ion binding
217627_at	ZNF573	-1.6	zinc finger protein 573	zinc ion binding
235690_at	ZNF594	-1.7	zinc finger protein 594	zinc ion binding
239007_at	ZNF616	-1.6	zinc finger protein 616	zinc ion binding
206188_at	ZNF623	-1.8	zinc finger protein 623	zinc ion binding
232272_at	ZNF624	-1.9	zinc finger protein 624	zinc ion binding
224492_s_at	ZNF627	-1.7	zinc finger protein 627	zinc ion binding
231950_at	ZNF658	-2.1	zinc finger protein 658	zinc ion binding
232563_at	ZNF684	-1.5	zinc finger protein 684	zinc ion binding

Table A-6. Expression of cell adhesion genes that are significantly different in the diaphragm after surgery

Probe set	Symbol	Fold change	Description	Function
231907_at	ABL2	2.0	v-abl Abelson murine leukemia viral oncogene homolog 2 (arg, Abelson-related gene)	cell adhesion
201883_s_at	B4GALT1	1.9	UDP-Gal:betaGlcNAc beta 1,4- galactosyltransferase, polypeptide 1	cell adhesion
216598_s_at	CCL2	8.2	chemokine (C-C motif) ligand 2	cell adhesion
217523_at	CD44	2.9	CD44 molecule (Indian blood group)	cell adhesion
203687_at	CX3CL1	2.6	chemokine (C-X3-C motif) ligand 1	cell adhesion
205898_at	CX3CR1	-2.6	chemokine (C-X3-C motif) receptor 1	cell adhesion
204359_at	FLRT2	-2.1	fibronectin leucine rich transmembrane protein 2	cell adhesion
222853_at	FLRT3	-2.6	fibronectin leucine rich transmembrane protein 3	cell adhesion
212070_at	GPR56	2.0	G protein-coupled receptor 56	cell adhesion
207316_at	HAS1	3.8	hyaluronan synthase 1	cell adhesion
203395_s_at	HES1	2.8	hairy and enhancer of split 1, (Drosophila)	cell adhesion
213620_s_at	ICAM2	1.8	intercellular adhesion molecule 2	cell adhesion
225806_at	JUB	-1.6	jub, ajuba homolog (Xenopus laevis)	cell adhesion
203780_at	MPZL2	2.3	myelin protein zero-like 2	cell adhesion
202149_at	NEDD9	2.3	neural precursor cell expressed, developmentally down-regulated 9	cell adhesion
225975_at	PCDH18	-2.3	protocadherin 18	cell adhesion
214212_x_at	PLEKHC1	1.7	pleckstrin homology domain containing, family C (with FERM domain) member 1	cell adhesion
210809_s_at	POSTN	1.8	periostin, osteoblast specific factor	cell adhesion
212099_at	RHOB	3.0	ras homolog gene family, member B	cell adhesion
212724_at	RND3	3.7	Rho family GTPase 3	cell adhesion
206211_at	SELE	6.0	selectin E (endothelial adhesion molecule 1)	cell adhesion
206026_s_at	TNFAIP6	4.1	tumor necrosis factor, alpha-induced protein 6	cell adhesion
202877_s_at	CD93	2.7	CD93 molecule	cell-cell adhesion
202638_s_at	ICAM1	3.4	intercellular adhesion molecule 1 (CD54), human rhinovirus receptor	regulation of cell adhesion

Table A-7. Expression of cell differentiation, growth, and proliferation genes that are significantly different in the diaphragm after surgery

Probe set	Symbol	Fold change	Description	Function
203725_at	GADD45A	3.0	growth arrest and DNA-damage-inducible, alpha	cell cycle arrest
202669_s_at	EFNB2	1.6	ephrin-B2	cell differentiation
209305_s_at	GADD45B	10.2	growth arrest and DNA-damage-inducible, beta	cell differentiation
204121_at	GADD45G	4.3	growth arrest and DNA-damage-inducible, gamma	cell differentiation
1559975_at	BTG1	2.3	B-cell translocation gene 1, anti-proliferative	cell growth
1555608_at	CAPRIN2	1.7	caprin family member 2	cell growth
223377_x_at	CISH	6.8	cytokine inducible SH2-containing protein	cell growth
209074_s_at	FAM107A	3.4	family with sequence similarity 107, member A	cell growth
205302_at	IGFBP1	1.6	insulin-like growth factor binding protein 1	cell growth
201830_s_at	NET1	3.0	neuroepithelial cell transforming gene 1	cell growth
222514_at	RRAGC	1.5	Ras-related GTP binding C	cell growth
202912_at	ADM	3.6	adrenomedullin	cell proliferation
206170_at	ADRB2	1.8	adrenergic, beta-2-, receptor, surface	cell proliferation
205290_s_at	BMP2	3.8	bone morphogenetic protein 2	cell proliferation
228176_at	C9orf47	2.8	chromosome 9 open reading frame 47	cell proliferation
204995_at	CDK5R1	1.6	cyclin-dependent kinase 5, regulatory subunit 1 (p35)	cell proliferation
213183_s_at	CDKN1C	-1.7	cyclin-dependent kinase inhibitor 1C (p57, Kip2)	cell proliferation
207442_at	CSF3	2.7	colony stimulating factor 3 (granulocyte)	cell proliferation
210762_s_at	DLC1	1.8	deleted in liver cancer 1	cell proliferation
213895_at	EMP1	3.8	epithelial membrane protein 1	cell proliferation
238500_at	EMP2	1.5	epithelial membrane protein 2	cell proliferation
203643_at	ERF	1.5	Ets2 repressor factor	cell proliferation

Table A-7. Continued.

Probe set	Symbol	Fold change	Description	Function
204420_at	FOSL1	3.3	FOS-like antigen 1	cell proliferation
1553613_s_at	FOXC1	2.6	forkhead box C1	cell proliferation
202723_s_at	FOXO1	1.9	forkhead box O1	cell proliferation
237403_at	GFI1B	2.2	growth factor independent 1B (potential regulator of CDKN1A, translocated in CML)	cell proliferation
209524_at	HDGFRP3	1.9	hepatoma-derived growth factor, related protein 3	cell proliferation
201626_at	INSIG1	2.7	insulin induced gene 1	cell proliferation
203275_at	IRF2	-1.6	interferon regulatory factor 2	cell proliferation
200712_s_at	MAPRE1	1.4	microtubule-associated protein, RP/EB family, member 1	cell proliferation
201502_s_at	NFKBIA	3.7	nuclear factor of kappa light polypeptide gene enhancer in B-cells inhibitor, alpha	cell proliferation
201695_s_at	NP	6.9	nucleoside phosphorylase	cell proliferation
218718_at	PDGFC	-1.6	platelet derived growth factor C	cell proliferation
223394_at	SERTAD1	3.0	SERTA domain containing 1	cell proliferation
203625_x_at	SKP2	-1.8	S-phase kinase-associated protein 2 (p45)	cell proliferation
214597_at	SSTR2	1.5	somatostatin receptor 2	cell proliferation
202286_s_at	TACSTD2	2.6	tumor-associated calcium signal transducer 2	cell proliferation
202241_at	TRIB1	3.3	tribbles homolog 1 (Drosophila)	cell proliferation
211527_x_at	VEGFA	1.8	vascular endothelial growth factor A	cell proliferation
201235_s_at	BTG2	6.0	BTG family, member 2	negative regulation of cell proliferation
213134_x_at	BTG3	2.6	BTG family, member 3	negative regulation of cell proliferation
201329_s_at	ETS2	4.9	v-ets erythroblastosis virus E26 oncogene homolog 2 (avian)	negative regulation of cell proliferation
218062_x_at	CDC42EP4	2.2	CDC42 effector protein (Rho GTPase binding) 4	regulation of cell shape

Table A-8. Expression of structural constituent or molecular activity genes that are significantly different in the diaphragm after surgery

Probe set	Symbol	Fold change	Description	Function
229218_at	COL1A2	-2.2	collagen, type I, alpha 2	extracellular matrix structural constituent
1563536_at	COL4A5	1.5	collagen, type IV, alpha 5 (Alport syndrome)	extracellular matrix structural constituent
37022_at	PRELP	1.6	proline/arginine-rich end leucine-rich repeat protein	extracellular matrix structural constituent
212086_x_at	LMNA	1.9	lamin A/C	structrual molecule activity
230289_at	EPB41L1	2.4	erythrocyte membrane protein band 4.1-like 1	structual molecular activity
203276_at	LMNB1	4.0	lamin B1	structual molecular activity
235086_at	THBS1	8.2	thrombospondin 1	structual molecular activity
1561705_at	TTBK2	1.6	tau tubulin kinase 2	structual molecular activity
209251_x_at	TUBA1C	1.5	tubulin, alpha 1c	structual molecular activity
208977_x_at	TUBB2C	1.6	tubulin, beta 2C	structual molecular activity
213476_x_at	TUBB3	1.7	tubulin, beta 3	structual molecular activity
209191_at	TUBB6	3.0	tubulin, beta 6	structual molecular activity
231853_at	TUBD1	-1.6	tubulin, delta 1	structual molecular activity
222142_at	CYLD	1.4	cylindromatosis (turban tumor syndrome)	structural constituent of ribosome

Table A-9. Expression of extracellular region, cell junction, and membrane genes that are significantly different in the diaphragm after surgery

Probe set	Symbol	Fold change	Description	Function
Extracellular region				
228190_at	ATG4C	-1.8	ATG4 autophagy related 4 homolog C (S. cerevisiae)	extracellular region
213528_at	C1orf156	-1.8	chromosome 1 open reading frame 156	extracellular region
224553_s_at	TNFRSF18	-1.6	tumor necrosis factor receptor superfamily, member 18	extracellular region
201858_s_at	SRGN	4.2	serglycin	extracellular region
219522_at	FJX1	2.4	four jointed box 1 (Drosophila)	extracellular region
221541_at	CRISPLD2	2.8	cysteine-rich secretory protein LCCL domain containing 2	extracellular region
220975_s_at	C1QTNF1	2.0	C1q and tumor necrosis factor related protein 1	extracellular region
229120_s_at	C1orf56	2.2	chromosome 1 open reading frame 56	extracellular region
223454_at	CXCL16	2.0	chemokine (C-X-C motif) ligand 16	extracellular region
203592_s_at	FSTL3	1.6	follistatin-like 3 (secreted glycoprotein)	extracellular region
221009_s_at	ANGPTL4	2.6	angiopoietin-like 4	extracellular region
205258_at	INHBB	4.3	inhibin, beta B	extracellular region
241557_x_at	TMEFF2	1.7	transmembrane protein with EGF-like and two follistatin-like domains 2	extracellular region
213425_at	WNT5A	-2.0	wingless-type MMTV integration site family, member 5A	extracellular region
226621_at	FGG	3.0	fibrinogen gamma chain	extracellular region
1570046_at	SCRG1	1.5	scrapie responsive protein 1	extracellular region
226977_at	LOC492311	-1.6	similar to bovine IgA regulatory protein	extracellular region
206552_s_at	TAC1	5.0	tachykinin, precursor 1 (substance K, substance P, neurokinin 1, neurokinin 2, neuromedin L, neurokinin alpha, neuropeptide K, neuropeptide gamma)	extracellular region
204597_x_at	STC1	7.8	stanniocalcin 1	extracellular region
209122_at	ADFP	1.9	adipose differentiation-related protein	extracellular region

Table A-9. Continued.

Probe set	Symbol	Fold change	Description	Function
Cell Junction				
227439_at	ANKS1B	1.8	ankyrin repeat and sterile alpha motif domain containing 1B	cell junction
210090_at	ARC	10.7	activity-regulated cytoskeleton-associated protein	cell junction
204715_at	PANX1	1.9	pannexin 1	cell junction
228263_at	GRASP	2.2	GRP1 (general receptor for phosphoinositides 1)-associated scaffold protein	cell junction
241771_at	RIMBP2	1.9	RIMS binding protein 2	cell junction
214827_at	PARD6B	1.8	par-6 partitioning defective 6 homolog beta (C. elegans)	cell junction
202085_at	TJP2	1.8	tight junction protein 2 (zona occludens 2)	cell junction
Membrane				
1559258_a_at	CXorf61	1.6	chromosome X open reading frame 61	plasma membrane
219492_at	CHIC2	1.8	cysteine-rich hydrophobic domain 2	plasma membrane
217291_at	CEACAM5	1.5	carcinoembryonic antigen-related cell adhesion molecule 5	anchored to membrane
1558511_s_at	FAM62B	1.6	family with sequence similarity 62 (C2 domain containing) member B	plasma membrane
218361_at	GOLPH3L	-1.9	golgi phosphoprotein 3-like	membrane
225222_at	HIAT1	1.7	hippocampus abundant transcript 1	integral to membrane
202181_at	KIAA0247	1.8	KIAA0247	integral to membrane
223800_s_at	LIMS3	2.4	LIM and senescent cell antigen-like domains 3	integral to membrane
229531_at	MCART6	-1.5	mitochondrial carrier triple repeat 6	mitochondrial inner membrane
228282_at	MFSD8	-1.7	major facilitator superfamily domain containing 8	lysosomal membrane
225673_at	MYADM	1.7	myeloid-associated differentiation marker	integral to membrane
1569641_at	PQLC1	1.5	PQ loop repeat containing 1	integral to membrane
226430_at	RELL1	1.6	RELT-like 1	integral to membrane
238829_at	SPG11	1.5	spastic paraplegia 11 (autosomal recessive)	integral to membrane
216920_s_at	TARP	-1.8	TCR gamma alternate reading frame protein	integral to membrane

Table A-9. Continued

Probe set	Symbol	Fold change	Description	Function
209387_s_at	TM4SF1	2.3	transmembrane 4 L six family member 1	integral to membrane
226489_at	TMCC3	1.7	transmembrane and coiled-coil domain family 3	integral to membrane
226825_s_at	TMEM165	2.0	transmembrane protein 165	integral to membrane
219253_at	TMEM185B	1.6	transmembrane protein 185B	integral to membrane
218113_at	TMEM2	3.3	transmembrane protein 2	integral to membrane
224917_at	TMEM49	4.3	transmembrane protein 49	integral to membrane
1557520_a_at	TMEM59	1.5	transmembrane protein 59	integral to membrane
219449_s_at	TMEM70	1.5	transmembrane protein 70	integral to membrane
223772_s_at	TMEM87A	1.8	transmembrane protein 87A	integral to membrane

Table A-10. Expression of neuronal factor, blood coagulation, catalytic activity, and miscellaneous genes that are significantly different in the diaphragm after surgery

Probe set	Symbol	Fold change	Description	Function
Neuronal Factor				
204622_x_at	NR4A2	3.7	nuclear receptor subfamily 4, group A, member 2	neuron differentiation
241583_x_at	SYT1	1.7	synaptotagmin I	neurotransmitter secretion
241652_x_at	LIN7A	2.1	lin-7 homolog A (C. elegans)	neurotransmitter secretion
1569916_at	SLC6A15	2.1	solute carrier family 6, member 15	neurotransmitter transport
204224_s_at	GCH1	4.6	GTP cyclohydrolase 1 (dopa-responsive dystonia)	neurotransmitter metabolic process
200815_s_at	PAFAH1B1	1.4	platelet-activating factor acetylhydrolase, isoform Ib, alpha subunit 45kDa	synaptic transmission
1565638_at	PMP22	1.6	peripheral myelin protein 22	synaptic transmission
203400_s_at	TF	1.4	transferrin	regulation of myelination
Blood coagulation				
205479_s_at	PLAU	3.3	plasminogen activator, urokinase	blood coagulation
210845_s_at	PLAUR	4.2	plasminogen activator, urokinase receptor	blood coagulation
202628_s_at	SERPINE1	8.6	serpin peptidase inhibitor, clade E (nexin, plasminogen activator inhibitor type 1), member 1	blood coagulation
203887_s_at	THBD	6.7	thrombomodulin	blood coagulation
218995_s_at	EDN1	1.8	endothelin 1	regulation of blood coagulation
Keratin filament				
234639_x_at	KRTAP9-8	-1.7	keratin associated protein 9-8	keratin filament
Ribokinase activity				
1568768_s_at	RBKS	6.7	ribokinase	ribokinase activity

Table A-10. Continued.

Probe set	Symbol	Fold change	Description	Function
Helicase activity				
1568815_a_at	DDX50	1.7	DEAD (Asp-Glu-Ala-Asp) box polypeptide 50	helicase activity
208152_s_at	DDX21	3.1	DEAD (Asp-Glu-Ala-Asp) box polypeptide 21	helicase activity
221031_s_at	APOLD1	5.6	apolipoprotein L domain containing 1	helicase activity
211787_s_at	EIF4A1	2.6	eukaryotic translation initiation factor 4A, isoform 1	helicase activity
208896_at	DDX18	1.6	DEAD (Asp-Glu-Ala-Asp) box polypeptide 18	helicase activity
204258_at	CHD1	2.8	chromodomain helicase DNA binding protein 1	helicase activity
212515_s_at	DDX3X	1.8	DEAD (Asp-Glu-Ala-Asp) box polypeptide 3, X-linked	helicase activity
205000_at	DDX3Y	2.0	DEAD (Asp-Glu-Ala-Asp) box polypeptide 3, Y-linked	helicase activity
Transferase activity				
51146_at	PIGV	-1.8	phosphatidylinositol glycan anchor biosynthesis, class V	transferase activity
209340_at	UAP1	2.8	UDP-N-acteylglucosamine pyrophosphorylase 1	transferase activity
221561_at	SOAT1	2.0	sterol O-acyltransferase (acyl-Coenzyme A: cholesterol acyltransferase) 1	transferase activity
1552611_a_at	JAK1	1.5	Janus kinase 1 (a protein tyrosine kinase)	transferase activity
225420_at	GPAM	-1.8	glycerol-3-phosphate acyltransferase, mitochondrial	transferase activity
202238_s_at	NNMT	4.0	nicotinamide N-methyltransferase	transferase activity
224454_at	ETNK1	4.0	ethanolamine kinase 1	transferase activity
203127_s_at	SPTLC2	1.7	serine palmitoyltransferase, long chain base subunit 2	transferase activity
203044_at	CHSY1	3.9	carbohydrate (chondroitin) synthase 1	transferase activity
227361_at	HS3ST3B1	2.0	heparan sulfate (glucosamine) 3-O-sulfotransferase 3B1	transferase activity
228772_at	HNMT	-1.8	histamine N-methyltransferase	transferase activity
205077_s_at	PIGF	-1.5	phosphatidylinositol glycan anchor biosynthesis, class F	transferase activity
1569136_at	MGAT4A	2.3	mannosyl (alpha-1,3-)-glycoprotein beta-1,4-N-acetylglucosaminyltransferase, isozyme A	transferase activity
1559391_s_at	B4GALT5	2.2	UDP-Gal:betaGlcNAc beta 1,4- galactosyltransferase, polypeptide 5	transferase activity

Table A-10. Continued.

Probe set	Symbol	Fold change	Description	Function
225612_s_at	B3GNT5	5.4	UDP-GlcNAc:betaGal beta-1,3-N-acetylglucosaminyltransferase 5	transferase activity
228762_at	LFNG	-2.0	LFNG O-fucosylpeptide 3-beta-N-acetylglucosaminyltransferase	transferase activity
203234_at	UPP1	3.2	uridine phosphorylase 1	transferase activity
238902_at	PCMTD1	-1.5	protein-L-isoaspartate (D-aspartate) O-methyltransferase domain containing 1	transferase activity
238346_s_at	TGS1	1.6	trimethylguanosine synthase homolog (S. cerevisiae)	transferase activity
206432_at	HAS2	4.5	hyaluronan synthase 2	transferase activity
204881_s_at	UGCG	5.0	UDP-glucose ceramide glucosyltransferase	transferase activity
213988_s_at	SAT1	2.8	spermidine/spermine N1-acetyltransferase 1	transferase activity
Hydrolase activity				
203708_at	PDE4B	2.6	phosphodiesterase 4B, cAMP-specific (phosphodiesterase E4 dunce homolog, Drosophila)	hydrolase activity
239516_at	LYPLAL1	-3.5	lysophospholipase-like 1	hydrolase activity
209355_s_at	PPAP2B	2.1	phosphatidic acid phosphatase type 2B	hydrolase activity
209585_s_at	MINPP1	-1.6	multiple inositol polyphosphate histidine phosphatase, 1	hydrolase activity
209457_at	DUSP5	2.5	dual specificity phosphatase 5	hydrolase activity
208893_s_at	DUSP6	2.5	dual specificity phosphatase 6	hydrolase activity
221752_at	SSH1	1.5	slingshot homolog 1 (Drosophila)	hydrolase activity
215095_at	ESD	-1.5	esterase D/formylglutathione hydrolase	hydrolase activity
201761_at	MTHFD2	2.4	methylenetetrahydrofolate dehydrogenase (NADP+ dependent) 2, methenyltetrahydrofolate cyclohydrolase	hydrolase activity
202716_at	PTPN1	2.2	protein tyrosine phosphatase, non-receptor type 1	hydrolase activity
224826_at	RP5-1022P6.2	1.7	hypothetical protein KIAA1434	hydrolase activity
238419_at	PHLDB2	2.0	pleckstrin homology-like domain, family B, member 2	hydrolase activity
219003_s_at	MANEA	-1.5	mannosidase, endo-alpha	hydrolase activity
206177_s_at	ARG1	4.5	arginase, liver	hydrolase activity
204014_at	DUSP4	1.8	dual specificity phosphatase 4	hydrolase activity

Table A-10. Continued.

Probe set	Symbol	Fold change	Description	Function
Ligase activity				
200648_s_at	GLUL	2.1	glutamate-ammonia ligase (glutamine synthetase)	ligase activity
Lyase activity				
201196_s_at	AMD1	2.3	adenosylmethionine decarboxylase 1	lyase activity
Spermatogenesis				
214911_s_at	BRD2	1.7	bromodomain containing 2	spermatogensis
Regulation of translation				
224692_at	PPP1R15B	2.1	protein phosphatase 1, regulatory (inhibitor) subunit 15B	regulation of translation

Table A-11. Expression of unknown function genes that are significantly different in the diaphragm after surgery

Probe set	Symbol	Fold change	Description	Function
222333_at	ALS2CL	1.9	ALS2 C-terminal like	unknown functions
231999_at	ANKRD11	1.5	ankyrin repeat domain 11	unknown functions
225735_at	ANKRD50	-1.5	ankyrin repeat domain 50	unknown functions
205239_at	AREG	5.7	amphiregulin (schwannoma-derived growth factor)	unknown functions
211947_s_at	BAT2D1	1.5	BAT2 domain containing 1	unknown functions
229437_at	BIC	2.7	BIC transcript	unknown functions
226383_at	C11orf46	-1.7	chromosome 11 open reading frame 46	unknown functions
218214_at	C12orf44	1.5	chromosome 12 open reading frame 44	unknown functions
227058_at	C13orf33	4.0	chromosome 13 open reading frame 33	unknown functions
227446_s_at	C14orf167	-1.9	chromosome 14 open reading frame 167	unknown functions
223474_at	C14orf4	1.6	chromosome 14 open reading frame 4	unknown functions
217682_at	C16orf72	1.9	chromosome 16 open reading frame 72	unknown functions
1553338_at	C1orf55	1.5	chromosome 1 open reading frame 55	unknown functions
209020_at	C20orf111	1.7	chromosome 20 open reading frame 111	unknown functions
1552605_s_at	C21orf74	1.5	chromosome 21 open reading frame 74	unknown functions
228067_at	C2orf55	2.4	chromosome 2 open reading frame 55	unknown functions
222309_at	C6orf62	2.4	chromosome 6 open reading frame 62	unknown functions
236634_at	C8orf48	-1.6	chromosome 8 open reading frame 48	unknown functions
222706_at	CCDC49	1.5	coiled-coil domain containing 49	unknown functions
1553214_a_at	CCDC7	-1.7	coiled-coil domain containing 7	unknown functions
227517_s_at	CENPL	2.0	centromere protein L	unknown functions
224991_at	CMIP	1.9	c-Maf-inducing protein	unknown functions
219397_at	COQ10B	1.9	coenzyme Q10 homolog B (S. cerevisiae)	unknown functions
1557954_at	CXorf15	1.4	chromosome X open reading frame 15	unknown functions

Table A-11. Continued.

Probe set	Symbol	Fold change	Description	Function
1556113_at	DKFZp451A211	2.5	DKFZp451A211 protein	unknown functions
1569987_at	DLEU7	-1.5	deleted in lymphocytic leukemia, 7	unknown functions
236649_at	DTWD1	-1.8	DTW domain containing 1	unknown functions
1563315_s_at	ERICH1	1.8	glutamate-rich 1	unknown functions
219216_at	ETAA1	-2.0	Ewing tumor-associated antigen 1	unknown functions
223038_s_at	FAM60A	1.7	family with sequence similarity 60, member A	unknown functions
244014_x_at	FAM92A1	-1.6	family with sequence similarity 92, member A1	unknown functions
1553797_a_at	FLJ30594	-2.3	hypothetical locus FLJ30594	unknown functions
229521_at	FLJ36031	4.8	hypothetical protein FLJ36031	unknown functions
241858_at	FPGT	-2.0	fucose-1-phosphate guanylyltransferase	unknown functions
232035_at	HIST1H4H	2.2	histone cluster 1, H4h	unknown functions
203023_at	HSPC111	1.9	hypothetical protein HSPC111	unknown functions
202081_at	IER2	2.9	immediate early response 2	unknown functions
218611_at	IER5	2.6	immediate early response 5	unknown functions
203144_s_at	KIAA0040	3.1	KIAA0040	unknown functions
228325_at	KIAA0146	5.6	KIAA0146	unknown functions
228334_x_at	KIAA1712	-1.6	KIAA1712	unknown functions
227099_s_at	LOC387763	3.8	hypothetical LOC387763	unknown functions
225857_s_at	LOC388796	1.8	hypothetical LOC388796	unknown functions
220770_s_at	LOC63920	-2.3	transposon-derived Buster3 transposase-like	unknown functions

Table A-11. Continued.

Probe set	Symbol	Fold change	Description	Function
224558_s_at	MALAT1	1.4	metastasis associated lung adenocarcinoma transcript 1 (non-coding RNA)	unknown functions
213761_at	MDM1	-1.6	Mdm4, transformed 3T3 cell double minute 1, p53 binding protein (mouse)	unknown functions
211456_x_at	MT1P2	3.2	metallothionein 1 pseudogene 2	unknown functions
236273_at	NBPF1	-1.4	neuroblastoma breakpoint family, member 1	unknown functions
218319_at	PELI1	3.0	pellino homolog 1 (Drosophila)	unknown functions
219093_at	PID1	-1.8	phosphotyrosine interaction domain containing 1	unknown functions
225699_at	SNORA9	2.5	small nucleolar RNA, H/ACA box 9	unknown functions
214965_at	SPATA2L	1.9	spermatogenesis associated 2-like	unknown functions
233242_at	WDR73	1.5	WD repeat domain 73	unknown functions
218647_s_at	YRDC	2.0	yrdC domain containing (E. coli)	unknown functions
228280_at	ZC3HAV1L	-1.6	zinc finger CCCH-type, antiviral 1-like	unknown functions

LIST OF REFERENCES

1. Liu LL, Gropper MA. Respiratory and hemodynamic management after cardiac surgery. *Curr Treat Options Cardiovasc Med* 2002;4:161-169.

2. Pappalardo F, Franco A, Landoni G, Cardano P, Zangrillo A, Alfieri O. Long-term outcome and quality of life of patients requiring prolonged mechanical ventilation after cardiac surgery. *Eur J Cardiothorac Surg* 2004;25:548-552.

3. Fagon JY, Chastre J, Domart Y, Trouillet JL, Pierre J, Darne C, Gibert C. Nosocomial pneumonia in patients receiving continuous mechanical ventilation. Prospective analysis of 52 episodes with use of a protected specimen brush and quantitative culture techniques. *Am Rev Respir Dis* 1989;139:877-884.

4. Scheinhorn DJ, Hassenpflug MS, Votto JJ, Chao DC, Epstein SK, Doig GS, Knight EB, Petrak RA. Ventilator-dependent survivors of catastrophic illness transferred to 23 long-term care hospitals for weaning from prolonged mechanical ventilation. *Chest* 2007;131:76-84.

5. Combes A, Costa MA, Trouillet JL, Baudot J, Mokhtari M, Gibert C, Chastre J. Morbidity, mortality, and quality-of-life outcomes of patients requiring >or=14 days of mechanical ventilation. *Crit Care Med* 2003;31:1373-1381.

6. Capdevila X, Lopez S, Bernard N, Rabischong E, Ramonatxo M, Martinazzo G, Prefaut C. Effects of controlled mechanical ventilation on respiratory muscle contractile properties in rabbits. *Intensive Care Med* 2003;29:103-110.

7. Le Bourdelles G, Viires N, Boczkowski J, Seta N, Pavlovic D, Aubier M. Effects of mechanical ventilation on diaphragmatic contractile properties in rats. *Am J Respir Crit Care Med* 1994;149:1539-1544.

8. Powers SK, Shanely RA, Coombes JS, Koesterer TJ, McKenzie M, Van Gammeren D, Cicale M, Dodd SL. Mechanical ventilation results in progressive contractile dysfunction in the diaphragm. *J Appl Physiol* 2002;92:1851-1858.

9. Sassoon CS, Caiozzo VJ, Manka A, Sieck GC. Altered diaphragm contractile properties with controlled mechanical ventilation. *J Appl Physiol* 2002;92:2585-2595.

10. Shanely RA, Zergeroglu MA, Lennon SL, Sugiura T, Yimlamai T, Enns D, Belcastro A, Powers SK. Mechanical ventilation-induced diaphragmatic atrophy is associated with oxidative injury and increased proteolytic activity. *Am J Respir Crit Care Med* 2002;166:1369-1374.

11. Yang L, Luo J, Bourdon J, Lin MC, Gottfried SB, Petrof BJ. Controlled mechanical ventilation leads to remodeling of the rat diaphragm. *Am J Respir Crit Care Med* 2002;166:1135-1140.

12. Zergeroglu MA, McKenzie MJ, Shanely RA, Van Gammeren D, DeRuisseau KC, Powers SK. Mechanical ventilation-induced oxidative stress in the diaphragm. *J Appl Physiol* 2003;95:1116-1124.

13. Levine S, Nguyen T, Taylor N, Friscia ME, Budak MT, Rothenberg P, Zhu J, Sachdeva R, Sonnad S, Kaiser LR, et al. Rapid disuse atrophy of diaphragm fibers in mechanically ventilated humans. *N Engl J Med* 2008;358:1327-1335.

14. Shanely RA, Van Gammeren D, Deruisseau KC, Zergeroglu AM, McKenzie MJ, Yarasheski KE, Powers SK. Mechanical ventilation depresses protein synthesis in the rat diaphragm. *Am J Respir Crit Care Med* 2004;170:994-999.

15. Bernard N, Matecki S, Py G, Lopez S, Mercier J, Capdevila X. Effects of prolonged mechanical ventilation on respiratory muscle ultrastructure and mitochondrial respiration in rabbits. *Intensive Care Med* 2003;29:111-118.

16. Radell P, Edstrom L, Stibler H, Eriksson LI, Ansved T. Changes in diaphragm structure following prolonged mechanical ventilation in piglets. *Acta Anaesthesiol Scand* 2004;48:430-437.

17. DeRuisseau KC, Shanely RA, Akunuri N, Hamilton MT, Van Gammeren D, Zergeroglu AM, McKenzie M, Powers SK. Diaphragm unloading via controlled mechanical ventilation alters the gene expression profile. *Am J Respir Crit Care Med* 2005;172:1267-1275.

18. Geiger PC, Cody MJ, Macken RL, Sieck GC. Maximum specific force depends on myosin heavy chain content in rat diaphragm muscle fibers. *J Appl Physiol* 2000;89:695-703.

19. Reid MB. Invited review: Redox modulation of skeletal muscle contraction: What we know and what we don't. *J Appl Physiol* 2001;90:724-731.

20. Shringarpure R, Davies KJ. Protein turnover by the proteasome in aging and disease. *Free Radic Biol Med* 2002;32:1084-1089.

21. Grisotto PC, dos Santos AC, Coutinho-Netto J, Cherri J, Piccinato CE. Indicators of oxidative injury and alterations of the cell membrane in the skeletal muscle of rats submitted to ischemia and reperfusion. *J Surg Res* 2000;92:1-6.

22. Vassilakopoulos T, Petrof BJ. Ventilator-induced diaphragmatic dysfunction. *Am J Respir Crit Care Med* 2004;169:336-341.

23. Argiles JM, Lopez-Soriano FJ. The ubiquitin-dependent proteolytic pathway in skeletal muscle: Its role in pathological states. *Trends Pharmacol Sci* 1996;17:223-226.

24. Jagoe RT, Goldberg AL. What do we really know about the ubiquitin-proteasome pathway in muscle atrophy? *Curr Opin Clin Nutr Metab Care* 2001;4:183-190.

25. Gomes MD, Lecker SH, Jagoe RT, Navon A, Goldberg AL. Atrogin-1, a muscle-specific f-box protein highly expressed during muscle atrophy. *Proc Natl Acad Sci U S A* 2001;98:14440-14445.

26. Sassoon CS, Zhu E, Caiozzo VJ. Assist-control mechanical ventilation attenuates ventilator-induced diaphragmatic dysfunction. *Am J Respir Crit Care Med* 2004;170:626-632.

27. Zhu E, Sassoon CS, Nelson R, Pham HT, Zhu L, Baker MJ, Caiozzo VJ. Early effects of mechanical ventilation on isotonic contractile properties and maf-box gene expression in the diaphragm. *J Appl Physiol* 2005;99:747-756.

28. DeRuisseau KC, Kavazis AN, Deering MA, Falk DJ, Van Gammeren D, Yimlamai T, Ordway GA, Powers SK. Mechanical ventilation induces alterations of the ubiquitin-proteasome pathway in the diaphragm. *J Appl Physiol* 2005;98:1314-1321.

29. Knisely AS, Leal SM, Singer DB. Abnormalities of diaphragmatic muscle in neonates with ventilated lungs. *J Pediatr* 1988;113:1074-1077.

30. Hunter RB, Stevenson E, Koncarevic A, Mitchell-Felton H, Essig DA, Kandarian SC. Activation of an alternative nf-kappab pathway in skeletal muscle during disuse atrophy. *FASEB J* 2002;16:529-538.

31. Jackman RW, Kandarian SC. The molecular basis of skeletal muscle atrophy. *Am J Physiol Cell Physiol* 2004;287:C834-843.

32. Kandarian SC, Jackman RW. Intracellular signaling during skeletal muscle atrophy. *Muscle Nerve* 2006;33:155-165.

33. Zhang P, Chen X, Fan M. Signaling mechanisms involved in disuse muscle atrophy. *Med Hypotheses* 2007;69:310-321.

34. Hunter RB, Kandarian SC. Disruption of either the nfkb1 or the bcl3 gene inhibits skeletal muscle atrophy. *J Clin Invest* 2004;114:1504-1511.

35. Cai D, Frantz JD, Tawa NE, Jr., Melendez PA, Oh BC, Lidov HG, Hasselgren PO, Frontera WR, Lee J, Glass DJ, et al. Ikkbeta/nf-kappab activation causes severe muscle wasting in mice. *Cell* 2004;119:285-298.

36. Stevenson EJ, Giresi PG, Koncarevic A, Kandarian SC. Global analysis of gene expression patterns during disuse atrophy in rat skeletal muscle. *J Physiol* 2003;551:33-48.

37. Lecker SH, Jagoe RT, Gilbert A, Gomes M, Baracos V, Bailey J, Price SR, Mitch WE, Goldberg AL. Multiple types of skeletal muscle atrophy involve a common program of changes in gene expression. *FASEB J* 2004;18:39-51.

38. Glass DJ. Skeletal muscle hypertrophy and atrophy signaling pathways. *Int J Biochem Cell Biol* 2005;37:1974-1984.

39. Glass DJ. Molecular mechanisms modulating muscle mass. *Trends Mol Med* 2003;9:344-350.

40. Sacheck JM, Ohtsuka A, McLary SC, Goldberg AL. Igf-i stimulates muscle growth by suppressing protein breakdown and expression of atrophy-related ubiquitin ligases, atrogin-1 and murf1. *Am J Physiol Endocrinol Metab* 2004;287:E591-601.

41. Hornberger TA, Hunter RB, Kandarian SC, Esser KA. Regulation of translation factors during hindlimb unloading and denervation of skeletal muscle in rats. *Am J Physiol Cell Physiol* 2001;281:C179-187.

42. Chen WS, Xu PZ, Gottlob K, Chen ML, Sokol K, Shiyanova T, Roninson I, Weng W, Suzuki R, Tobe K, et al. Growth retardation and increased apoptosis in mice with homozygous disruption of the akt1 gene. *Genes Dev* 2001;15:2203-2208.

43. Peng XD, Xu PZ, Chen ML, Hahn-Windgassen A, Skeen J, Jacobs J, Sundararajan D, Chen WS, Crawford SE, Coleman KG, et al. Dwarfism, impaired skin development, skeletal muscle atrophy, delayed bone development, and impeded adipogenesis in mice lacking akt1 and akt2. *Genes Dev* 2003;17:1352-1365.

44. Carlsson P, Mahlapuu M. Forkhead transcription factors: Key players in development and metabolism. *Dev Biol* 2002;250:1-23.

45. Brunet A, Bonni A, Zigmond MJ, Lin MZ, Juo P, Hu LS, Anderson MJ, Arden KC, Blenis J, Greenberg ME. Akt promotes cell survival by phosphorylating and inhibiting a forkhead transcription factor. *Cell* 1999;96:857-868.

46. Ramaswamy S, Nakamura N, Sansal I, Bergeron L, Sellers WR. A novel mechanism of gene regulation and tumor suppression by the transcription factor fkhr. *Cancer Cell* 2002;2:81-91.

47. Stitt TN, Drujan D, Clarke BA, Panaro F, Timofeyva Y, Kline WO, Gonzalez M, Yancopoulos GD, Glass DJ. The igf-1/pi3k/akt pathway prevents expression of muscle atrophy-induced ubiquitin ligases by inhibiting foxo transcription factors. *Mol Cell* 2004;14:395-403.

48. Kamei Y, Miura S, Suzuki M, Kai Y, Mizukami J, Taniguchi T, Mochida K, Hata T, Matsuda J, Aburatani H, et al. Skeletal muscle foxo1 (fkhr) transgenic mice have less skeletal muscle mass, down-regulated type i (slow twitch/red muscle) fiber genes, and impaired glycemic control. *J Biol Chem* 2004;279:41114-41123.

49. Sandri M, Sandri C, Gilbert A, Skurk C, Calabria E, Picard A, Walsh K, Schiaffino S, Lecker SH, Goldberg AL. Foxo transcription factors induce the atrophy-related ubiquitin ligase atrogin-1 and cause skeletal muscle atrophy. *Cell* 2004;117:399-412.

50. Primeau AJ, Adhihetty PJ, Hood DA. Apoptosis in heart and skeletal muscle. *Can J Appl Physiol* 2002;27:349-395.

51. Lecker SH, Solomon V, Mitch WE, Goldberg AL. Muscle protein breakdown and the critical role of the ubiquitin-proteasome pathway in normal and disease states. *J Nutr* 1999;129:227S-237S.

52. Du J, Wang X, Miereles C, Bailey JL, Debigare R, Zheng B, Price SR, Mitch WE. Activation of caspase-3 is an initial step triggering accelerated muscle proteolysis in catabolic conditions. *J Clin Invest* 2004;113:115-123.

53. McClung JM, Kavazis AN, DeRuisseau KC, Falk DJ, Deering MA, Lee Y, Sugiura T, Powers SK. Caspase-3 regulation of diaphragm myonuclear domain during mechanical ventilation-induced atrophy. *Am J Respir Crit Care Med* 2007;175:150-159.

54. Powers SK, Kavazis AN, McClung JM. Oxidative stress and disuse muscle atrophy. *J Appl Physiol* 2007;102:2389-2397.

55. Chen M, Won DJ, Krajewski S, Gottlieb RA. Calpain and mitochondria in ischemia/reperfusion injury. *J Biol Chem* 2002;277:29181-29186.

56. Dupont-Versteegden EE. Apoptosis in skeletal muscle and its relevance to atrophy. *World J Gastroenterol* 2006;12:7463-7466.

57. Dupont-Versteegden EE, Strotman BA, Gurley CM, Gaddy D, Knox M, Fluckey JD, Peterson CA. Nuclear translocation of endog at the initiation of disuse muscle atrophy and apoptosis is specific to myonuclei. *Am J Physiol Regul Integr Comp Physiol* 2006;291:R1730-1740.

58. Ferreira R, Neuparth MJ, Vitorino R, Appell HJ, Amado F, Duarte JA. Evidences of apoptosis during the early phases of soleus muscle atrophy in hindlimb suspended mice. *Physiol Res* 2008;57:601-611.

59. Ventadour S, Attaix D. Mechanisms of skeletal muscle atrophy. *Curr Opin Rheumatol* 2006;18:631-635.

60. Mayer RJ. The meteoric rise of regulated intracellular proteolysis. *Nat Rev Mol Cell Biol* 2000;1:145-148.

61. Hicke L. Gettin' down with ubiquitin: Turning off cell-surface receptors, transporters and channels. *Trends Cell Biol* 1999;9:107-112.

62. Hicke L, Dunn R. Regulation of membrane protein transport by ubiquitin and ubiquitin-binding proteins. *Annu Rev Cell Dev Biol* 2003;19:141-172.

63. Goll DE, Thompson VF, Li H, Wei W, Cong J. The calpain system. *Physiol Rev* 2003;83:731-801.

64. Huang J, Forsberg NE. Role of calpain in skeletal-muscle protein degradation. *Proc Natl Acad Sci U S A* 1998;95:12100-12105.

65. Bartoli M, Richard I. Calpains in muscle wasting. *Int J Biochem Cell Biol* 2005;37:2115-2133.

66. Attaix D, Ventadour S, Codran A, Bechet D, Taillandier D, Combaret L. The ubiquitin-proteasome system and skeletal muscle wasting. *Essays Biochem* 2005;41:173-186.

67. Solomon V, Baracos V, Sarraf P, Goldberg AL. Rates of ubiquitin conjugation increase when muscles atrophy, largely through activation of the n-end rule pathway. *Proc Natl Acad Sci U S A* 1998;95:12602-12607.

68. Taillandier D, Aurousseau E, Meynial-Denis D, Bechet D, Ferrara M, Cottin P, Ducastaing A, Bigard X, Guezennec CY, Schmid HP, et al. Coordinate activation of lysosomal, ca 2+-activated and atp-ubiquitin-dependent proteinases in the unweighted rat soleus muscle. *Biochem J* 1996;316 (Pt 1):65-72.

69. Bodine SC, Latres E, Baumhueter S, Lai VK, Nunez L, Clarke BA, Poueymirou WT, Panaro FJ, Na E, Dharmarajan K, et al. Identification of ubiquitin ligases required for skeletal muscle atrophy. *Science* 2001;294:1704-1708.

70. Powers SK, Kavazis AN, DeRuisseau KC. Mechanisms of disuse muscle atrophy: Role of oxidative stress. *Am J Physiol Regul Integr Comp Physiol* 2005;288:R337-344.

71. Kondo H, Miura M, Itokawa Y. Oxidative stress in skeletal muscle atrophied by immobilization. *Acta Physiol Scand* 1991;142:527-528.

72. Appell HJ, Duarte JA, Soares JM. Supplementation of vitamin e may attenuate skeletal muscle immobilization atrophy. *Int J Sports Med* 1997;18:157-160.

73. Betters JL, Criswell DS, Shanely RA, Van Gammeren D, Falk D, Deruisseau KC, Deering M, Yimlamai T, Powers SK. Trolox attenuates mechanical ventilation-induced diaphragmatic dysfunction and proteolysis. *Am J Respir Crit Care Med* 2004;170:1179-1184.

74. Haddad JJ. Antioxidant and prooxidant mechanisms in the regulation of redox(y)-sensitive transcription factors. *Cell Signal* 2002;14:879-897.

75. Li YP, Schwartz RJ, Waddell ID, Holloway BR, Reid MB. Skeletal muscle myocytes undergo protein loss and reactive oxygen-mediated nf-kappab activation in response to tumor necrosis factor alpha. *FASEB J* 1998;12:871-880.

76. Cuschieri J, Maier RV. Mitogen-activated protein kinase (mapk). *Crit Care Med* 2005;33:S417-419.

77. Kramer HF, Goodyear LJ. Exercise, mapk, and nf-kappab signaling in skeletal muscle. *J Appl Physiol* 2007;103:388-395.

78. Kefaloyianni E, Gaitanaki C, Beis I. Erk1/2 and p38-mapk signalling pathways, through msk1, are involved in nf-kappab transactivation during oxidative stress in skeletal myoblasts. *Cell Signal* 2006;18:2238-2251.

79. Childs TE, Spangenburg EE, Vyas DR, Booth FW. Temporal alterations in protein signaling cascades during recovery from muscle atrophy. *Am J Physiol Cell Physiol* 2003;285:C391-398.

80. Shen HM, Liu ZG. Jnk signaling pathway is a key modulator in cell death mediated by reactive oxygen and nitrogen species. *Free Radic Biol Med* 2006;40:928-939.

81. Macgowan NA, Evans KG, Road JD, Reid WD. Diaphragm injury in individuals with airflow obstruction. *Am J Respir Crit Care Med* 2001;163:1654-1659.

82. Mercadier JJ, Schwartz K, Schiaffino S, Wisnewsky C, Ausoni S, Heimburger M, Marrash R, Pariente R, Aubier M. Myosin heavy chain gene expression changes in the diaphragm of patients with chronic lung hyperinflation. *Am J Physiol* 1998;274:L527-534.

83. Moore AJ, Stubbings A, Swallow EB, Dusmet M, Goldstraw P, Porcher R, Moxham J, Polkey MI, Ferenczi MA. Passive properties of the diaphragm in copd. *J Appl Physiol* 2006;101:1400-1405.

84. 84. Ottenheijm CA, Heunks LM, Dekhuijzen RP. Diaphragm adaptations in patients with copd. *Respir Res* 2008;9:12.

85. Ottenheijm CA, Heunks LM, Hafmans T, van der Ven PF, Benoist C, Zhou H, Labeit S, Granzier HL, Dekhuijzen PN. Titin and diaphragm dysfunction in chronic obstructive pulmonary disease. *Am J Respir Crit Care Med* 2006;173:527-534.

86. Ottenheijm CA, Heunks LM, Li YP, Jin B, Minnaard R, van Hees HW, Dekhuijzen PN. Activation of the ubiquitin-proteasome pathway in the diaphragm in chronic obstructive pulmonary disease. *Am J Respir Crit Care Med* 2006;174:997-1002.

87. Ottenheijm CA, Heunks LM, Sieck GC, Zhan WZ, Jansen SM, Degens H, de Boo T, Dekhuijzen PN. Diaphragm dysfunction in chronic obstructive pulmonary disease. *Am J Respir Crit Care Med* 2005;172:200-205.

88. Ottenheijm CA, Jenniskens GJ, Geraedts MC, Hafmans T, Heunks LM, van Kuppevelt TH, Dekhuijzen PN. Diaphragm dysfunction in chronic obstructive pulmonary disease: A role for heparan sulphate? *Eur Respir J* 2007;30:80-89.

89. Li C, Hung Wong W. Model-based analysis of oligonucleotide arrays: Model validation, design issues and standard error application. *Genome Biol* 2001;2:RESEARCH0032.

90. Holter NS, Mitra M, Maritan A, Cieplak M, Banavar JR, Fedoroff NV. Fundamental patterns underlying gene expression profiles: Simplicity from complexity. *Proc Natl Acad Sci U S A* 2000;97:8409-8414.

91. Storey JD, Tibshirani R. Statistical significance for genomewide studies. *Proc Natl Acad Sci U S A* 2003;100:9440-9445.

92. Khatri P, Voichita C, Kattan K, Ansari N, Khatri A, Georgescu C, Tarca AL, Draghici S. Onto-tools: New additions and improvements in 2006. *Nucleic Acids Res* 2007;35:W206-211.

93. Haddad F, Zaldivar F, Cooper DM, Adams GR. Il-6-induced skeletal muscle atrophy. *J Appl Physiol* 2005;98:911-917.

94. Metcalf D, Greenhalgh CJ, Viney E, Willson TA, Starr R, Nicola NA, Hilton DJ, Alexander WS. Gigantism in mice lacking suppressor of cytokine signalling-2. *Nature* 2000;405:1069-1073.

95. Kang SW, Baines IC, Rhee SG. Characterization of a mammalian peroxiredoxin that contains one conserved cysteine. *J Biol Chem* 1998;273:6303-6311.

96. Da Silva-Azevedo L, Jahne S, Hoffmann C, Stalder D, Heller M, Pries AR, Zakrzewicz A, Baum O. Up-regulation of the peroxiredoxin-6 related metabolism of reactive oxygen species in skeletal muscle of mice lacking neuronal nitric oxide synthase. *J Physiol* 2008.

97. Wang X, Phelan SA, Forsman-Semb K, Taylor EF, Petros C, Brown A, Lerner CP, Paigen B. Mice with targeted mutation of peroxiredoxin 6 develop normally but are susceptible to oxidative stress. *J Biol Chem* 2003;278:25179-25190.

98. Richter C, Park JW, Ames BN. Normal oxidative damage to mitochondrial and nuclear DNA is extensive. *Proc Natl Acad Sci U S A* 1988;85:6465-6467.

99. Falk DJ, Deruisseau KC, Van Gammeren DL, Deering MA, Kavazis AN, Powers SK. Mechanical ventilation promotes redox status alterations in the diaphragm. *J Appl Physiol* 2006;101:1017-1024.

100. Chen Y, Cai J, Jones DP. Mitochondrial thioredoxin in regulation of oxidant-induced cell death. *FEBS Lett* 2006;580:6596-6602.

101. 101. Matsushima Y, Nanri H, Nara S, Okufuji T, Ohta M, Hachisuka K, Ikeda M. Hindlimb unloading decreases thioredoxin-related antioxidant proteins and increases thioredoxin-binding protein-2 in rat skeletal muscle. *Free Radic Res* 2006;40:715-722.

102. Hirota K, Murata M, Sachi Y, Nakamura H, Takeuchi J, Mori K, Yodoi J. Distinct roles of thioredoxin in the cytoplasm and in the nucleus. A two-step mechanism of redox regulation of transcription factor nf-kappab. *J Biol Chem* 1999;274:27891-27897.

103. Thomason DB, Booth FW. Atrophy of the soleus muscle by hindlimb unweighting. *J Appl Physiol* 1990;68:1-12.

104. Chen YW, Gregory CM, Scarborough MT, Shi R, Walter GA, Vandenborne K. Transcriptional pathways associated with skeletal muscle disuse atrophy in humans. *Physiol Genomics* 2007;31:510-520.

105. 1Nordquist J, Hoglund AS, Norman H, Tang X, Dworkin B, Larsson L. Transcription factors in muscle atrophy caused by blocked neuromuscular transmission and muscle unloading in rats. *Mol Med* 2007;13:461-470.

106. Mitch WE, Goldberg AL. Mechanisms of muscle wasting. The role of the ubiquitin-proteasome pathway. *N Engl J Med* 1996;335:1897-1905.

107. Murton AJ, Constantin D, Greenhaff PL. The involvement of the ubiquitin proteasome system in human skeletal muscle remodelling and atrophy. *Biochim Biophys Acta* 2008;1782:730-743.

108. de Boer MD, Selby A, Atherton P, Smith K, Seynnes OR, Maganaris CN, Maffulli N, Movin T, Narici MV, Rennie MJ. The temporal responses of protein synthesis, gene expression and cell signalling in human quadriceps muscle and patellar tendon to disuse. *J Physiol* 2007;585:241-251.

109. Menconi MJ, Wei W, Yang H, Wray CJ, Hasselgren PO. Treatment of cultured myotubes with the calcium ionophore a23187 increases proteasome activity via a camk ii-caspase-calpain-dependent mechanism. *Surgery* 2004;136:135-142.

110. Smith IJ, Dodd SL. Calpain activation causes a proteasome-dependent increase in protein degradation and inhibits the akt signalling pathway in rat diaphragm muscle. *Exp Physiol* 2007;92:561-573.

111. Tidball JG, Spencer MJ. Expression of a calpastatin transgene slows muscle wasting and obviates changes in myosin isoform expression during murine muscle disuse. *J Physiol* 2002;545:819-828.

112. Lo AS, Liew CT, Ngai SM, Tsui SK, Fung KP, Lee CY, Waye MM. Developmental regulation and cellular distribution of human cytosolic malate dehydrogenase (mdh1). *J Cell Biochem* 2005;94:763-773.

113. Grant PM, Roderick SL, Grant GA, Banaszak LJ, Strauss AW. Comparison of the precursor and mature forms of rat heart mitochondrial malate dehydrogenase. *Biochemistry* 1987;26:128-134.

114. Kwon HS, Huang B, Ho Jeoung N, Wu P, Steussy CN, Harris RA. Retinoic acids and trichostatin a (tsa), a histone deacetylase inhibitor, induce human pyruvate dehydrogenase kinase 4 (pdk4) gene expression. *Biochim Biophys Acta* 2006;1759:141-151.

115. Sugden MC, Holness MJ. Recent advances in mechanisms regulating glucose oxidation at the level of the pyruvate dehydrogenase complex by pdks. *Am J Physiol Endocrinol Metab* 2003;284:E855-862.

116. Wittwer M, Fluck M, Hoppeler H, Muller S, Desplanches D, Billeter R. Prolonged unloading of rat soleus muscle causes distinct adaptations of the gene profile. *FASEB J* 2002;16:884-886.

117. Mazzatti DJ, Smith MA, Oita RC, Lim FL, White AJ, Reid MB. Muscle unloading-induced metabolic remodeling is associated with acute alterations in ppardelta and ucp-3 expression. *Physiol Genomics* 2008;34:149-161.

118. Edmondson DG, Olson EN. Helix-loop-helix proteins as regulators of muscle-specific transcription. *J Biol Chem* 1993;268:755-758.

119. Adams GR, Haddad F, Baldwin KM. Time course of changes in markers of myogenesis in overloaded rat skeletal muscles. *J Appl Physiol* 1999;87:1705-1712.

120. Staib JL, Swoap SJ, Powers SK. Diaphragm contractile dysfunction in myod gene-inactivated mice. *Am J Physiol Regul Integr Comp Physiol* 2002;283:R583-590.

121. Tajbakhsh S, Rocancourt D, Buckingham M. Muscle progenitor cells failing to respond to positional cues adopt non-myogenic fates in myf-5 null mice. *Nature* 1996;384:266-270.

122. Zammit PS, Carvajal JJ, Golding JP, Morgan JE, Summerbell D, Zolnerciks J, Partridge TA, Rigby PW, Beauchamp JR. Myf5 expression in satellite cells and spindles in adult muscle is controlled by separate genetic elements. *Dev Biol* 2004;273:454-465.

123. Kosek DJ, Kim JS, Petrella JK, Cross JM, Bamman MM. Efficacy of 3 days/wk resistance training on myofiber hypertrophy and myogenic mechanisms in young vs. Older adults. *J Appl Physiol* 2006;101:531-544.

124. Pope RK, Pestonjamasp KN, Smith KP, Wulfkuhle JD, Strassel CP, Lawrence JB, Luna EJ. Cloning, characterization, and chromosomal localization of human superillin (svil). *Genomics* 1998;52:342-351.

125. Blake DJ, Weir A, Newey SE, Davies KE. Function and genetics of dystrophin and dystrophin-related proteins in muscle. *Physiol Rev* 2002;82:291-329.

126. Lee MA, Joo YM, Lee YM, Kim HS, Kim JH, Choi JK, Ahn SJ, Min BI, Kim CR. Archvillin anchors in the z-line of skeletal muscle via the nebulin c-terminus. *Biochem Biophys Res Commun* 2008;374:320-324.

127. Takizawa N, Ikebe R, Ikebe M, Luna EJ. Supervillin slows cell spreading by facilitating myosin ii activation at the cell periphery. *J Cell Sci* 2007;120:3792-3803.

128. Potthoff MJ, Arnold MA, McAnally J, Richardson JA, Bassel-Duby R, Olson EN. Regulation of skeletal muscle sarcomere integrity and postnatal muscle function by mef2c. *Mol Cell Biol* 2007;27:8143-8151.

129. Yamakuchi M, Higuchi I, Masuda S, Ohira Y, Kubo T, Kato Y, Maruyama I, Kitajima I. Type i muscle atrophy caused by microgravity-induced decrease of myocyte enhancer factor 2c (mef2c) protein expression. *FEBS Lett* 2000;477:135-140.

130. O'Shea JJ, Park H, Pesu M, Borie D, Changelian P. New strategies for immunosuppression: Interfering with cytokines by targeting the jak/stat pathway. *Curr Opin Rheumatol* 2005;17:305-311.

131. Rawlings JS, Rosler KM, Harrison DA. The jak/stat signaling pathway. *J Cell Sci* 2004;117:1281-1283.

132. Bennett M, Macdonald K, Chan SW, Luzio JP, Simari R, Weissberg P. Cell surface trafficking of fas: A rapid mechanism of p53-mediated apoptosis. *Science* 1998;282:290-293.

133. Liebermann DA, Hoffman B. Gadd45 in stress signaling. *J Mol Signal* 2008;3:15.

134. Schuler M, Green DR. Mechanisms of p53-dependent apoptosis. *Biochem Soc Trans* 2001;29:684-688.

135. Yu J, Zhang L. The transcriptional targets of p53 in apoptosis control. *Biochem Biophys Res Commun* 2005;331:851-858.

136. Siu PM, Alway SE. Id2 and p53 participate in apoptosis during unloading-induced muscle atrophy. *Am J Physiol Cell Physiol* 2005;288:C1058-1073.

137. Boles JM, Bion J, Connors A, Herridge M, Marsh B, Melot C, Pearl R, Silverman H, Stanchina M, Vieillard-Baron A, et al. Weaning from mechanical ventilation. *Eur Respir J* 2007;29:1033-1056.

138. Carson SS. Outcomes of prolonged mechanical ventilation. *Curr Opin Crit Care* 2006;12:405-411.

139. MacIntyre NR, Cook DJ, Ely EW, Jr., Epstein SK, Fink JB, Heffner JE, Hess D, Hubmayer RD, Scheinhorn DJ. Evidence-based guidelines for weaning and discontinuing ventilatory support: A collective task force facilitated by the american college of chest physicians; the american association for respiratory care; and the american college of critical care medicine. *Chest* 2001;120:375S-395S.

140. Tobin MJ. Breathing pattern analysis. *Intensive Care Med* 1992;18:193-201.

141. Appendini L, Purro A, Patessio A, Zanaboni S, Carone M, Spada E, Donner CF, Rossi A. Partitioning of inspiratory muscle workload and pressure assistance in ventilator-dependent copd patients. *Am J Respir Crit Care Med* 1996;154:1301-1309.

142. Capdevila X, Perrigault PF, Ramonatxo M, Roustan JP, Peray P, d'Athis F, Prefaut C. Changes in breathing pattern and respiratory muscle performance parameters during difficult weaning. *Crit Care Med* 1998;26:79-87.

143. Del Rosario N, Sassoon CS, Chetty KG, Gruer SE, Mahutte CK. Breathing pattern during acute respiratory failure and recovery. *Eur Respir J* 1997;10:2560-2565.

144. Jubran A, Tobin MJ. Pathophysiologic basis of acute respiratory distress in patients who fail a trial of weaning from mechanical ventilation. *Am J Respir Crit Care Med* 1997;155:906-915.

145. Tobin MJ, Perez W, Guenther SM, Semmes BJ, Mador MJ, Allen SJ, Lodato RF, Dantzker DR. The pattern of breathing during successful and unsuccessful trials of weaning from mechanical ventilation. *Am Rev Respir Dis* 1986;134:1111-1118.

146. Wysocki M, Cracco C, Teixeira A, Mercat A, Diehl JL, Lefort Y, Derenne JP, Similowski T. Reduced breathing variability as a predictor of unsuccessful patient separation from mechanical ventilation. *Crit Care Med* 2006;34:2076-2083.

147. Bien MY, Hseu SS, Yien HW, Kuo BI, Lin YT, Wang JH, Kou YR. Breathing pattern variability: A weaning predictor in postoperative patients recovering from systemic inflammatory response syndrome. *Intensive Care Med* 2004;30:241-247.

148. El-Khatib M, Jamaleddine G, Soubra R, Muallem M. Pattern of spontaneous breathing: Potential marker for weaning outcome. Spontaneous breathing pattern and weaning from mechanical ventilation. *Intensive Care Med* 2001;27:52-58.

149. Engoren M. Approximate entropy of respiratory rate and tidal volume during weaning from mechanical ventilation. *Crit Care Med* 1998;26:1817-1823.

150. Esteban A, Alia I, Tobin MJ, Gil A, Gordo F, Vallverdu I, Blanch L, Bonet A, Vazquez A, de Pablo R, et al. Effect of spontaneous breathing trial duration on outcome of attempts to discontinue mechanical ventilation. Spanish lung failure collaborative group. *Am J Respir Crit Care Med* 1999;159:512-518.

151. Lemaire F. Difficult weaning. *Intensive Care Med* 1993;19 Suppl 2:S69-73.

152. Vallverdu I, Calaf N, Subirana M, Net A, Benito S, Mancebo J. Clinical characteristics, respiratory functional parameters, and outcome of a two-hour t-piece trial in patients weaning from mechanical ventilation. *Am J Respir Crit Care Med* 1998;158:1855-1862.

153. Benchetrit G, Bertrand F. A short-term memory in the respiratory centres: Statistical analysis. *Respir Physiol* 1975;23:147-158.

154. Kuratomi Y, Okazaki N, Ishihara T, Arai T, Kira S. Variability of breath-by-breath tidal volume and its characteristics in normal and diseased subjects. Ventilatory monitoring with electrical impedance pneumography. *Jpn J Med* 1985;24:141-149.

155. Tobin MJ, Yang KL, Jubran A, Lodato RF. Interrelationship of breath components in neighboring breaths of normal eupneic subjects. *Am J Respir Crit Care Med* 1995;152:1967-1976.

156. Bruce EN. Chemoreflex and vagal afferent mechanisms enhance breath to breath variability of breathing. *Respir Physiol* 1997;110:237-244.

157. Jubran A, Tobin MJ. Effect of isocapnic hypoxia on variational activity of breathing. *Am J Respir Crit Care Med* 2000;162:1202-1209.

158. Khatib MF, Oku Y, Bruce EN. Contribution of chemical feedback loops to breath-to-breath variability of tidal volume. *Respir Physiol* 1991;83:115-127.

159. Van den Aardweg JG, Karemaker JM. Influence of chemoreflexes on respiratory variability in healthy subjects. *Am J Respir Crit Care Med* 2002;165:1041-1047.

160. Brack T, Jubran A, Tobin MJ. Effect of elastic loading on variational activity of breathing. *Am J Respir Crit Care Med* 1997;155:1341-1348.

161. Brack T, Jubran A, Tobin MJ. Effect of resistive loading on variational activity of breathing. *Am J Respir Crit Care Med* 1998;157:1756-1763.

162. Tobin MJ, Mador MJ, Guenther SM, Lodato RF, Sackner MA. Variability of resting respiratory drive and timing in healthy subjects. *J Appl Physiol* 1988;65:309-317.

163. Krieger BP, Chediak A, Gazeroglu HB, Bizousky FP, Feinerman D. Variability of the breathing pattern before and after extubation. *Chest* 1988;93:767-771.

164. Yang KL. Reproducibility of weaning parameters. A need for standardization. *Chest* 1992;102:1829-1832.

165. Ballanyi K, Onimaru H, Homma I. Respiratory network function in the isolated brainstem-spinal cord of newborn rats. *Prog Neurobiol* 1999;59:583-634.

166. Davenport P.W. RRL. Cerebral cortex and respiration. In: Dempsey JAP, A.I., editor. Regulation of breathing,. New York: Marcel Dekker; 1995. p. 365-388.

167. Modarreszadeh M, Bruce EN. Ventilatory variability induced by spontaneous variations of paco2 in humans. *J Appl Physiol* 1994;76:2765-2775.

168. Preas HL, 2nd, Jubran A, Vandivier RW, Reda D, Godin PJ, Banks SM, Tobin MJ, Suffredini AF. Effect of endotoxin on ventilation and breath variability: Role of cyclooxygenase pathway. *Am J Respir Crit Care Med* 2001;164:620-626.

169. Brack T, Jubran A, Tobin MJ. Dyspnea and decreased variability of breathing in patients with restrictive lung disease. *Am J Respir Crit Care Med* 2002;165:1260-1264.

170. Ponikowski P, Anker SD, Chua TP, Francis D, Banasiak W, Poole-Wilson PA, Coats AJ, Piepoli M. Oscillatory breathing patterns during wakefulness in patients with chronic heart failure: Clinical implications and role of augmented peripheral chemosensitivity. *Circulation* 1999;100:2418-2424.

171. Feld H, Priest S. A cyclic breathing pattern in patients with poor left ventricular function and compensated heart failure: A mild form of cheyne-stokes respiration? *J Am Coll Cardiol* 1993;21:971-974.

172. Lahiri S, Hsiao C, Zhang R, Mokashi A, Nishino T. Peripheral chemoreceptors in respiratory oscillations. *J Appl Physiol* 1985;58:1901-1908.

173. Ponikowski P, Chua TP, Piepoli M, Ondusova D, Webb-Peploe K, Harrington D, Anker SD, Volterrani M, Colombo R, Mazzuero G, et al. Augmented peripheral chemosensitivity as a potential input to baroreflex impairment and autonomic imbalance in chronic heart failure. *Circulation* 1997;96:2586-2594.

174. Arold SP, Mora R, Lutchen KR, Ingenito EP, Suki B. Variable tidal volume ventilation improves lung mechanics and gas exchange in a rodent model of acute lung injury. *Am J Respir Crit Care Med* 2002;165:366-371.

175. Mutch WA, Harms S, Ruth Graham M, Kowalski SE, Girling LG, Lefevre GR. Biologically variable or naturally noisy mechanical ventilation recruits atelectatic lung. *Am J Respir Crit Care Med* 2000;162:319-323.

176. Marini JJ. Breathing patterns as integrative weaning preditors: Variations on a them. *Crit Care Med* 2006;34:2241-2243.

177. Donaldson GC. The chaotic behaviour of resting human respiration. *Respir Physiol* 1992;88:313-321.

178. Dejours P, Flandrois R, Lefrancois R, Teillac A. [study of the regulation of ventilation during muscular exercise in man.]. *J Physiol (Paris)* 1961;53:321-322.

179. Morganroth ML, Morganroth JL, Nett LM, Petty TL. Criteria for weaning from prolonged mechanical ventilation. *Arch Intern Med* 1984;144:1012-1016.

180. Sahn SA, Lakshminarayan S. Bedside criteria for discontinuation of mechanical ventilation. *Chest* 1973;63:1002-1005.

181. Yang KL, Tobin MJ. A prospective study of indexes predicting the outcome of trials of weaning from mechanical ventilation. *N Engl J Med* 1991;324:1445-1450.

182. Purro A, Appendini L, De Gaetano A, Gudjonsdottir M, Donner CF, Rossi A. Physiologic determinants of ventilator dependence in long-term mechanically ventilated patients. *Am J Respir Crit Care Med* 2000;161:1115-1123.

183. Whitelaw WA, Derenne JP. Airway occlusion pressure. *J Appl Physiol* 1993;74:1475-1483.

184. Vassilakopoulos T, Zakynthinos S, Roussos C. The tension-time index and the frequency/tidal volume ratio are the major pathophysiologic determinants of weaning failure and success. *Am J Respir Crit Care Med* 1998;158:378-385.

185. Caminal P, Domingo L, Giraldo BF, Vallverdu M, Benito S, Vazquez G, Kaplan D. Variability analysis of the respiratory volume based on non-linear prediction methods. *Med Biol Eng Comput* 2004;42:86-91.

186. Loveridge B, West P, Anthonisen NR, Kryger MH. Breathing patterns in patients with chronic obstructive pulmonary disease. *Am Rev Respir Dis* 1984;130:730-733.

187. Fiamma MN, Straus C, Thibault S, Wysocki M, Baconnier P, Similowski T. Effects of hypercapnia and hypocapnia on ventilatory variability and the chaotic dynamics of ventilatory flow in humans. *Am J Physiol Regul Integr Comp Physiol* 2007;292:R1985-1993.

188. Reissmann HK, Ranieri VM, Goldberg P, Gottfried SB. Continuous positive airway pressure facilitates spontaneous breathing in weaning chronic obstructive pulmonary disease patients by improving breathing pattern and gas exchange. *Intensive Care Med* 2000;26:1764-1772.

189. Pincus S. Approximate entropy (apen) as a complexity measure. *Chaos* 1995;5:110-117.

190. BuSha BF, Stella MH. State and chemical drive modulate respiratory variability. *J Appl Physiol* 2002;93:685-696.

191. Costa M, Goldberger AL, Peng CK. Multiscale entropy analysis of complex physiologic time series. *Phys Rev Lett* 2002;89:068102.

BIOGRAPHICAL SKETCH

Tseng Tien Huang was born in Yuan-Lin town, Taiwan, and graduated salutatorian of his high school class in 1993. He received his bachelor's degree in Physical Therapy from National Cheng-Kung University, Tainan, Taiwan in July of 1996. Then, he was on the military duty from 1996-1998 in Taiwan. In 2002, he began a master's program in physical therapy at the University of Florida in Gainesville, Florida and received a master degree in physical therapy in 2004. Deciding to focus his carrier in rehabilitation science research, Tseng began his doctoral work at the University of Florida in 2004 under the direction of A.D. Martin. Tseng focused his studies on pulmonary physiology and inspiratory muscle training in difficult-to-wean patients. He received his PhD in May 2009.